Experimental and Numerical study of submerged inclined buoyant jet discharges into stagnant saline ambient water

Yilin Guo

Thesis submitted to the University of Ottawa

in partial Fulfillment of the requirements for the

Master of Applied Science in Civil Engineering

Department of Civil Engineering

Faculty of Engineering

University of Ottawa

Abstract

Treated and untreated liquid that is discharged from industrial and desalination plants is one of the main factors that break the ecological balance and destroys aquatic habitat in lakes, rivers and coastal areas where the effluent is discharged. Positively and negatively buoyant jets are two categories of outfalls which are generated because of the destiny difference between the effluent and ambient fluid. In order to ensure minimal impact of the effluent on the environment, it is necessary to estimate the dilution of the jet and compare it with environmental regulations on the level of required dilution to ensure that the concentration of the effluent is diluted quickly enough and the concentration of the effluent at different points does not exceed the allowed concentrations. This study investigated the positively buoyant jet, which happens near the coastal and near water area. For instance, cooling water that flows out from a power plant or factory, wasted water that is discharged from an industrial plant near river, submerged drainage from civil municipal sewer systems and treated water from desalination plant in coastal area. Density difference, velocity and inclined angle of the jet were considered as the main factors that contribute to the jet spreading and were compared to develop the best solution for its dilution. The jet was discharged inclined downward to allow for more mixing and dilution of the effluent with the ambient water. In order to simulate a positive jet, tap water was injected in saline ambient. A large number of experiments were conducted in the laboratory and using camera imaging. The jet trajectory was estimated from the images using image processing and the impact of various parameters such as Froude number and jet velocity were investigated. The opensource software OpenFOAM, was employed for numerical simulations which is a finite volume model ensures mass conservation and allows for flexible mesh size for further accuracy and optimization of computational cost. Using this Computational Fluid Dynamics (CFD) model, the numerical simulations were performed, and the results were compared with laboratory experiments. A Reynold-Averaged Navier-Stokes (RANS) approach was employed in the numerical simulations which offers a good balance between accuracy and computational cost. It was found that the numerical model in conjunction with the second order turbulence model called Launder-Reece-Rodi model (LRR) had a reasonable agreement with the experimental data.

Acknowledgements

First and foremost, I would like to express my sincere gratitude to my supervisor Dr. Majid Mohammadian. Without his encouragement and support on my study, I would not be able to complete the project and thesis. His rigorous scientific spirit and positive attitude towards life really impressed me. That is lifetime treasure for me. Thank so much for all his help and guidance during my study period at the University of Ottawa.

Secondly, I would like to thank Dr. Hassan Alfaifi, a former PHD student at the University of Ottawa who sheared his experience with me and helped me a lot on setting up my experiments.

I would like to thank Proust Allan and Diyuan Wang for their great cooperation during the experimental process.

I would like to thank all the good friends who helped me during the past years.

Finally, I would like to thank my mother and father who give me great love, broad vision and continuous support in my whole life.

Table of Contents

List of Figures

List of Tables

List of Acronyms

CFD: Computational Fluid Dynamics

LRR: Launder-Reece-Rodi

LA: Light Attenuation

LIF: Laser-Induced Fluorescence

LES Large Eddy Simulations

OpenFOAM: Open Field Operation And Manipulation

PIV: Particle Image Velocimetry

RANS: Reynolds-Averaged Navier–Stokes

List of Symbols

Re: Reynolds Number

U_0: Jet initial velocity (m/s)

Q_0: Nozzle flow flux (m^3/s)

ρ : Fluid density (kg/m^3)

u: Flow velocity(m/s)

L: Characteristic linear dimension (m)

μ: Fluid dynamic vsicosity ($kg/(m \cdot s)$)

ν: Fluid kinematic viscosity(m^2/s)

R_0: Initial jet Richardson number

M_0 : Jet initial momentum flux

B_0 : Jet initial buoyancy-generated momentum flux

M_B: Buoyancy-generated-momentum

s： Distance to the nozzle on the U_0 direction

n: Distance to the nozzle on the vertical direction to U_0.

F_0: Jet initial Froude number

ρ_a: Ambient density (kg/m^3)

ρ_0 : Jet initial density (kg/m^3)

S: Salinity

S_a: Ambient Salinity

S_0: Jet initial Salinity

T: Jet initial temperature (℃)

ρ: Ambient density, kg/m^3

ρ_t : Density of water at temperature T, in this project ρ_t is jet initial density, kg/m^3

L_M : The momentum length scale

L_Q : Discharge length scale

d_0 : Nozzle diameter (m)

g_0: Relatively gravity acceleration (m^2/s)

Fd: Densimetric Froude number

V_a : Volume of salinity liquid body in tank 2, $V_a = 0.045m^3$.

m_0: Water weight (kg)

m_s: Salt (99% NaCl) weight(kg)

${D_{ij}}^v$: Viscous diffusion

${D_{ij}}^T$: Turbulent diffusion

κ: Turbulent kinetic energy

ε: Dissipation rate

$DeltaT$: Time step size

α , θ_0: Inclined discharge angles

Chapter 1 Introduction

1.1 Background

In this study, near-field characteristics of the inclined jet and saline ambient will be specifically examined. More importantly, we study the relationship between the mixing of the effluent and different jet velocities, density differences, and inclined angles. In real applications, the environmental problems due to industrial and urban outfalls have tripped due to the developments in many regions. Water is the key factor that leads a country to a prosperity phase and a significant safeguard for all its citizens' daily water consumption. Desalination, for instant, is an option for many cities which suffer from drought and in possession of marine resources with dissolved minerals (like salt) and produce clean and potable water for its population. However, with saline water flows in and purified water flows out, the auxiliary product - hypersaline brine discharges into to the near-field surroundings, which not only changes the water quality but also has a negative influence on biodiversity. Thermal liquid from power plant, treated or untreated water from municipal sewer systems and outflow from commercial or industrial factories that finally enter into rivers, lakes or marine area all are the realistic examples that refers to effluent problems.

During more than four decades in the past, effluent issues have been widely studied worldwide. Many researchers have tried to find out the optimum solution to reduce the influence from the outfall on the environment.

1.1.1 Environmental impacts of effluent discharges

From the point of view of outfall problem solution, it is technically necessary to learn the environmental impacts of the outfall, in an attempt to guide the exploration of potential methods to reduce its negative influence on ecosystem and living environment. An estimation reveals that

up to 25 million cubic meters of desalinated water is produced every day on the planet (Lattemann and Hopner, 2008). It is extensively observed that the operation of desalination plants has great and detrimental impacts on receiving marine environments both physicochemically and ecologically. (Winters et al., 1979; Miri and Chouikhi, 2005; Maugin and Corsin, 2005).

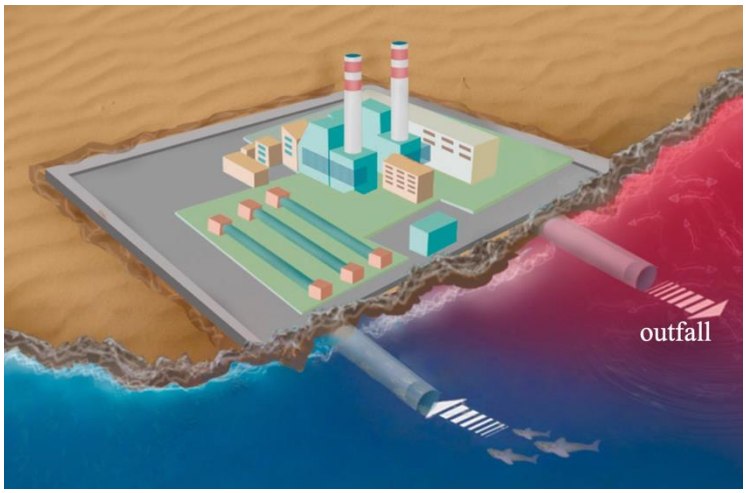

(a) Cooling water discharge

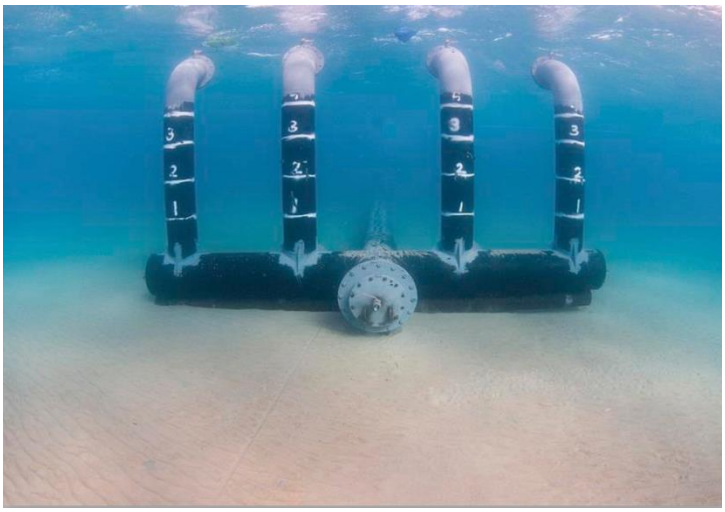

(b) Industrial power plant

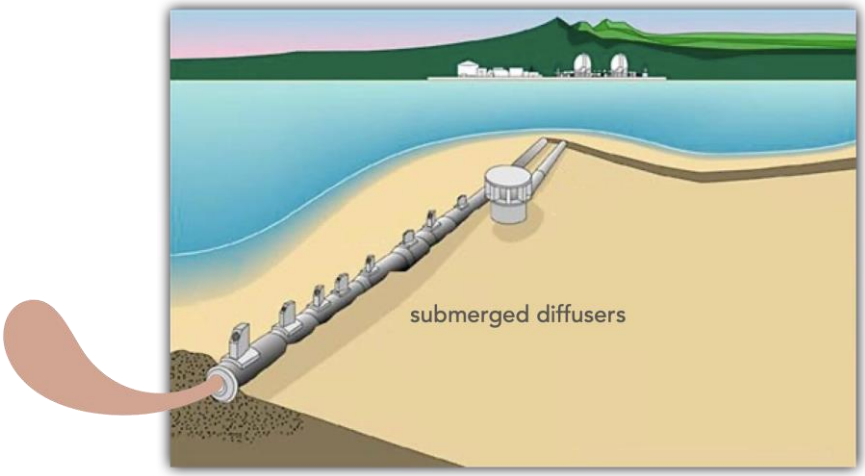

(c) Drainage water effluent

(d)Desalination plant

(e)Industrial wastewater

Fig.1.1 Jet discharge under different circumstance

1.1.2 About buoyant jet

Jet discharge is an essential part in the process of industrial plants, desalination plants, sewage treatment plants. etc. The dilution and transmission behaviors of a fluid flow has been inspected both experimentally and numerically in previous studies. One of the terminal goals of these studies is engaged in maximizing the mixing level between the jet and the ambient. However, nowadays, there is still a long way to study the flow characteristics and features on every aspect to predict or solve related engineering problems. Depending on the characteristics of the effluent and the receiving environment, such as salinity and temperature difference, velocity and stream angle, the jet could act as laminar, turbulent, buoyant jet, plume, etc.

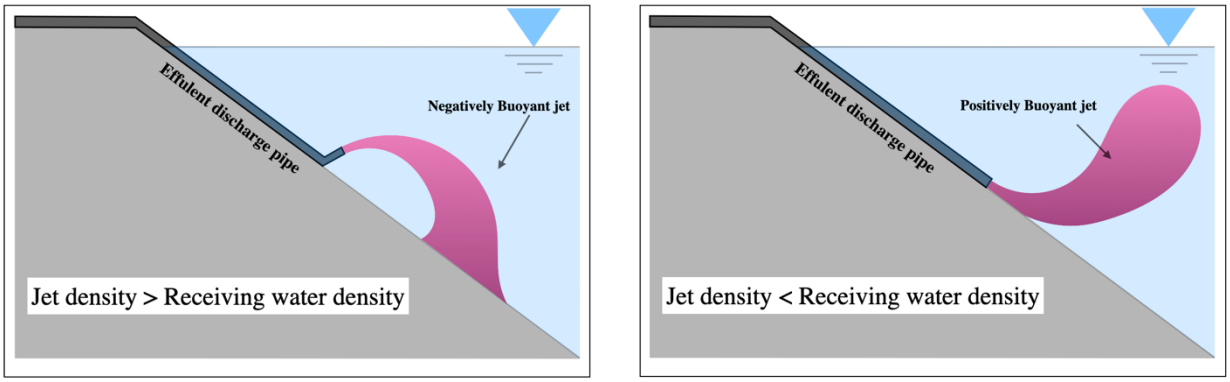

a. Negetively Buoyant Jet

b. Positively Buoyant Jet

Fig 1.2 Negatively and positively jets

In this thesis, the behaviour of an inclined positive buoyant jet with a round discharge shape was studied. By definition, a buoyant jet is a continuous fluid flow with both momentum and buoyancy. A jet with an initial velocity which has a higher density than the receiving ambient could be categorized as a negatively buoyant jet; while if the moving jet has lower density than the surroundings, it could be called a positively buoyant jet. According to the initial features, the jet could be classified into two main categories. One is non-buoyant jet, the other is a jet with density difference. The density difference of the jet and the receiving environment emerges from the difference in concentration and temperature between the flow and the ambient. This study focused on the impact of density difference related to concentration, or in other words, salinity. All the laboratory experiments were carried at the same temperature. The environment that the jet enters also plays an essential role, it could be divided into two groups: stagnant ambient and

flowing ambient. In the experimental section of this study, stagnant and uniform salty liquid was chosen for the receiving body.

The factors that dominate the movement, the shape and mixing of a jet are primarily dependent on the condition of the jet and the ambient water that it enters into. Many aspects are taken into account as initial variables in the design phase of experiments and simulations in this thesis. From the consideration of momentum contribution, jets with velocity at 0.2m/s, 0.41m/s and 0.6m/s were investigated. As the buoyancy was determined based on the salinity difference and the jet was tap water mixed with dye without any salt, fully mixed uniform salty water with various salinity values was employed for the ambient liquid. Actually, a complex parameter - densimetric Froude number ("Fd" or "Froude number" are short for densimetric Froude number in this thesis) that contains the effects of velocity and density difference was considered in this study. Experiments were carried under Froude number values at 10, 20, 30, 50 and 100. Froude number is a crucial indicator. It could largely simplify the predicting procedure of jet movement. Except for the above variables, jet discharge angle was also changed and studied. Experimental results with jet at 30° and 60° inclined angle downwards will be presented in Chapter 3.

The Froude Number is given by

$$F_d = \frac{U_0}{\sqrt{g'D}} \tag{1}$$

Where, U_0 is the velocity, D is the jet diameter, and g' is reduced gravitational acceleration.

$$g' = g\frac{\rho_a - \rho_0}{\rho_0} \tag{2}$$

Where, ρ_0 is the jet density and ρ_a is the ambient density.

Image analysis using camara records was applied to extract data from laboratory experiments. Centerline of each jet at fully developed stage was analyzed.

Due to the high costs and time requirements of laboratory research, numerical simulation of fluids is a good substitute for laboratory and field studies and tend to have higher demand in practice. In this project, a series of numerical simulations were conducted to compare with the

laboratory experimental results and evaluate the accuracy of the selected numerical model and turbulence scheme.

Computational fluid dynamics (CFD) is a widely used approach by using finite volume numerical simulation (or other methods such as finite difference, finite element, boundary element, etc.) based on massive calculations on computers. Open Field Operation and Manipulation (OpenFOAM), a free and open-source tool was used for the simulations in this study.

In the field of numerical studies on fluid flow, the selection of turbulence model is a key step in getting accurate simulation outcomes. Fluid flow is a complex problem and not easy to predict especially with turbulence effects. However, since Navier-Stokes(N-S) equations were introduced about 200 years ago, they offered more ways to describe and analyze flow behavior. Launder-Reece-Rodi (LRR) turbulence model, which is a second-order model, can be used with Reynold-Averaged Navier-Stokes (RANS) equations. It was used for numerical simulation of turbulence in Chapter 4. As a result, most of numerical calculations in this study predicted jet results which were in reasonable agreement with laboratory experiments in Chapter 3.

1.2 Objectives

Buoyant jets exist in many circumstances. The study of their dynamic properties and dilution rules could help us design related structures in an optimal way. By deeply understanding the buoyant jet behavior, we can minimize the effluent impacts on the ecosystem and living environment. The main objectives of this project are:

- Study the characteristics of inclined positive buoyant jets experimentally and numerically
- Find out the relationship between the submerged inclined buoyant jets behavior and their parameters including velocity, angle and Froude number.
- Conduct CFD simulations in OpenFOAM under the same initial conditions as in the laboratory investigations

- Chose appropriate turbulence model and solver to use in OpenFOAM for this project
- Compare experimental result with numerical data

1.3 Novelty of the Study

In previous studies, investigations related to dense jet and negative buoyant jet were widely conducted. However, researchers have rarely focused on the positively buoyant jet with inclined discharge angle. Much less examples are focused on the factors that impact the behavior of such jets. This project was targeted at learning the submerged inclined positive buoyant jet properties both experimentally and numerically. The outcome of this study may contribute to the effluent structure design process to improve the fluid dilution efficiency at lower cost and at the same time to protect the environment with less disturbance.

More specifically, the subject of this study is focused on the factors that could govern the spreading of a positively buoyant jet. Jet velocity, Froude number, discharge angle and density difference were considered in the experimental preparation stage. The selection of the LRR turbulence model with the utilization of a modified solver in OpenFOAM on the inclined positively buoyant jet study are also other novel aspects of this investigation.

1.4 Outline of the thesis

This thesis is presented in a monograph form and contains five chapters.

Chapter 1 gives an introduction that provides an overview of the whole project.

Chapter 2 provides a literature review. In this chapter, a background description is demonstrated. Previous experimental studies about negatively and positively buoyant jet discharged into stagnant environment are discussed. A review of CFD studies of negatively and positively buoyant jet in OpenFOAM is also presented in this chapter.

Chapter 3 presents the experimental study. This Chapter contains the key research content of the

laboratory investigation on the submerged inclined positive jet behavior in stagnant ambient.

Chapter 4 demonstrates the numerical simulations. This chapter shows a CFD method that makes use of computer technologies to predict jet movement by employing OpenFOAM. The numerical simulation results show good agreement with laboratory experimental results in Chapter 3.

Chapter 5 presents some concluding remarks. This chapter gives a summary view of the whole project, and also provides some suggestions for future work.

Chapter 2 Literature Review

2.1 Introduction

Outfall designs have a close influence on energy cost, environmental impact and outfall structure construction type. It is always desirable to enhance the mixing in the process of the liquid discharge. A large number of studies have been conducted to learn about the properties that may contribute to diffusion efficiency of the jet. According to previous studies, the research methods could be divided into two groups, laboratorial experiments and numerical simulations.

2.1.1 Outfall types and fundamental theory

Table 2.1 Outfall categories on different classification standard

<table>
<tr><td>Classification parameter</td><td colspan="3">Categories</td></tr>
<tr><td rowspan="2">Driving force</td><td rowspan="2">Plume</td><td colspan="2">Buoyant jet</td></tr>
<tr><td>Positive buoyant jet</td><td>Negative buoyant jet</td></tr>
<tr><td>Density difference type</td><td>Jet with salinity difference</td><td colspan="2">Jet with temperature difference jet</td></tr>
<tr><td>Discharge location</td><td>Surface jet</td><td colspan="2">Submerged jet</td></tr>
<tr><td>Discharge ports</td><td>Single</td><td colspan="2">Multiport</td></tr>
<tr><td>Reynolds number</td><td>Laminar flow</td><td colspan="2">Turbulent flow</td></tr>
<tr><td>Discharge angle</td><td>Inclined jet</td><td colspan="2">Vertical jet/Horizontal jet</td></tr>
<tr><td>Receiving liquid dynamic characteristics</td><td>Stagnant ambient</td><td colspan="2">Flowing ambient</td></tr>
</table>

An effluent may turn into various regimes depending on the jet and flow features. Table 2.1 provides a range of possible types that could describe a discharge. Most of the industrial outflows could be divided into two types. The first category is positively buoyant jet that has lower density than the environment. Under this circumstance, the jet has a tendency to rise in the

receiving body. The second category is called negatively buoyant jet, it eventually moves towards the bottom. However, the density depends on both salinity and temperature. The exporting location also matters. Discharges can be categorised in two groups: surface flow and submerged flow. In practical applications, inclined discharge angles and multiport diffusers have been introduced to help buoyant jets spread more efficiently within a limited time and space. The jet behaviors could also be affected by the ambient water. Two cases can be distinguished; one is stagnant ambient the other is flowing ambient. In the process of jet movement, the Reynolds Number (Re) has been introduced to distinguish turbulence flow, transitional flow and laminar flow. The Reynolds number is the ratio of inertial forces to viscous forces. It is defined as

$$Re = \frac{inertial\ forces}{visous\ forces} \tag{3}$$

or

$$Re = \frac{\rho u L}{\mu} = \frac{uL}{\nu} \tag{4}$$

where

ρ : fluid density (kg/m^3)

u: flow velocity(m/s)

L: characteristic linear dimension (m)

μ: fluid dynamic vsicosity $(kg/(m \cdot s))$

ν: fluid kinematic viscosity(m^2/s)

Table 2.2 Flow classification in terms of the Reynolds number.(Andrew, John and Martin, 2013)

Re < 2000	Laminar flow
2000 < Re < 4000	Transitional flow
Re > 4000	Turbulent flow

Table 2.2 shows flow classification in terms of the Reynolds number. The table only provide a rough reference range of flow types. In some cases, Reynold Number for initiation of turbulence was found to be over 4000. (Chadwicket al., 2013)

2.1.2 Negatively buoyant jet

A typical submerged negatively buoyant jet has a tendency to eventually move towards the bottom of its ambient water. This phenomenon generally occurs in the outfall area of desalination and industrial plants. The use of the inclined discharge angles can enhance the dilution efficiency of the jet and reduce its density to a lower level rapidly within a relatively short distance.

Fig 2.1 shows the sketch of an inclined dense jet spreading into a still uniform environment (Kikkert et al., 2007). Some key information about the inclined negatively buoyant jet can be described in the form of a group of formulas.

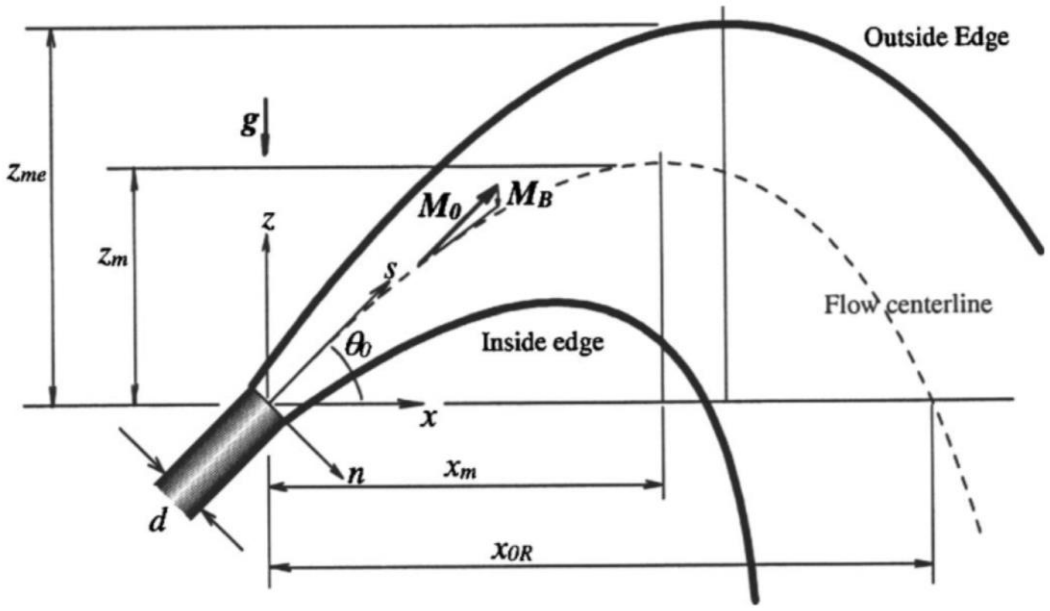

Fig.2.1 Sketch of an inclined negatively buoyant jet discharged into a stagnant ambient (Kikkert et al., 2007)

The liquid flows from a round nozzle with a diameter d, upward discharge angleθ_0, and intial velocity U_0, jet density ρ_0, ambient density ρ_a, jet initial momentum M_0, buoyancy-generated-momentum M_B. It reaches the highest point z_m (centerline) and z_{me}(edge). Parameter x_m indicates the horizontal location of the peak of the centerline, while X_{OR} represents the location when the jet returns to its nozzle height (return point). In the Fig. 2.1, x stands for the horizontal direction, z means vertical direction, s indicates the direction of initial velocity and n is perpendicular to s.

The trajectory of the inclined negatively buoyant jet normally includes three phases. It is important to characterize these phases, because the jet properties like dilution rate, jet centerline shape, even entrainment activities with the surroundings are different in each zone.

In the near nozzle area (jet-like area), the momentum flux M_0 governs the effluent behavior, it is much larger in magnitude compared to buoyancy-generated- momentum M_B, where $M_0 \gg M_B$ （Kikkert et al., 2007）. The buoyancy-generated momentum M_B plays a role to prevent the jet from sinking. The jet initial volume flux is defined as

$$M_0 = U_0 Q_0 \tag{5}$$

$$Q_0 = \frac{1}{4}\pi d^2 U_0 \tag{6}$$

U_0 : jet initial velocity

Q_0: nozzle flow flux

Jet trajectory can be demonstrated by the relevant momentum flux ratio

$$\frac{dn_*}{ds_*} = \frac{M_{B^*} \cos\theta_0}{1 - M_{B^*} \sin\theta_0} \tag{7}$$

s and n represent for the distance to the nozzle on the U_0 direction and the vertical direction to U_0.

M_{B^*} is a dimensionless buoyancy-generated momentum flux and is estimated as

$$M_{B^*} = \frac{I_\Delta k}{I_{Q\Delta}} \left[\frac{I_m}{\pi}\right]^{1/2} \frac{1}{{F_0}^2} {s_*}^2 \tag{8}$$

Where:

Δ is centerline buoyancy($\Delta = \frac{\rho - \rho_a}{\rho_a}$, ρ is centerline density, ρ_a is ambient density),

F_0 is the jet initial Froude number ($F_0 = \frac{U_0}{\sqrt{d\Delta_0}}$),

The integral constants are given by $I_m = 1.7$, $I_Q = 2.0$,

Jet Gaussian velocity spread constant is estimated as k=0.11,

The symbol * represents a dimensionless parameter.

The second region for the jet is around where $M_0 \approx M_B$. In this region, the buoyancy-generated momentum flux has the same magnitude as initial momentum flux and the jet transforms from a jet-like zone to plume-like zone. The transition length-scale in this stage can be evaluated by S_{JP}.

$$S_{JP^*} \approx \left[\frac{I_{Q\Delta}}{I_\Delta} \frac{1}{k} \left(\frac{\pi}{I_m}\right)^{\frac{1}{2}}\right]^{\frac{1}{2}} F_0 \tag{9}$$

In 2000, Davidson and Pun investigated the jet-like zone to plume-like zone by using the idea of $M_0 \approx M_B$. They proved that the maximum height was always located in the near nozzle jet-like area.

The last region is a plume like one, where $M_0 \ll M_B$. In this region, buoyancy-generated-momentum dominates the jet behavior.

2.1.3 Positively buoyant jet

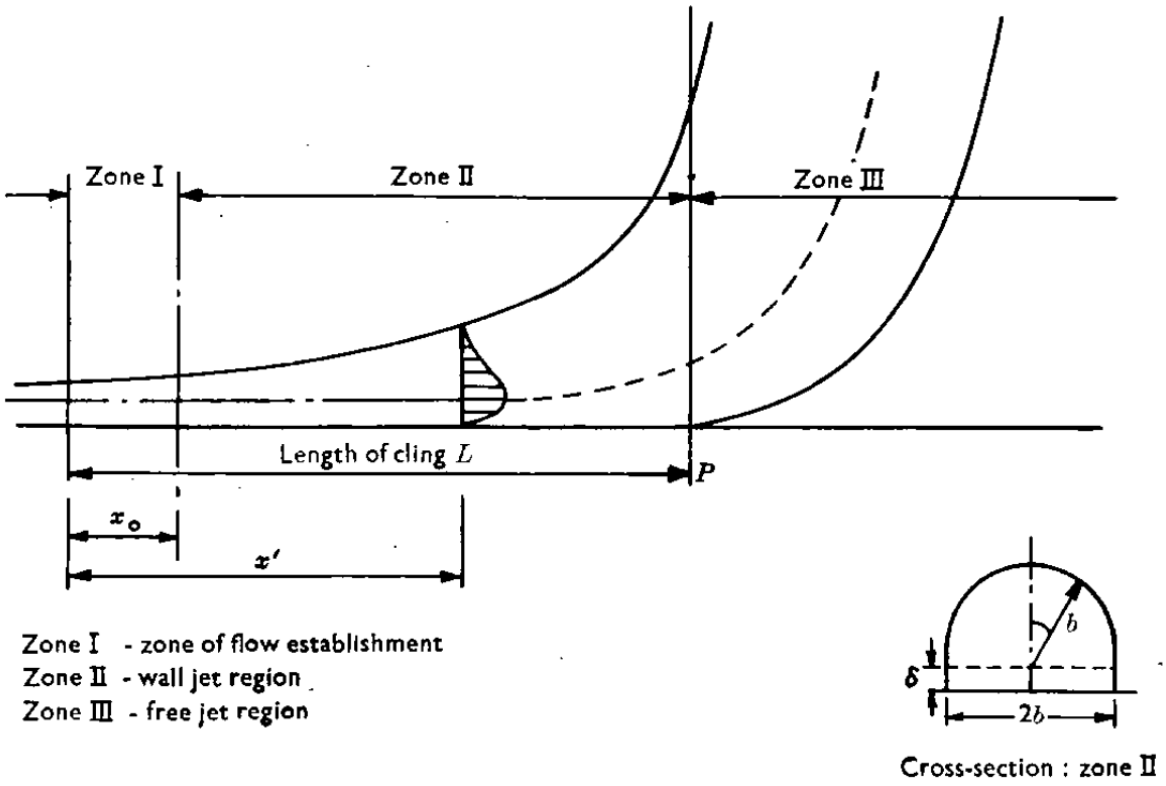

Fig. 2.2. Schematic of submerged horizontal positively buoyant jet. Sharp (1975,1977).

The positively buoyant jet happens frequently for thermal outfall near river and liquid that discharges into marine area with hazardous contaminant. In 1975, Sharp's theory and analysis about positively buoyant wall jet was introduced. Their group were pioneers to conduct the experiments on submerged horizontal thermal jet. Fig. 2.2 demonstrates a schematic of the outfall in their study. The jet flowed into the receiving environment horizontally along the bottom. The positively buoyant effluent acted as a wall jet after the initial discharged area. It clung to the bottom until it reached to the next phase. The second stage of the discharge developed as a free jet and eventually climbed up to the water surface.

2.2 Previous experimental studies

2.2.1 Previous experimental studies on negatively buoyant jet

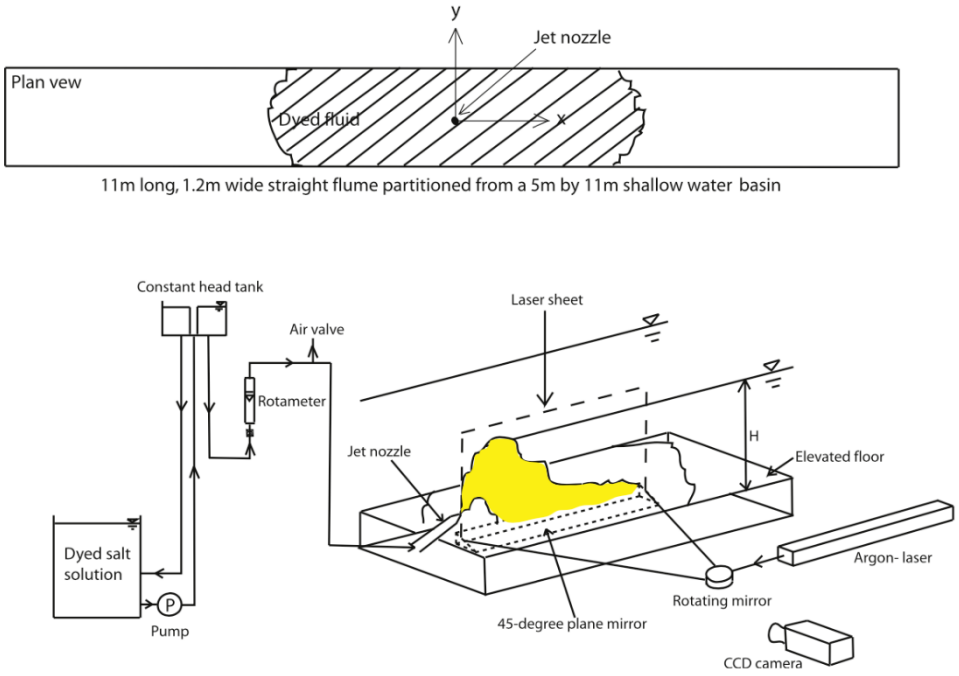

Fig 2.3.1 Experiments apparatus of Inclined dense jets discharged into steady ambient. Lai, C. C., & Lee, J. H (2012)

In 2012, inclined dense jets into a stagnant ambient were experimentally studied by Lai and Lee. The planar laser-induced fluorescence (LIF) and the Particle Image Velocimetry (PIV) methods were used during the experiments. Fig 2.3.1 shows the experimental apparatus. From their data on vertical velocity measurement, it can be observed that the mixing process is jet-like before the outfall reached to the maximum point.

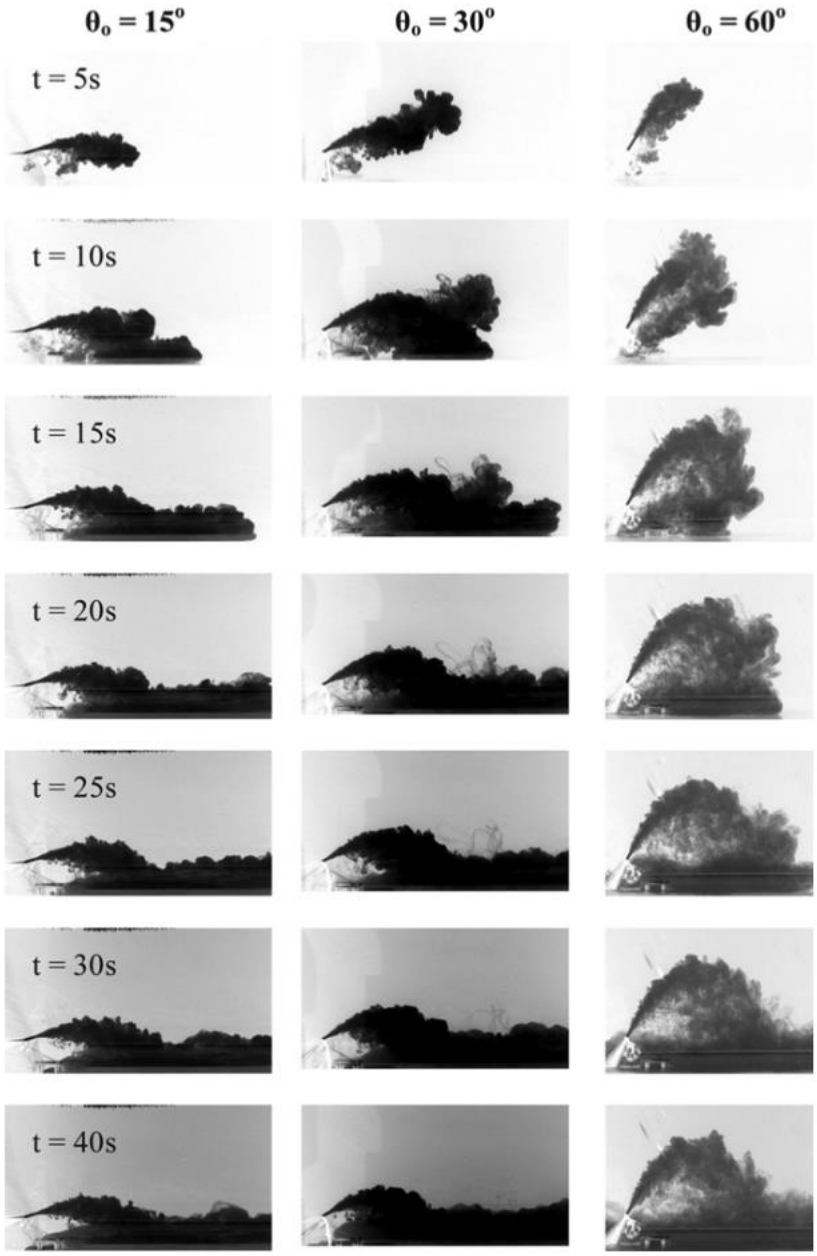

Fig.2.3.2 Inclined dense jets behavior comparisons on different angles over time with Froude number at 16.

Their tests were conducted on jets discharged at six angles (15°, 30°, 38°, 45°, 52° & 60°) , and Froude numbers were in the range of 20 to 40.

Fig.2.3.2 shows the buoyant flow transformation process with Froude number of 16 and discharge angles at 15°, 30°, 60°. From their study on image analysis and concentration data, the

jet detrainment was proved to be existed and had a crucial impact on jet with $\theta_0 > 15°$. The discharge behavior was jet-like before it arrived the highest point. The dilution difference was negligible for jets between $38°\sim60°$.

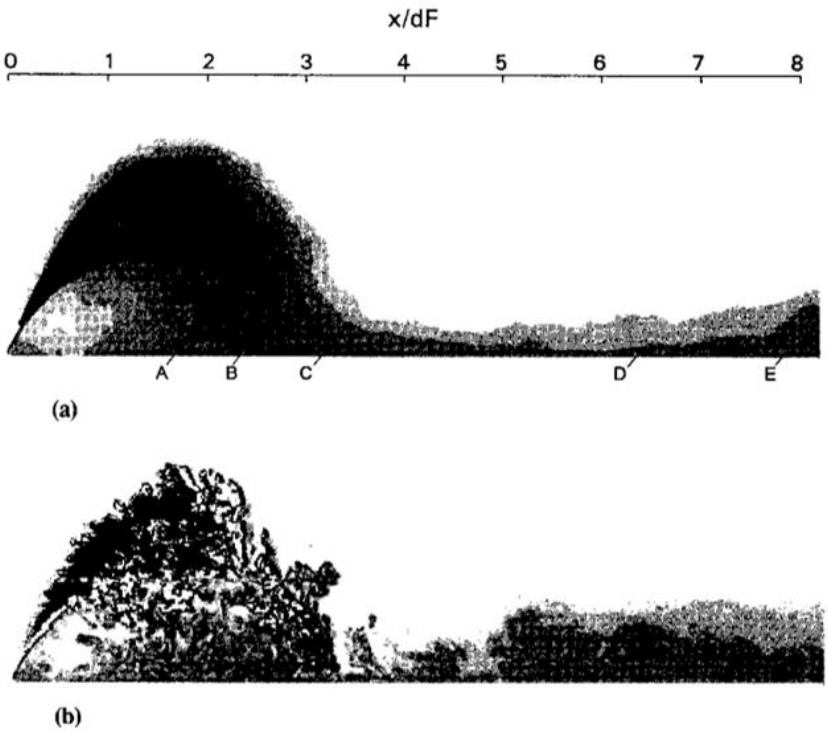

Fig.2.4.1 Laser-Induced Fluorescence Images of Dense jet (a) Time-average Image (b) Instantaneous Image. (Roberts et. al., 1997).

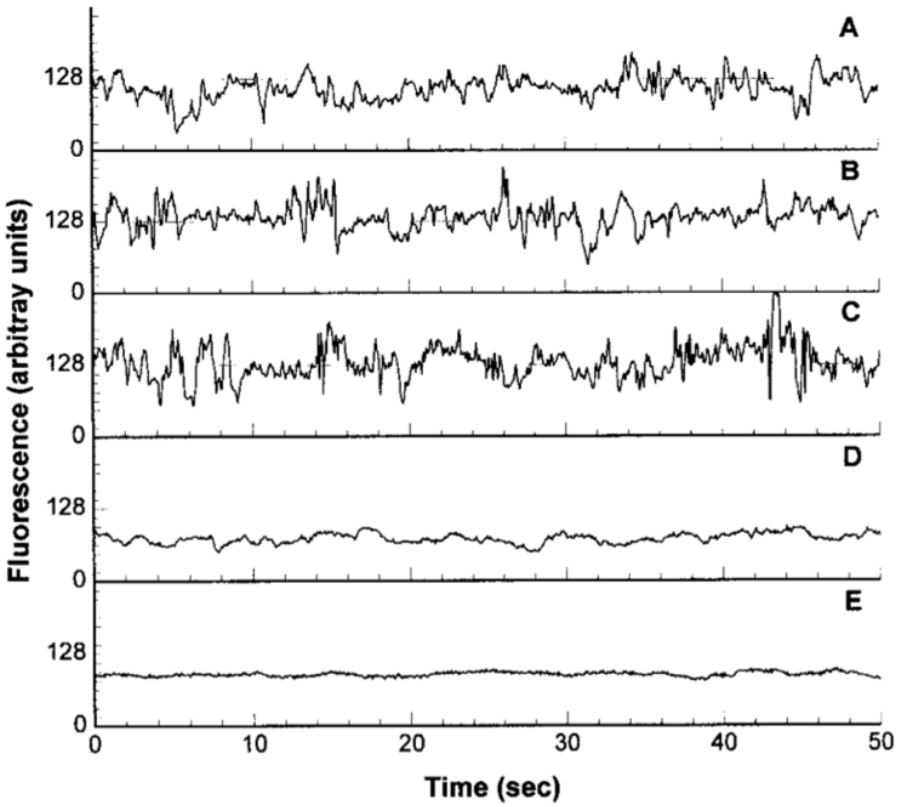

Fig. 2.4.2 Simultaneous Tracer Concentrations from locations ABCDE.

Negatively buoyant jets with upward angle at 60° discharged into still environment were inspected by Roberts et al. in 1997. They used laser-induced fluorescence (LIF) and micro-conductivity probe in the laboratory to track the jet properties. Fig.2.4.1 Shows the laser-induced fluorescence images of the dyed dense jet, the shade is related to the jet concentration level. The shade turned brighter around the impact point. Thus, dilution activity became more intense and the concentration decreased from the impact point. Fig.2.4.2 presents information of concentration variation at points A, B, C, D and E simultaneously as in Fig.2.4.1.

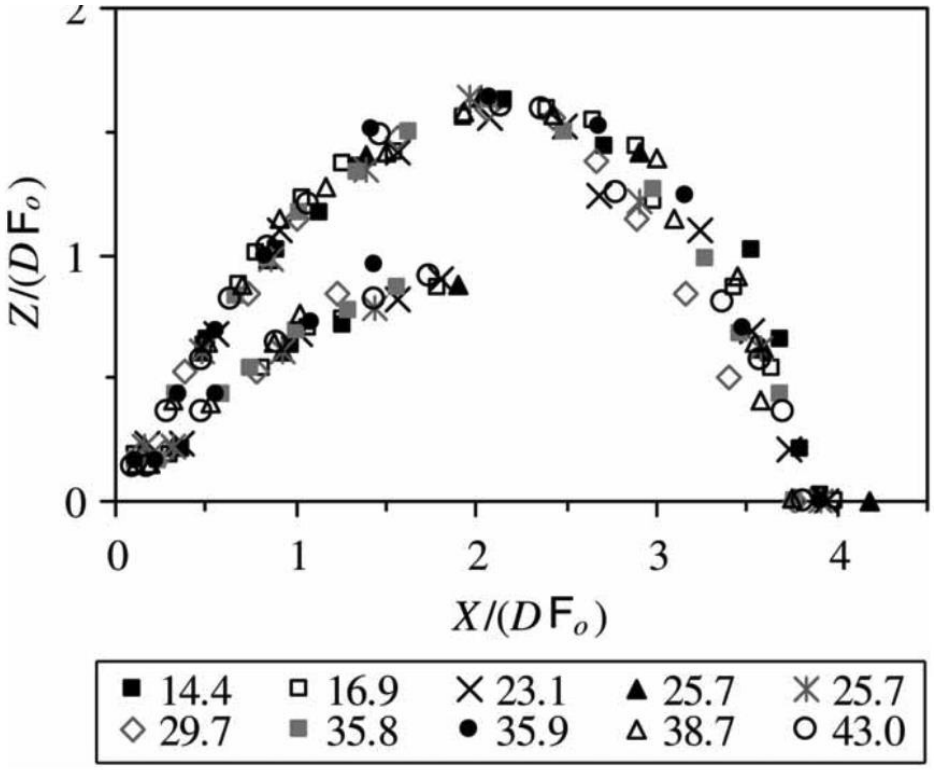

Fig.2.5 Inclined (45°) dense jets' trajectories with different Froude number (F_0 = 14.44~43)

Papakonstantis et al. (2011) also conducted experiments on submerged inclined negatively buoyant jet. Fig.2.5 indicates that with dimensionless analysis, the upper outside edge of the jets overlapped each other when they had the same discharge angle even when the Froude number varied. However, the lower edge of the jet trajectory was hard to distinguish. This may be attributed to the impact of gravity that made the jet sink immediately after the flow began.

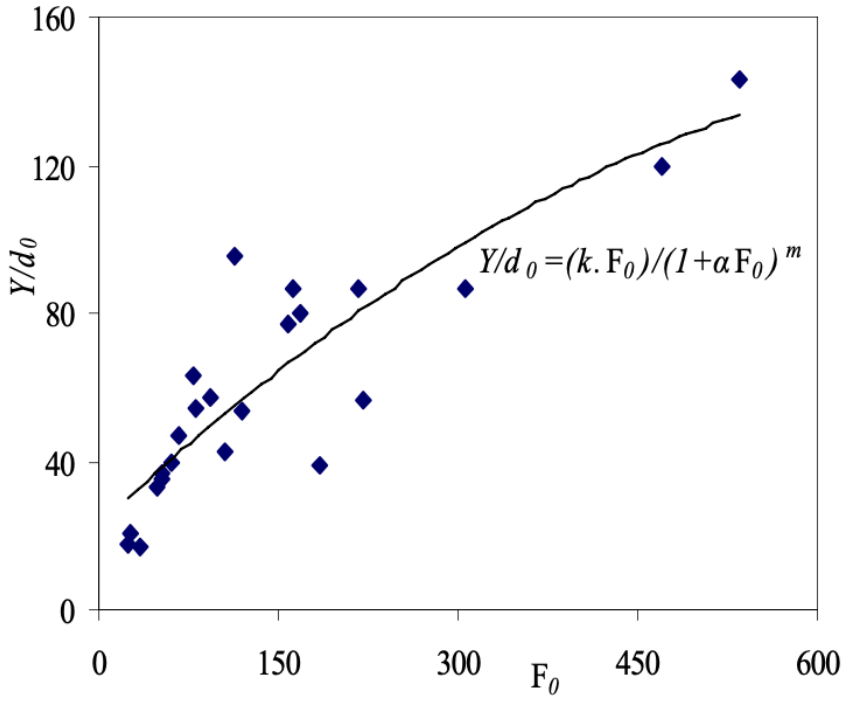

Fig. 2.6 Normalized maximum jet centerline level as a function of Froude number of jet with *30°* discharge angle. (Bashitialshaaer et al., 2013)

Experimental investigation on brine discharges were conducted by Bashitialshaaer et al. in 2013 in a tank of 150cm long, 60cm wide and 60cm high. In their study, tap water temperature ranged from 20 C° to 22 C° and density was 995.7 kg/m. The jet had higher density than the environment and it was dyed by KM_nO_4. The concentrations of the jet were set at 2%, 4% and 6%, (20 g/L, 40 g/L and 60), equivalent density values were 1011, 1024 and 1035 kg/m^3.

Experimental results obtained from Bashitialshaaer's study on inclined dense jet are shown in Fig.2.6. In Fig.2.6, d_0 is nozzle diameter, F_0 is Froude number, k and α are empirical coefficients obtained from fitting against data. With the increase of the Froude number, the jet trajectory length extended. More intense fluctuation was recorded in jets with larger Froude number than the smaller ones. From their study, the terminal rise elevation of the jet centerline was associated with the jet initial Froude number. Several equations about the jet trajectory were presented from their research. This could guide desalination plant designers to enhance the mixing based on the presented data of the effluent mixing.

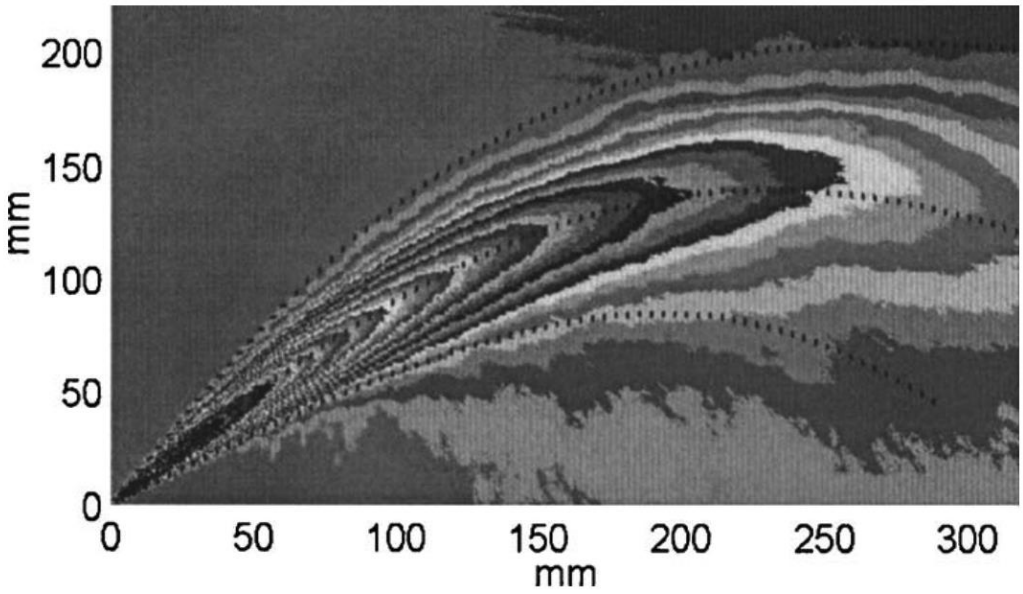

Fig. 2.7 Averaged LIF image of negatively buoyant jet in with nozzle diameter 2.45mm, discharge angle *45*° and initial Froude number 48.66.(Kikkert et al.,2007)

Kikkert et al., (2007) did experimental studies on negatively buoyant jets and tried to develop some predictive solutions analytically. Their analysis proved that the jet upper edge of terminal rise could be accurately predicted analytically for those jets which have a discharge angle between 0° to 75° and Froude number in the range of 14 to 99. However, the lower edge of jet terminal rise was not precisely predicted. (Fig.2.7)

Christodoulou et al. (2015) drew conclusions from brine effluent experiments. From their study, a correlation between discharge angles and dilution was found. For the design of brine discharge facilities, the range of 60°~ 75° angles were suggested to be used for the submerged dense jets from a deep location and the range of 30~45° was advised for the jets in shallow water to get enough dilution. The selection of outfall diameter also matters, because it affects the Froude number which contributes to the jet spreading. Indeed, the Froude number has a great influence on the impact point dilution in 20° to 30°, but this effect was negligible for jets from 30° to 75°.

2.2.2 Previous experimental studies on positively buoyant jet

Experimental studies on the dense and thermal discharges were carried by Michas et al. (2009). The initial properties are shown in Table. 2.3.

Table. 2.3 Initial settings for jet and ambient. (Michas et. al, 2009).

Type	#Runs	ρ_a(g/L)	ρ_0(g/L)	R_e	R_0
Salt water -Trajectory	15	1000.4~1001.5	1013.0~1015.0	660~4060	0.030~0.799
Type	#Runs	T_a(℃)	T_0(℃)	R_e	R_0
Hot water - Trajectory	16	14.40-14.47	53.90-59.00	1380-9060	0.041-0.841
Hot water - Temperature	27	19.0~26.30	49.30~64.70	1340~13190	0.014~0.842

The jet trajectories of saline and thermal outfalls were analysed in their study. Reynolds number for saline ones was between 660 to 4060, while for the thermal ones it was in the range of 1380 to 9060. Richardson number (a ratio of length scales L_Q and L_M) was used. The equations are written as follows.

Initial jet Richardson number R_0:

$$R_0 = \frac{L_Q}{L_M} = \left(\frac{1}{4}\right)^{\frac{1}{4}} \frac{\sqrt{g_0' d_0}}{U_0} = \left(\frac{\pi}{4}\right)^{\frac{1}{4}} {F_0}^{-1} \tag{10}$$

Where,

F_0 is initial Froude number

U_0 is jet initial velocity

d_0 is nozzle diameter

g_0 is relatively gravity acceleration

$$L_Q = \frac{Q_0}{{M_0}^{1/2}} \tag{11}$$

$$L_M = \frac{{M_0}^{3/4}}{{B_0}^{1/2}} \tag{12}$$

L_Q and L_M are characteristic length scales.

$$Q_0 = \frac{\pi {d_0}^2 U_0}{4} \tag{13}$$

$$M_0 = Q_0 U_0 \tag{14}$$

$$B_0 = {g_0}' Q_0 \tag{15}$$

$${g_0}' = \frac{\rho_a - \rho_0}{\rho_a} g \tag{16}$$

ρ_a is ambient density

ρ_0 is jet initial density

M_0 is jet initial momentum flux

B_0 is jet initial buoyancy-generated momentum flux

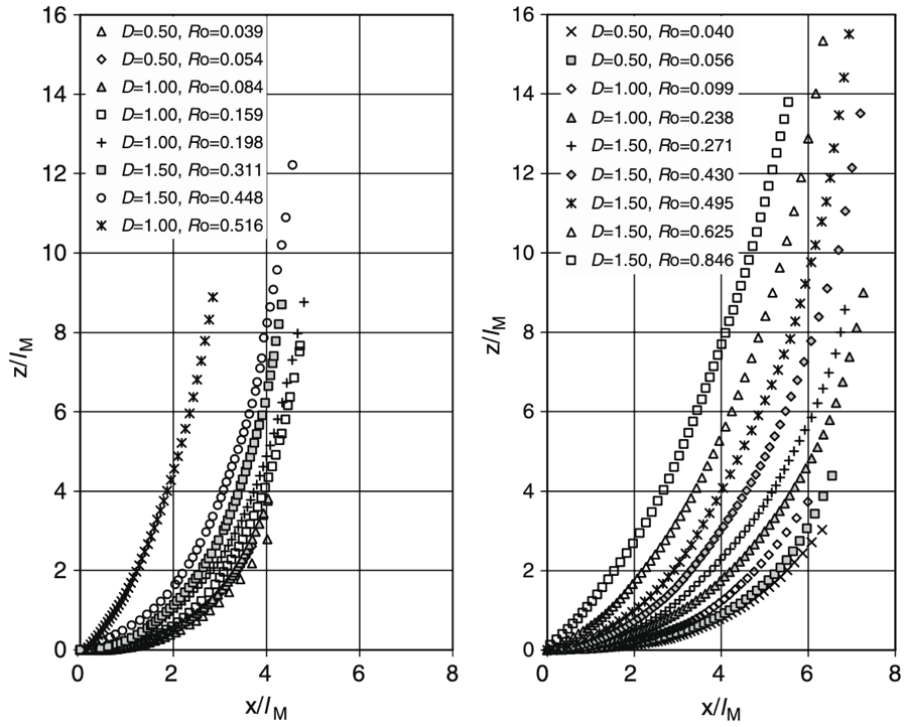

Fig.2.8 Horizontal round nozzle discharge of brine jet (left (upside down)) and thermal jet(right) at a range of initial Richardson numbers. Michas et. al (2009).

From Fig.2.8, the trajectories for brine jet and thermal jet can be distinguished. For the saline jets, the jets' trajectories were plotted upside-down in order to compare with the hot jets.

By comparing these two groups of jets, thermal jet seems to extend longer on the horizontal level than the dense jet to reach the same dimensionless vertical height Z/L_M. Initial Richardson number affects the jet effluent spreading process. Smaller nozzle diameter worked more efficient to discharge liquid to farther locations.

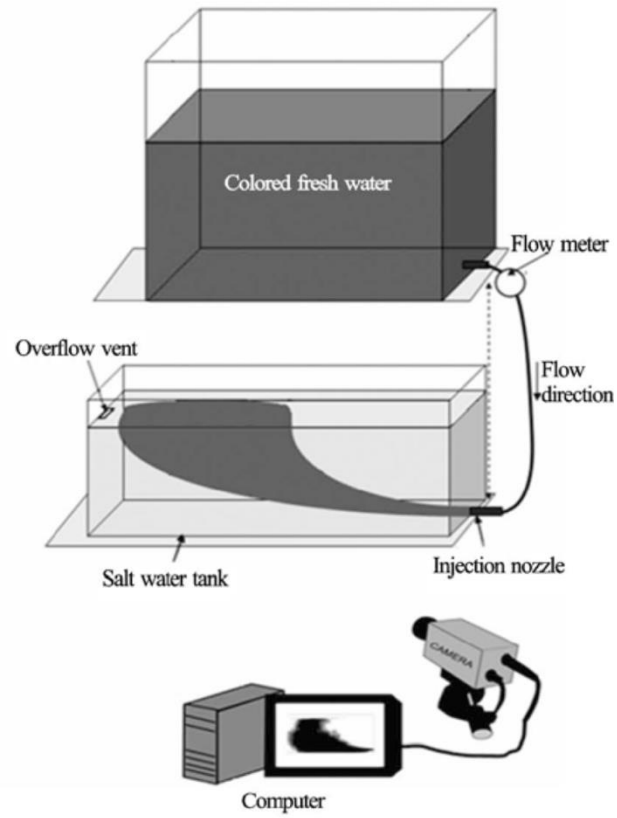

Fig.2.9.1 Experiment setup. (Belcaid et.al 2015)

Study of fresh water entering into a salty, stagnant and homogeneous environment ambient was conducted by Belcaid et al. (2015). Their experiment setup condition is shown in Fig 2.9.1. Reynolds number varied from 2000 to 6000 and Froude number was between 1 to 75.

Fig. 2.9.2 and Fig 2.9.3 reveal that the jet transformation behavior was related to the change of the salinity difference and Reynolds number. They found that the jet was mainly controlled by the buoyancy-generated momentum. For those jets that clung to the bottom with the Coanda effect, higher salinity difference contributed to longer cling length. The jet radius and spreading had a linear correlation with the Froude number. Thus, the larger the Froude number was, the more efficient the jet was diluted.

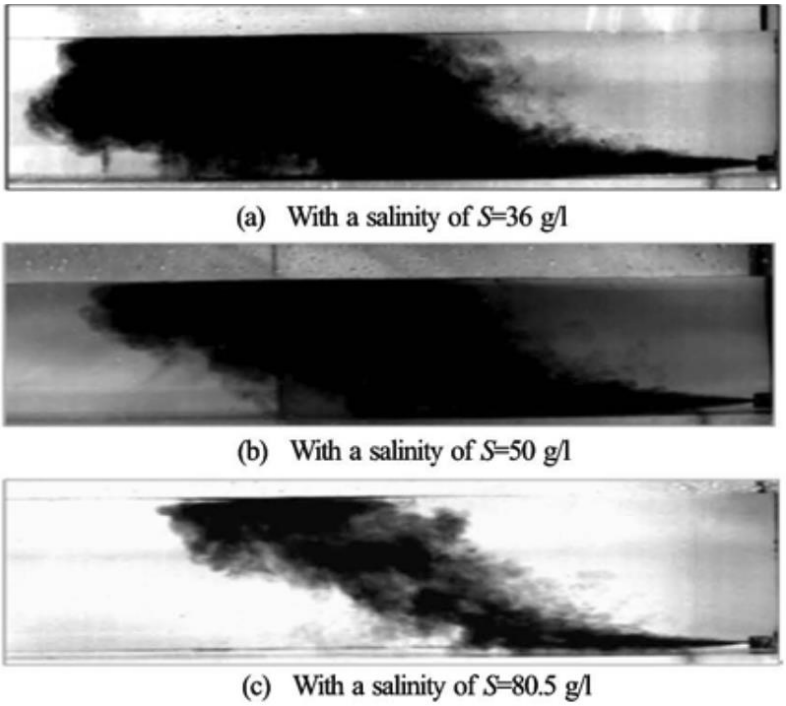

Fig. 2.9.2 Comparison of jets performance with Re=7500 into the ambient of various salinity(a)(b)(c). (Belcaid et.al 2015)

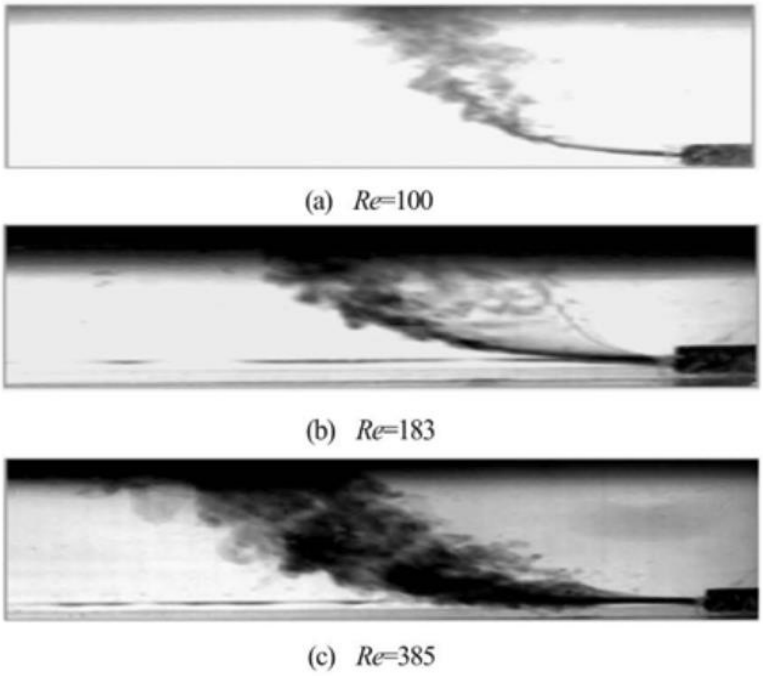

Fig. 2.9.3 Comparison of jets performance at different Reynolds numbers (a)(b)(c). (Belcaid et.al 2015)

2.3 Previous numerical studies

2.3.1 Previous numerical studies on negatively buoyant jet

An accurate description and prediction of outfall behavior is always needed. With the development of computer technology, the numerical simulation which requires intensive calculations became very popular and was extensively employed during the past two decades.

Computational Fluid Dynamics (CFD) is a technique that uses numerical approaches to solve and predict problems of fluid flows. CFD was initially explored as an alternative method to substitute the large-scale, and costly experiments in aerospace domain. With the comprehensive improvement of CFD technology, it became widely implemented on the jet study in both academic and industrial fields.

OpenFOAM, a free, opensource approach is widely adopted on numerical simulations of the effluent discharge. It is based on past experiences that the mesh density and the selection of turbulence models mostly determine the accuracy and the reliability of modeling results in OpenFOAM. However, it is impractical to always use high-resolution meshes due to the huge computational demand. Finer mesh sizes in near-outfall zone are generally suggested and relatively coarse meshes can be used in the zones farther away. According to earlier studies, several turbulence models have been validated with good outcomes on different fluid flow cases. These models are widely used in jet investigation: Standard k-ε model, Reliable k-ε model, Launder-Reece-Rodi (LRR) model, Reynolds-Averaged Navier-Stokes (RANS) model and Large Eddy Simulations (LES) model etc.

Vafeiadou et al. (2005) were the pioneers to study and predict jet properties using CFD method. This study concentrated on brine jets that flow out from an inclined nozzle into a quiescent ambient. They employed the k-ε model and the Shear Stress Transport (SST) model in ANSYS CFX. The results in their 3-D simulation were consistent with the experimental data from Bloomfield et. al (2002).

Table. 2.4 Numerical cases parameters. (Gildeh et. al, 2015)

Test#	Inclined angle θ	Inlet Diameter (mm)	Initial inlet height y_0(mm)	$\Delta\rho_0/\rho_a$ (mm)	Discharge velocity U_0 (m/s)	Temperature difference ΔT(℃)	Densimetric Froude # F_d	Jet to plume characteristic length scale L_m(mm)	Bed proximity parameter y_0/L_m
1	30°	6.5	11.17	1.984	1.000	0.5	28.10	172.00	0.065
2	30°	6.5	11.17	0.995	0.531	1.5	21.10	129.00	0.086
3	30°	6.5	11.17	1.984	0.356	1.0	10.00	61.00	0.180
4	45°	6.5	12.92	1.984	1.173	0.5	23.30	193.00	0.070
5	45°	6.5	12.92	0.995	0.515	1.5	21.30	120.00	0.108
6	45°	6.5	12.92	1.984	0.345	1.0	10.00	57.00	0.228

Numerical experiments in OpenFOAM on inclined dense jet (angles at 30° and 45°) discharged into still water surroundings were operated by Gildeh et al. (2015). The primary objective of this study was to find out the relation between the selection of turbulence models and the jet activities in simulations. Five RANS models were hired in comparison: the LRR model, the RNG k-ε model, the reliable k-ε model, the nonlinear k-ε model, the Launder-Gibson Reynolds stress model. These five models were applied in 6 cases. Table. 2.4 shows the parameters that considered in these cases.

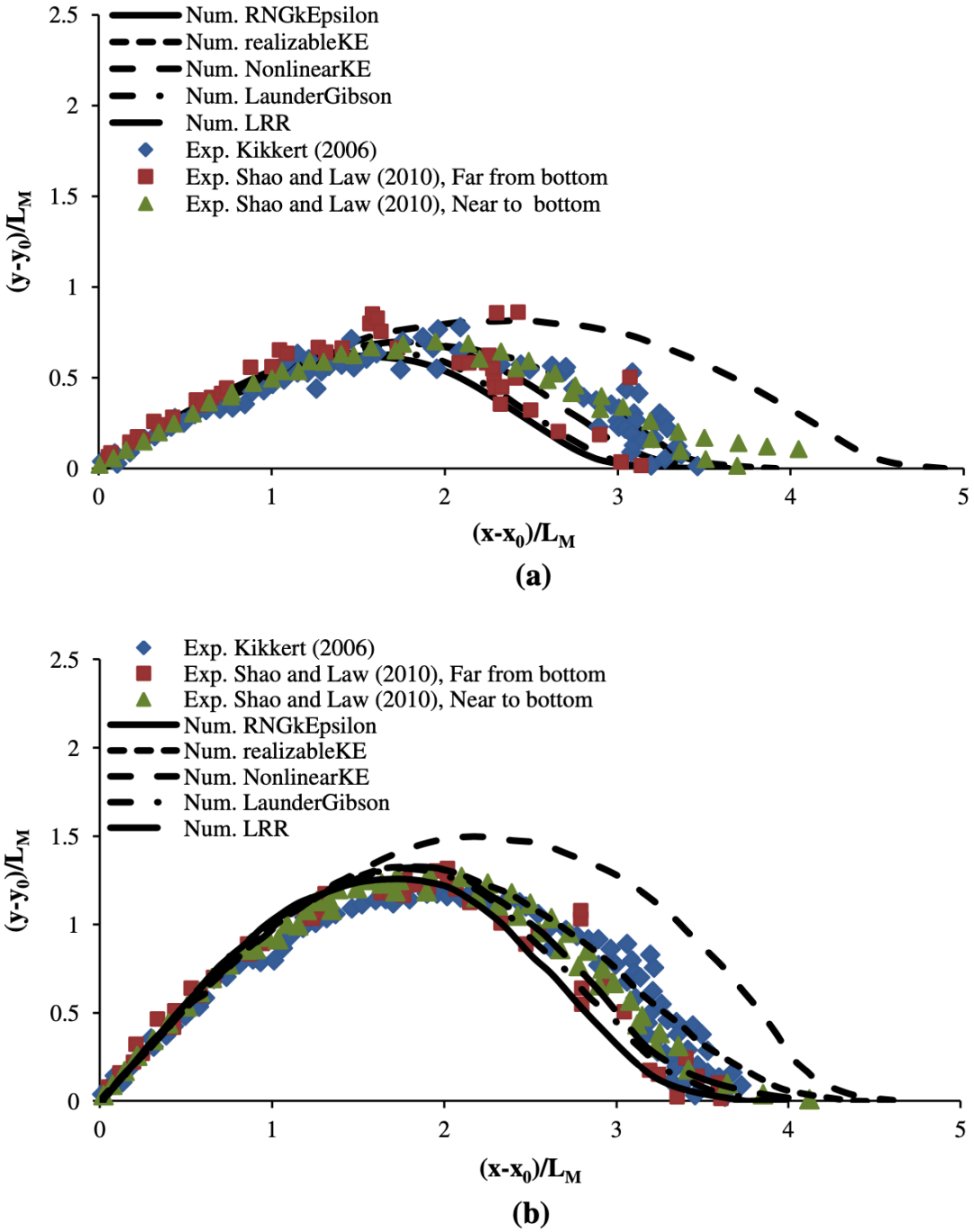

Fig. 2.10 Normalized jet trajectories (a) 30°, Froude number at 28.10 (b) 45°, Froude number at 34.30. (Gildeh et. al, 2015)

The trajectory centerlines of numerical results in this study matched the experimental data from Shao et. al (2010). Fig. 2.10 shows the normalized trajectory comparison under the

aforementioned turbulence models and Shao's physical experiments. Figure 2.10(a) and Figure 2.10(b) represent the jet centerline path for 30° and 45°. In both groups, the reliable k-ε model developed the longest trajectory compared to others. The RNG k-ε model underestimated the centerline data in the latter stage after the jet arrived at the maximum rise height. In both groups, results from Reliable k-ε model and Nonlinear k-ε model were overpredicted. LRR and Launder-Gibson model performed better in the comparisons.

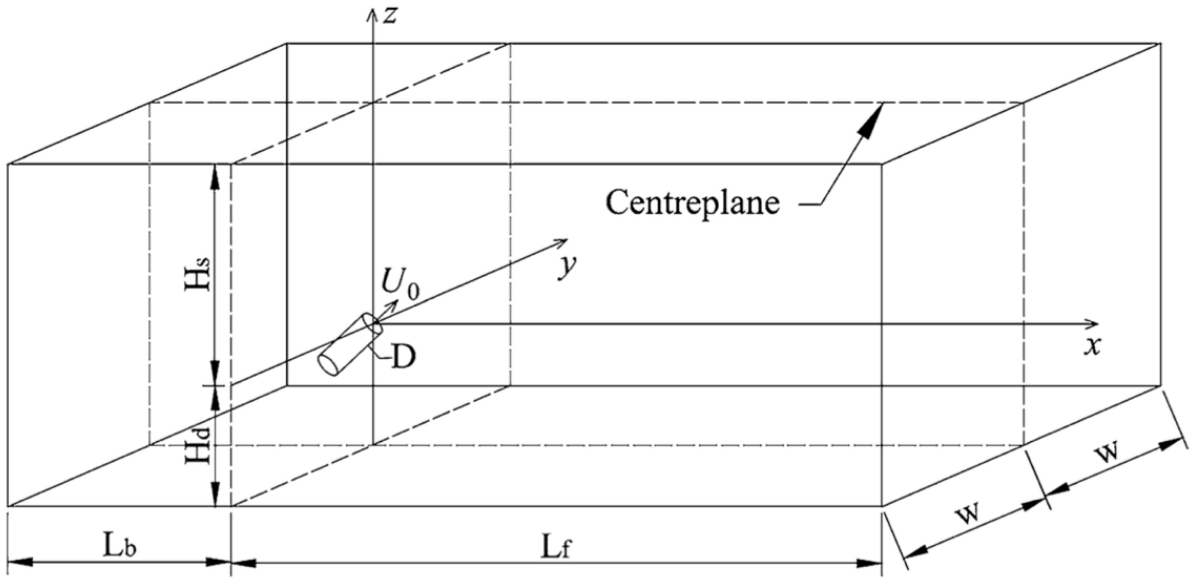

Fig. 2.11.1 Computational domain for inclined (45°) dense jet. (Zhang et.al 2016)

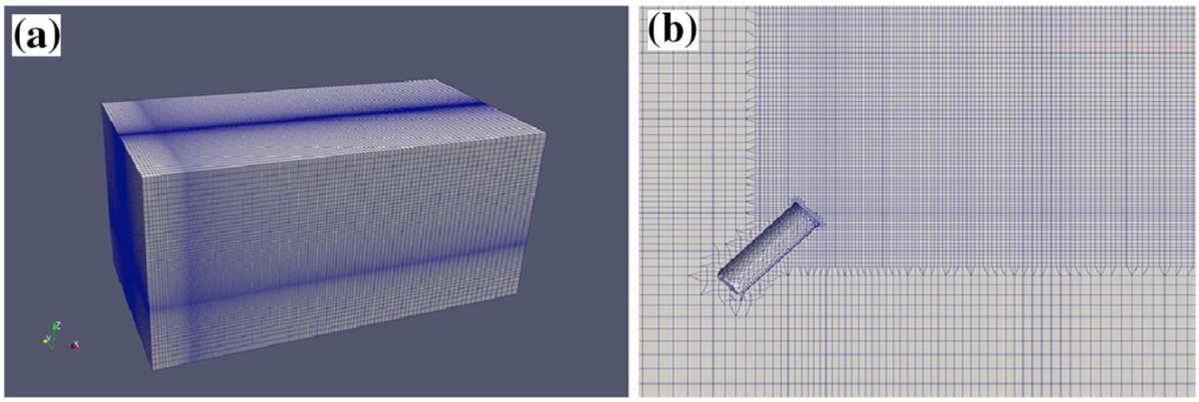

Fig. 2.11.2 Refined mesh scheme in OpenFOAM. (Zhang et.al 2016)

Zhang et.al (2016) made use of OpenFOAM to investigate the inclined (45°) dense jet problems

numerically. Fig. 2.11.1 shows the domain of this experiment, the nozzle was submerged in the middle plane between the front and the back walls. In this research, Smagorinsky and Dynamic Smagorinsky (SGS) models were used in the large eddy simulations (LES). SnappyHexMesh was used to build the refined mesh as shown in Fig. 2.11.2.

Fig. 2.11.3 demonstrates a typical example of concentration contour for inclined (45°) buoyant jet in this study. The dilution process and the jet path can be understood visually. By comparing with experimental data in the same task and from previous related studies, the LES simulations were found to be a reliable way for modeling the jet movement. Fig. 2.11.4 shows a comparison of jet trajectory experimentally and numerically.

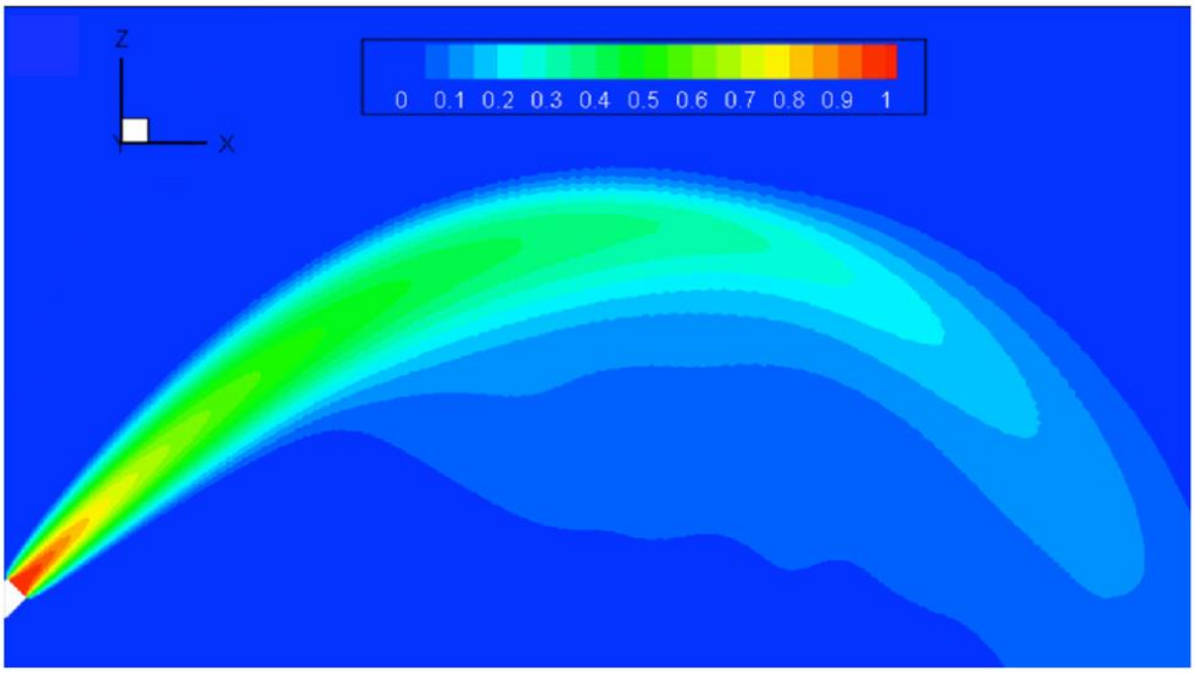

Fig 2.11.3 Dimensionless brine jet (45°) concentration distribution in numerical study. (Zhang et.al 2016)

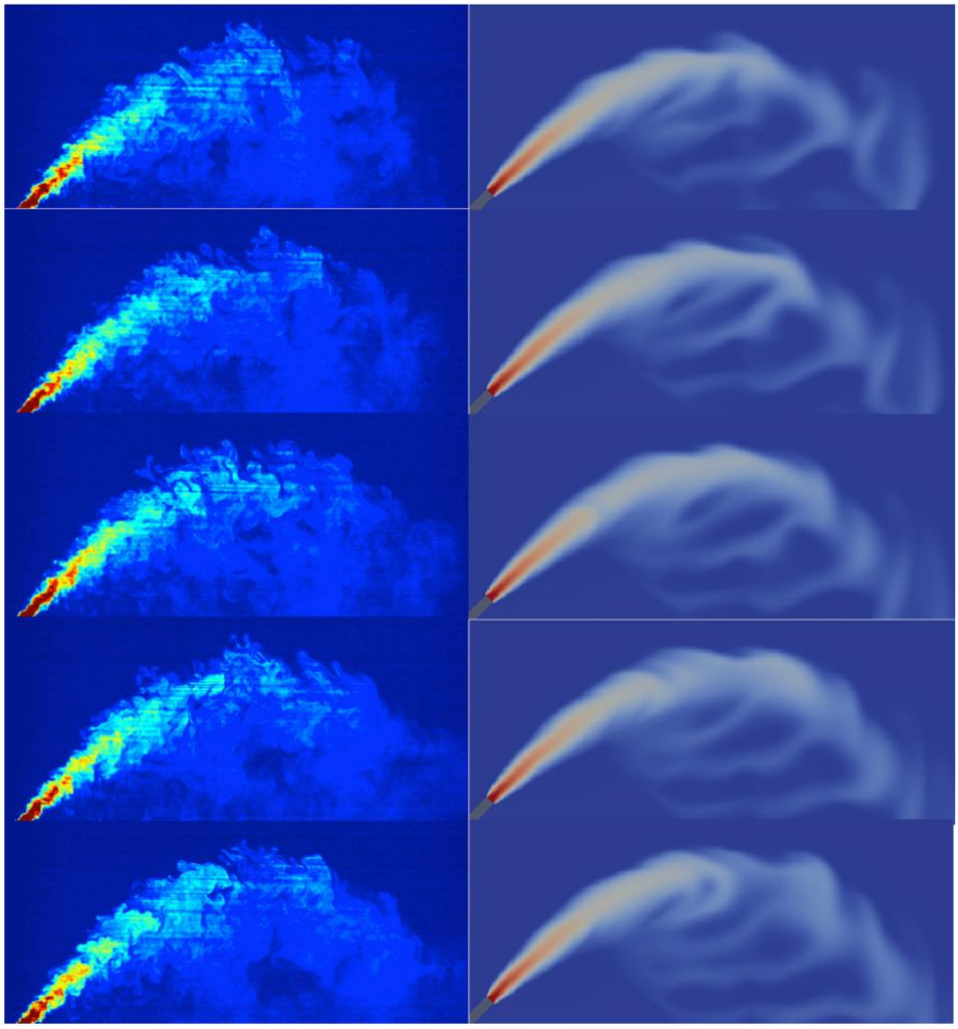

Fig 2.11.4 Jet performance comparison between experimental result (Left) and LES modeling (Right). (Zhang et.al 2016)

2.3.2 Previous numerical studies on positively buoyant jet

Numerical studies on the positively buoyant jets are limited. These jets are not studied as widely as the negatively buoyant jets. However, problems related to the positively buoyant jets commonly emerge near some desalination outlets and the area adjacent to the cooling water outfalls. Thus, investigation on the mixing properties under such conditions is necessary.

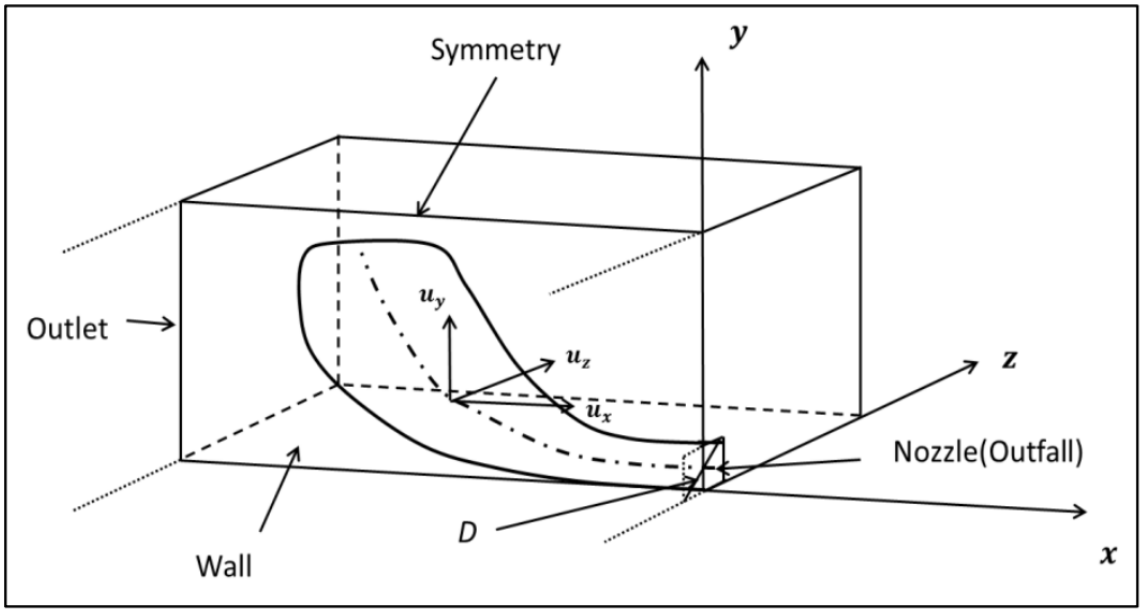

Fig. 2.12 Overview of the symmetric numerical domain. (Alfaifi et. al, 2015)

Alfaifi et. al (2015) conducted research of thermal buoyant wall jet that was horizontally discharged into a calm and uniform environment from a submerged diffuser. In this study, the simulation domain was half of the full domain because the jet was symmetric by the middle plane where the nozzle was located. Froude number as a key factor of the study was set to 10 and 15. In OpenFOAM, Alfaifi chose the Reliable k-ε model and LRR model for calculation. The jet trajectories in these four scenarios are presented in the Fig. 2.13. By analyzing these graphs, we can observe that these two RANS models can both predict the jet behaviors in similar background, but the LRR model is slightly better in performance than the k-ε model. Here, larger Froude number played a role in extending the jet trajectories to longer distances.

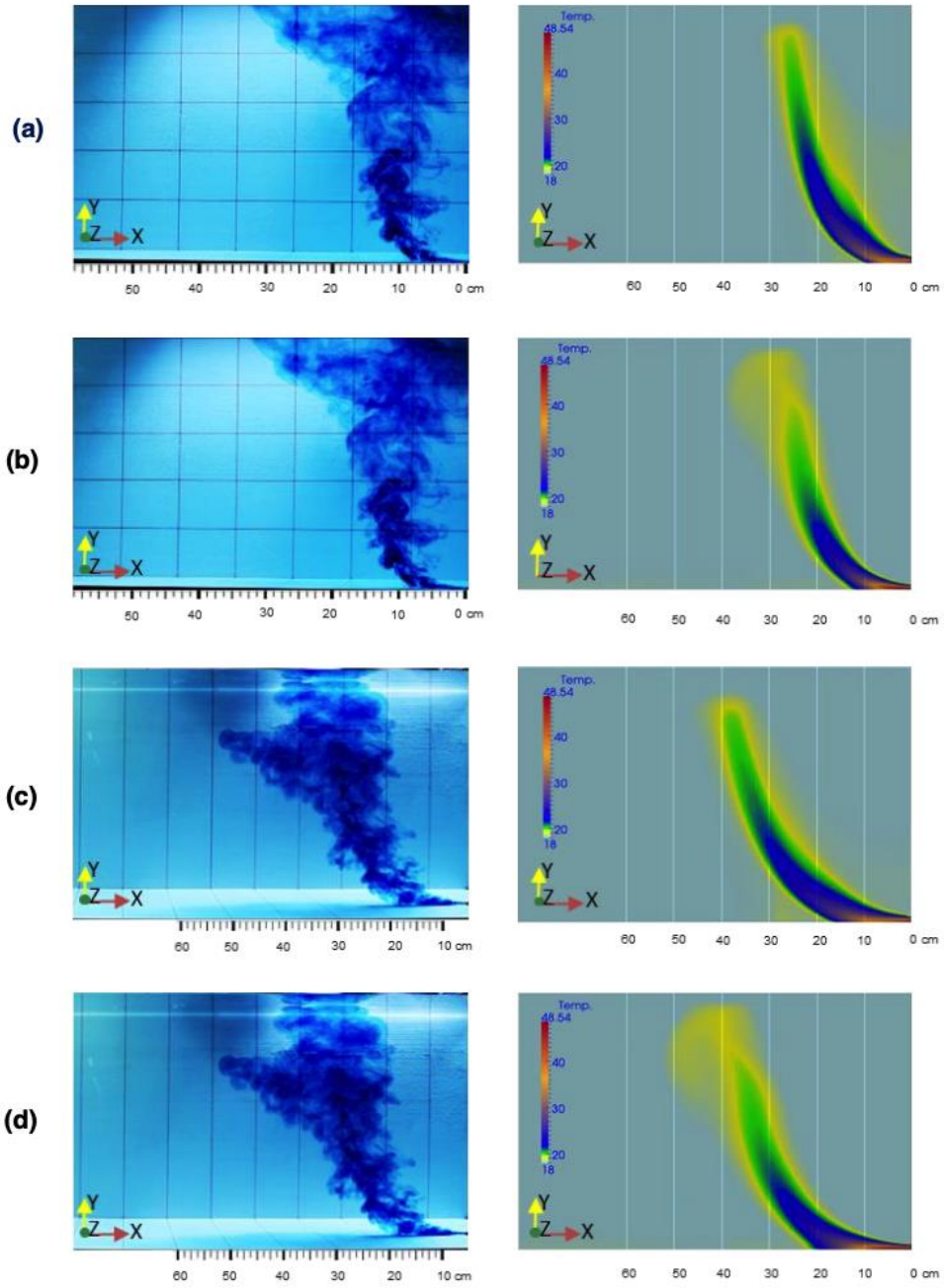

Fig. 2.13 Jet trajectory comparison between different models and Froude numbers in experiments (left) and simulations (right). (a) Reliable k-ε, Froude number at 10 (b) LRR, Froude number at 10 (c) Reliable k-ε, Froude number at 15 (d) LRR, Froude number at 15

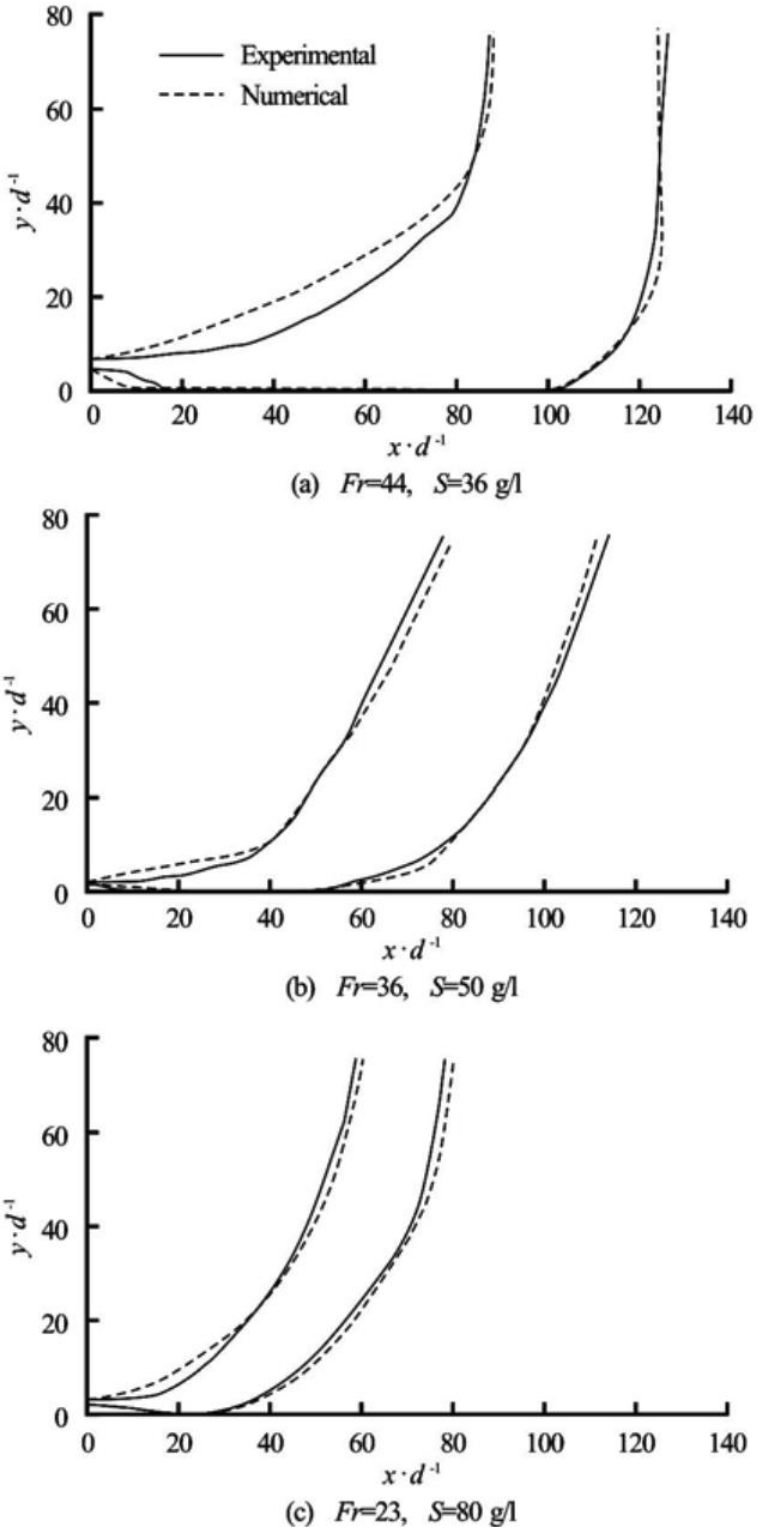

Fig. 2.14 Comparison of Jet upper and lower boundaries in experiments and simulations, initial velocity at 1.31m/s, Reynolds number at 5700. (Belcaid et. al, 2015).

Belcaid et. al (2015) inspected the dynamic characteristics of horizontal wall jet with fresh water discharged into the still salty homogenous ambient both in the laboratory and by CFD. They used the standard k-ε model in the OpenFOAM for simulation. Fig. 2.14 provides three groups of their experiments and related numerical results. Although the Froude numbers and salinity varies among groups, the simulations were consistent with experimental data.

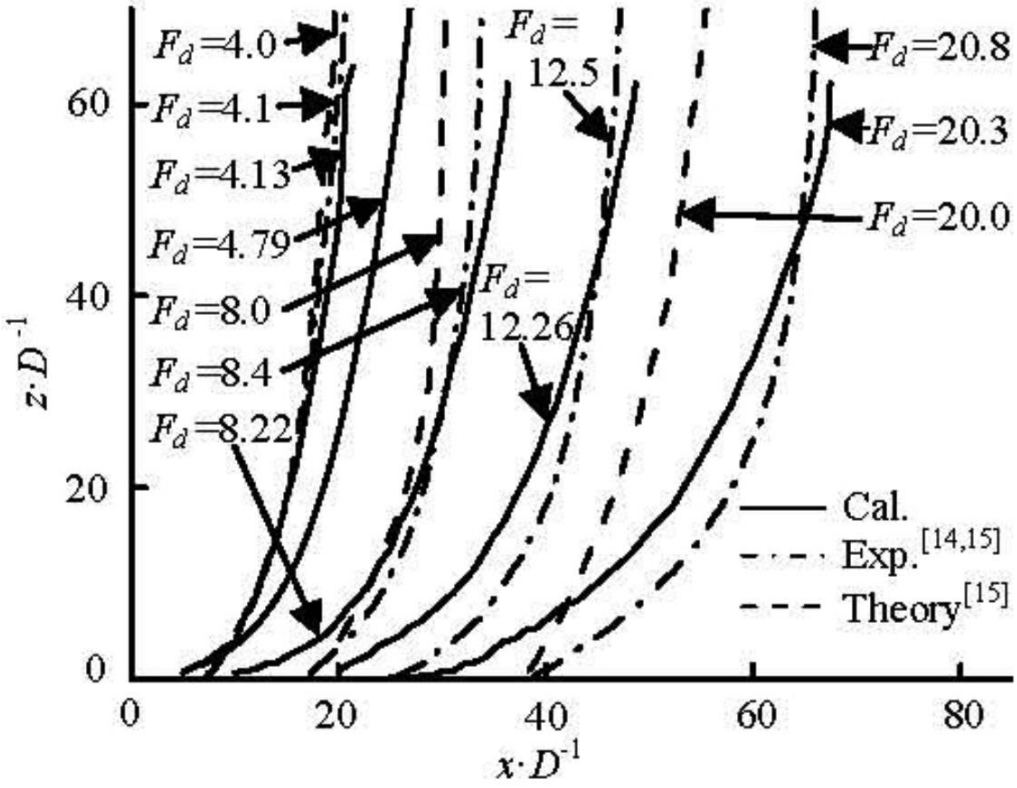

Fig. 2.15 Jet centerline comparison between experiments, simulations and mathematical approaches. (Huai et. al, 2010)

Fig.2.15 displays the numerical simulations by Huai et. al (2010) that employed Realizable k-ε model for the simulation of buoyant wall jet with a range of Froude umbers. The lines reveal that the jet travels longer with the increase of Froude number. The data in Realizable k-ε model was very close to the experimental results. Thus, the Realizable k-ε model was found to be applicable to predict positively buoyant wall jets.

Chapter 3 Experimental study

3.1 Experiment objectives

Submerged outfall systems are employed to discharge the treated or untreated liquid into ambient waters in an efficient way that enhances the mixing.

In this project, the primary objective of experiments was to study the behaviour of a submerged inclined jet from a round nozzle with an angle downward into calm homogeneous saline ambient. A series of laboratory experiments have been designed in this project to study the positively buoyant jets' behaviors under the same temperature but different jet velocities and density differences.

3.2 Apparatus and experiment procedure

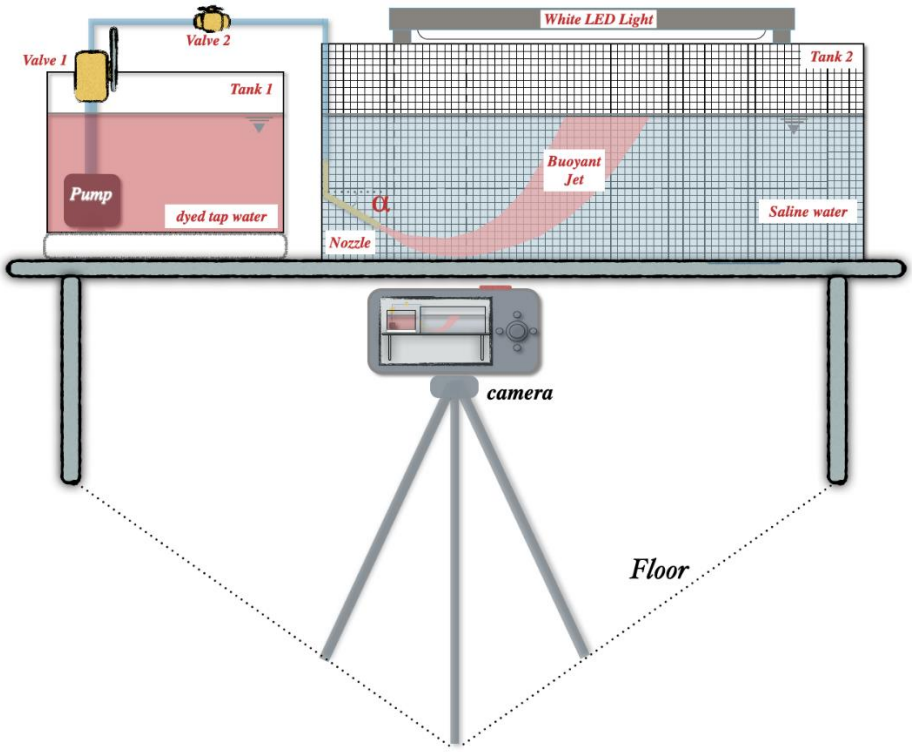

(a)

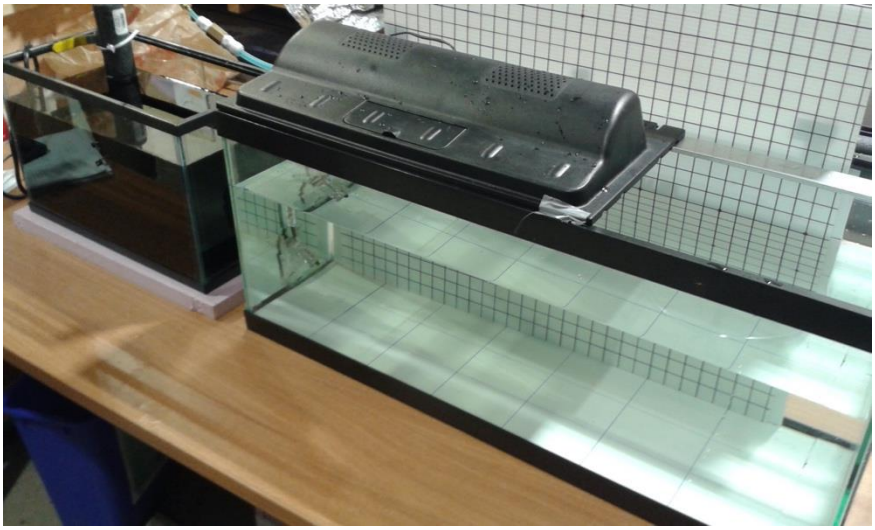

(b)

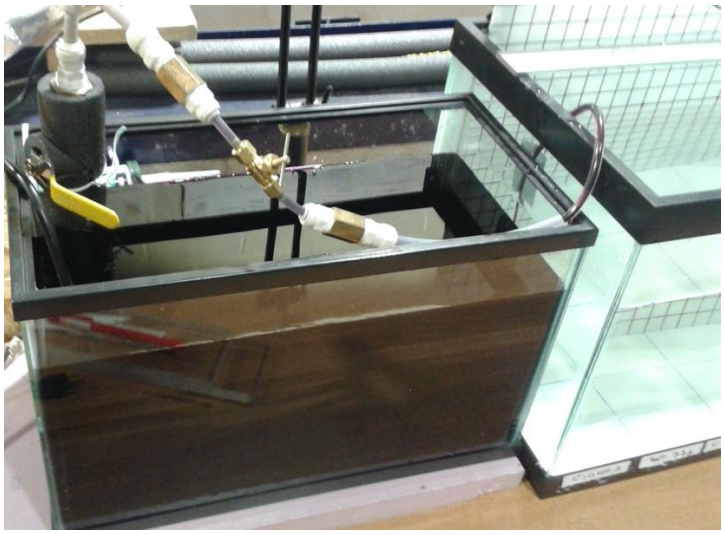

(c)

Figure. 3.1 Experimental Apparatus of submerged buoyant jet discharged into stagnant saline ambient (a) Schematic (b) Jet tank (c) Discharge tank.

The experiments were carried out at the Water Resources Laboratory of the University of Ottawa in two rectangular tanks, which were connected together by a transparent hose.

The jet was discharged from the left small tank (tank 1) with tap water into the right large tank (tank 2) of salted water, which simulated the positive buoyant jet released to higher salinity surrounding. The technique applied in this experiment was based on the image analysis system that extracted the dyed jet trajectory data by using the videos and image records in the camera.

Food coloring was used in tank 1 as tracer for the jet. Over the tank, a white LED light was placed. A plastic board with a 2cm-by-2cm mesh was attached to the back wall, a 10cm by 10cm grid marked plastic board was located on the bottom. An electric pump was immersed in tank 1 provided the energy and delivered the fluid, controlled by a ball valve - valve 1. A check valve (non-return valve) – Valve 2 was used for adjusting the flux and velocity through the nozzle.

The tank 2 was 0.75m long, 0.3m wide and 0.3m high. Connected with water pipe from tank 1, jet nozzle was positioned at the middle in the transverse direction in tank 2, within homogeneous environment. In this way, the flow would act symmetrically across the width. All movements were recorded by a digital video camera which was located parallel to the tank 2, 3.5 meters away, far enough for the parallax to be ignored.

In this project, three main parameters were studied, density difference, outflow velocity and discharge angle. Jet density is a variable dependent on salinity and jet initial temperature. In this study, all experiments were operated under the same temperature, removing the effects of temperature, thus the salinity became the only factor. For the salt, 99.99% $NaCl$ was chosen and mixed with tap water to get the optimum salinity. The density is linked to salinity and temperature based on the following equations:

$$\rho = f(S,T) \tag{17}$$

$$A = 8.24493 \times 10^{-1} - 4.0899 \times 10^{-3}T + 7.6438 \times 10^{-5}T^2 \\ -8.2467 \times 10^{-7}T^3 + 5.3875 \times 10^{-9}T^4 \tag{18}$$

$$B = -5.72466 \times 10^{-3} + 1.0227 \times 10^{-4}T - 1.6546 \times 10^{-6}T^2 \tag{19}$$

$$C = 4.8314 \times 10^{-4} \tag{20}$$

$$\rho = \rho_t + AS + BS^{3/2} + CS \tag{21}$$

$$\rho_t = 999.842594 + 6.793952 \times 10^{-2}T - 9.095290 \times 10^{-3}T^2 \\ +1.001685 \times 10^{-4}T^3 - 1.120083 \times 10^{-6}T^4 + 6.536336 \times 10^{-9}T^5 \tag{22}$$

where

S: Salinity

T: jet initial temperature, T=18.8℃

ρ: ambient density, kg/m^3

ρ_t : density of water at temperature T, in this project ρ_t is jet initial density, $\mathrm{kg/m^3}$

(equation of ρ_t was published in British Journal of Applied Physics, by Bigg et. al, 1967).

According to previous studies, is was numerically found that, with stable initial velocity, temperature and a settled outfall nozzle diameter, the initial jet density could be directly represented by a simple character— (densimetric) Froude number with stable initial velocity and same outfall nozzle diameter.

$$F_d = \frac{U_0}{\sqrt{g'D}} \tag{23}$$

$$g' = g\frac{\rho_a - \rho_0}{\rho_0} \tag{24}$$

where

D : outfall nozzle diameter, m

U_0: jet initial velocity, m/s

ρ_0 : jet initial density, jet is tap water, $\rho_0 = 1000\, kg/m^3$

ρ_a : ambient water density, kg/m^3

F_d : (densimetric) Froude number

g : gravitational acceleration, $g = 9.81\, m/s^2$

g' : reduced gravitational acceleration

$$\rho_a = \frac{m_a}{V_a} = \frac{m_s + \rho V_a}{V_a} \tag{25}$$

$$m_s = \frac{\rho_0\, g\, V_a\, {U_0}^2}{{F_d}^2\, D} \tag{26}$$

$$S = \frac{g\ salt}{kg\ sea\ water} \tag{27}$$

$$\frac{g'}{g} = \frac{\rho_a - \rho_0}{\rho_0} = \frac{m_s}{m_0} \tag{28}$$

$$V_a = L \times W \times H \tag{29}$$

Where

V_a : Volume of saline liquid body in tank 2, length L=0.74m, wide W=0.3m, height H=0.2m, $V_a = 0.045 m^3$.

m_0: Water weight, kg

m_s: Salt (99% NaCl) weight, kg.

Experiments were conducted for various nozzle angles (-30°, -60°), jet velocity (0.2m/s, 0.4m/s, 0.6m/s), and Froude Number (10, 20, 30, 50, 100). For every single experiment, the Salt weight was measured according to Table 3.1

Table 3.1 Salt weight m_s of experiments under different U_0 and F_d

m_s (g)	$F_d = 10$	$F_d = 20$	$F_d = 30$	$F_d = 50$	F_d =100
U_0=0.2m/s	0.465	0.116	0.052	0.019	0.005
U_0=0.41m/s	1.920	0.480	0.213	0.077	0.019
U_0=0.6m/s	4.197	1.049	0.466	0.168	0.142

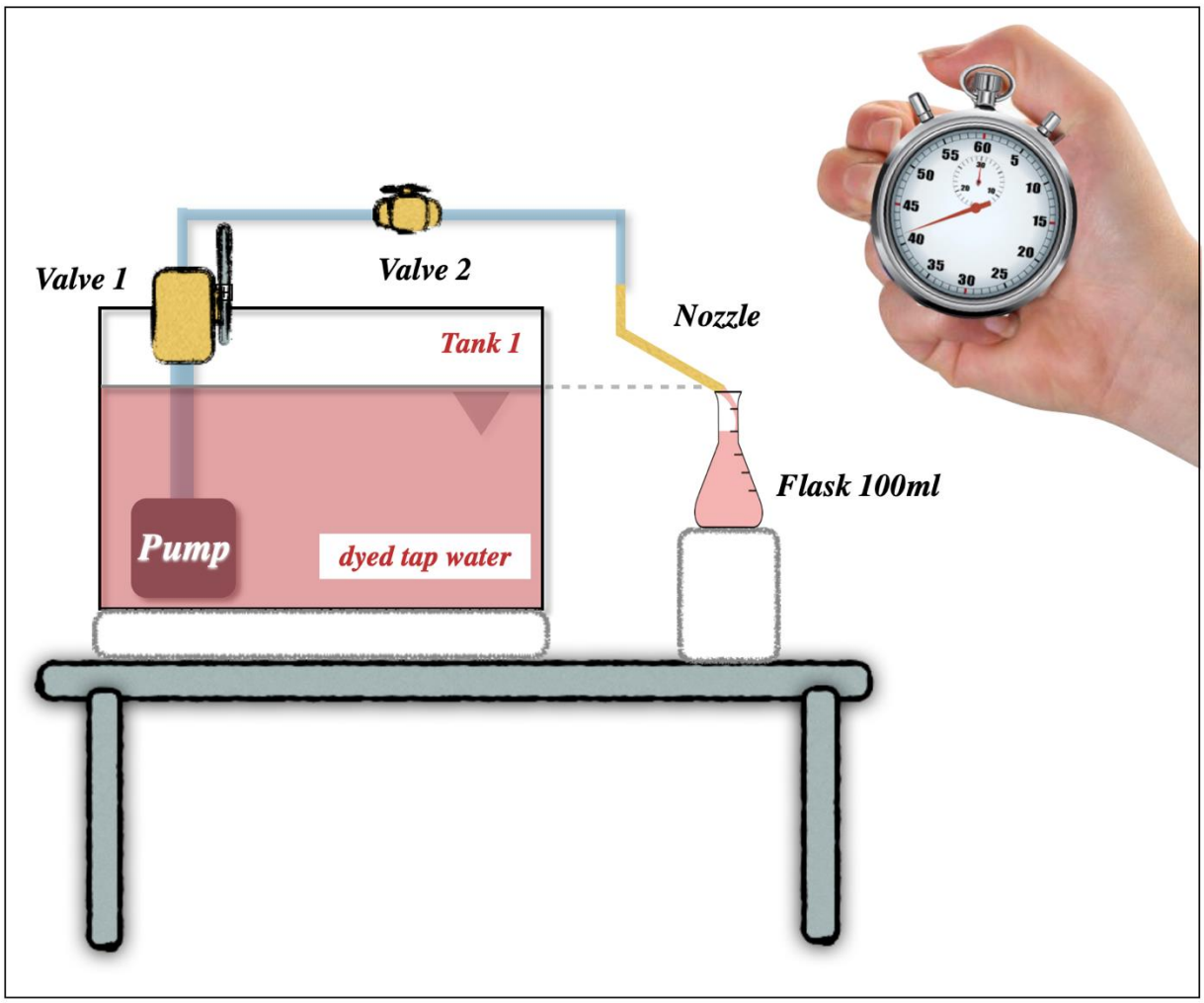

Fig. 3.2 Nozzle velocity measurement.

Round nozzle diameter was measured by vernier scale, the average result after 5 measurements was 3.929mm. Jet velocity was adjusted by calculating the time that needs to fill a 100ml graduated flask. The nozzle was placed at the same elevation as water surface in Tank 1 to avoid being affected by water depth and velocity. As shown in Fig. 3.2, valve 1 controlled the pump under the water and valve 2 worked as an accurate adjuster to refine nozzle velocity. With the coordination of a stopwatch, the most precise position for valve 2 would be obtained after several trails. Delicate adjustment for Value 2 was needed to get the desirable result. (Table. 3.2)

$$t = \frac{V}{Q} \tag{30}$$

$$Q = \frac{\pi}{4} D^2 U \tag{31}$$

where

Q: discharge flow rate, m^3/s.

U: fluid velocity from nozzle, m/s.

D: nozzle diameter, $D = 0.003929m$, measured by a varnier caliper.

Fig. 3.3 Nozzle diameter measurement.

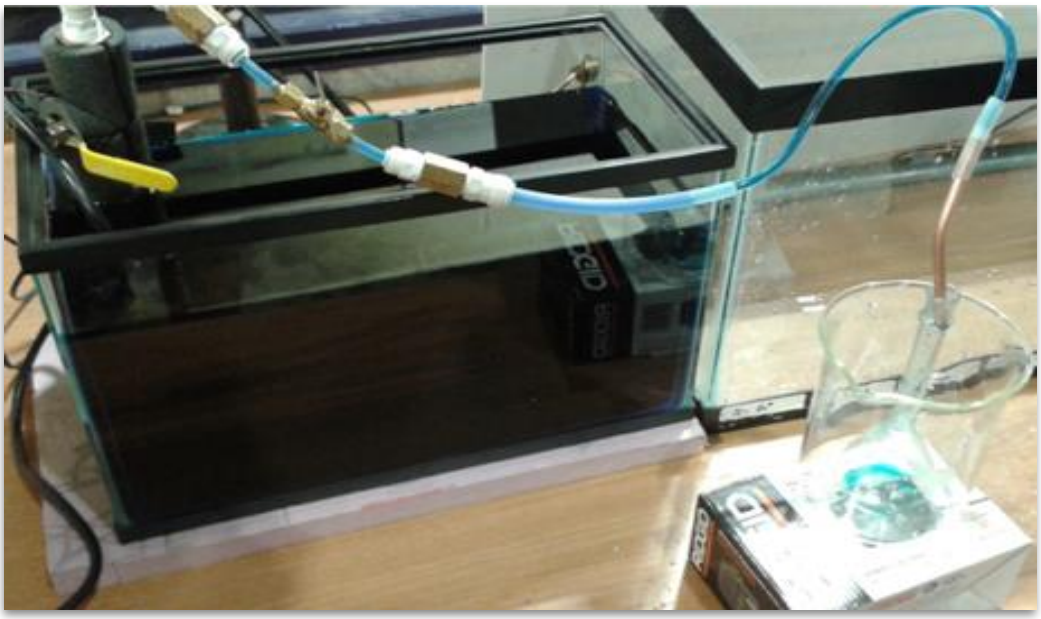

Figure 3.4 Jet velocity measurement.

Table 3.2 velocity measurement record.

	Record Time(s)	Average Time	Jet Velocity(m/s)
Velocity 1	41.60	41.34	0.2
	41.43		
	41.44		
Velocity 2	20.40	20.35	0.41
	20.31		
	20.33		
Velocity 3	13.66	13.76	0.6
	13.75		
	13.38		

3.3 Experiment results and discussion

In this study the positive buoyant jet was discharged through a downward angle, to analyse the trajectory in different settings in a dimensionless way. The momentum length scale L_M and discharge length scale L_Q are defined as (Fisher et al, 1979),

$$L_M = \frac{{M_0}^{3/4}}{{B_0}^{1/2}} \tag{32}$$

$$L_Q = \frac{Q_0}{{M_0}^{1/2}} \tag{33}$$

Where,

B_0: initial buoyancy flux

M_0: initial kinematic momentum flux

Q_0: initial volume flux

$$Mo = \frac{\pi}{4} D^2 {U_0}^2 \tag{34}$$

$$B_0 = g' Q_0 \tag{35}$$

$$Q_0 = \frac{\pi}{4} D^2 U_0 \tag{36}$$

$$L_Q = D\sqrt{\frac{\pi}{4}} = 0.00348 \tag{37}$$

Table. 3.3 Momentum length scale L_M calculation.

2cm/L_M	$F_d = 10$	$F_d = 20$	$F_d = 30$	$F_d = 50$	F_d =100
U_0=0.2m/s	0.541132	0.270275	0.180958	0.109384	0.056113
U_0=0.41m/s	0.541147	0.270573	0.180241	0.108370	0.053832
U_0=0.6m/s	0.541208	0.270572	0.180338	0.108280	0.054140

Table. 3.4 Discharge length scale L_Q calculation.

2cm/L_M	$F_d = 10$	$F_d = 20$	$F_d = 30$	$F_d = 50$	F_d =100
U_0=0.2m/s	0.541132	0.270275	0.180958	0.109384	0.056113
U_0=0.41m/s	0.541147	0.270573	0.180241	0.108370	0.053832
U_0=0.6m/s	0.541208	0.270572	0.180338	0.108280	0.054140

L_MSubmerged inclined buoyant jets in this study either touched the bed or did not. Those which did not touch the bottom boundary follow the schematic in Fig. 3.5. For most of jets in the near nozzle section, the jet is dominated by momentum. In this section, the buoyant fluid with

different speed has a tendency to follow the initial direction at an angle α towards the bottom. Due to entrainment with the saline ambient, the kinetic energy of the jet decreases. From the lowest point, buoyancy starts dominating the jet behaviour. After this point, the trajectory moves upward with a tendency to spread toward the surface of the receiving ambient water.

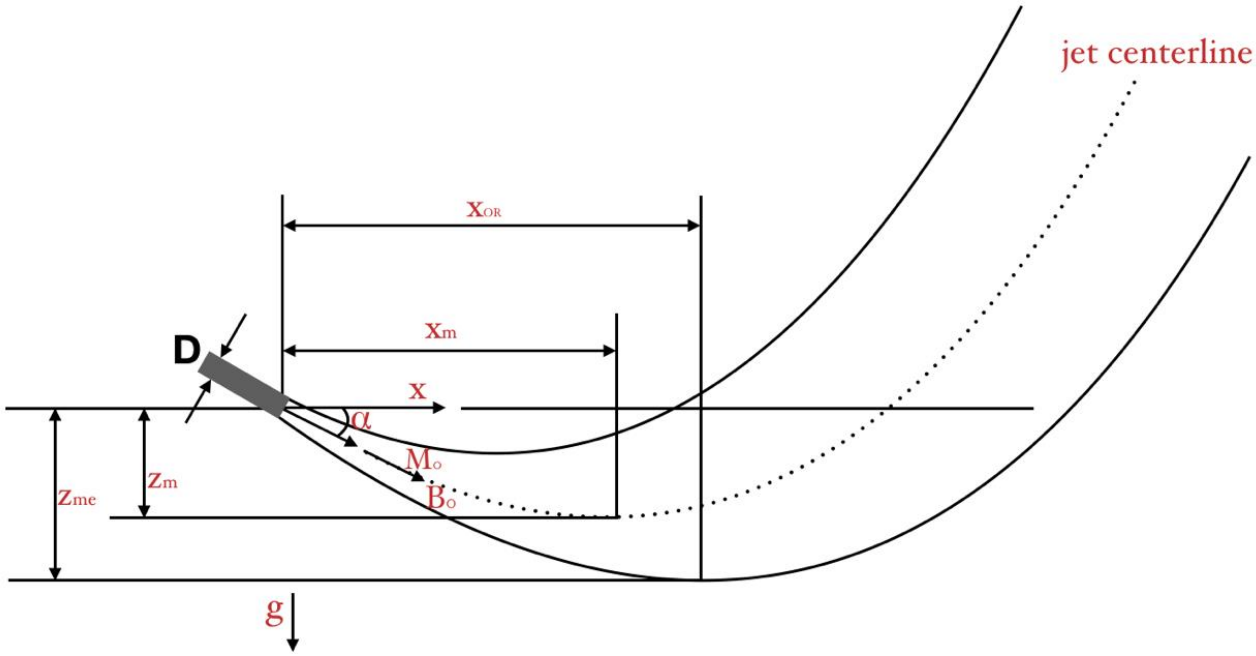

Fig. 3.5 A schematic of a submerged inclined buoyant jet discharged into stable saline ambient.

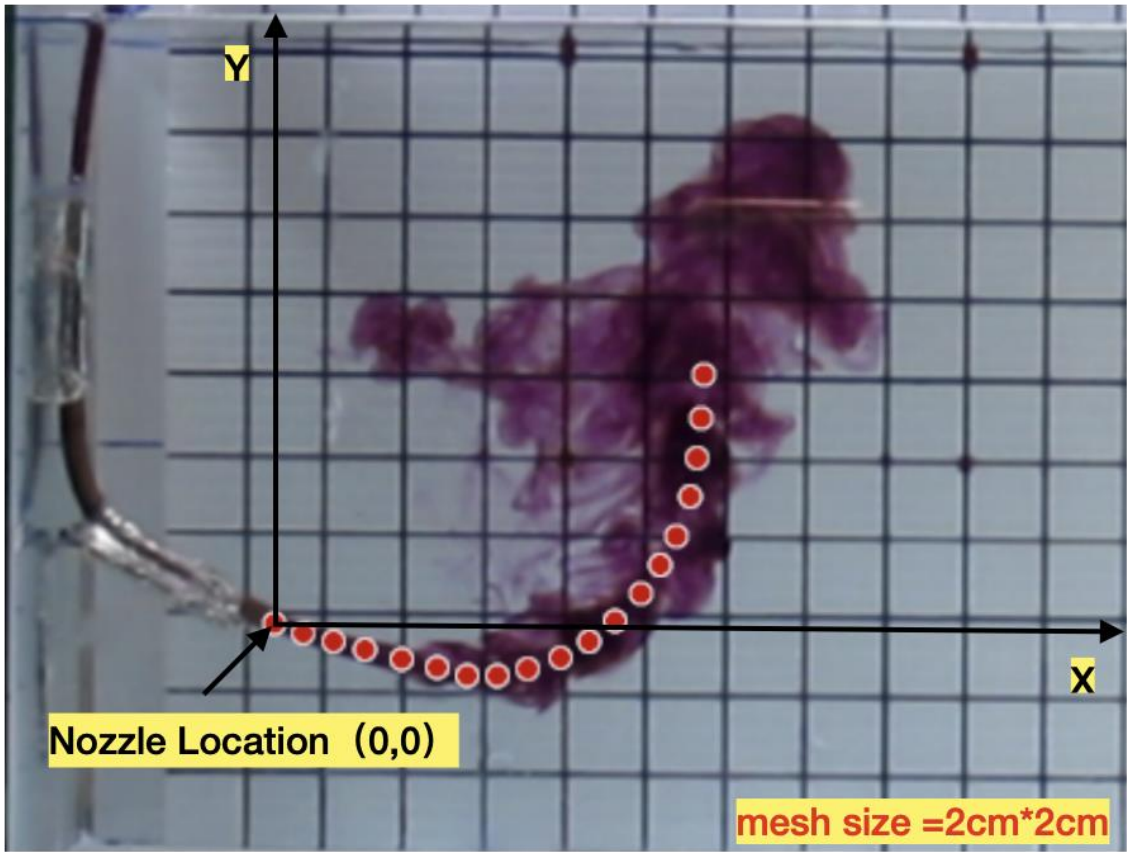

Fig. 3.6.1 A typical photograph about the centerline data collection of buoyant jet (jet shape at 10s in angle -30°, initial velocity 0.2m/s and Froud Number 10) trajectory using WebPlotDigitizer.

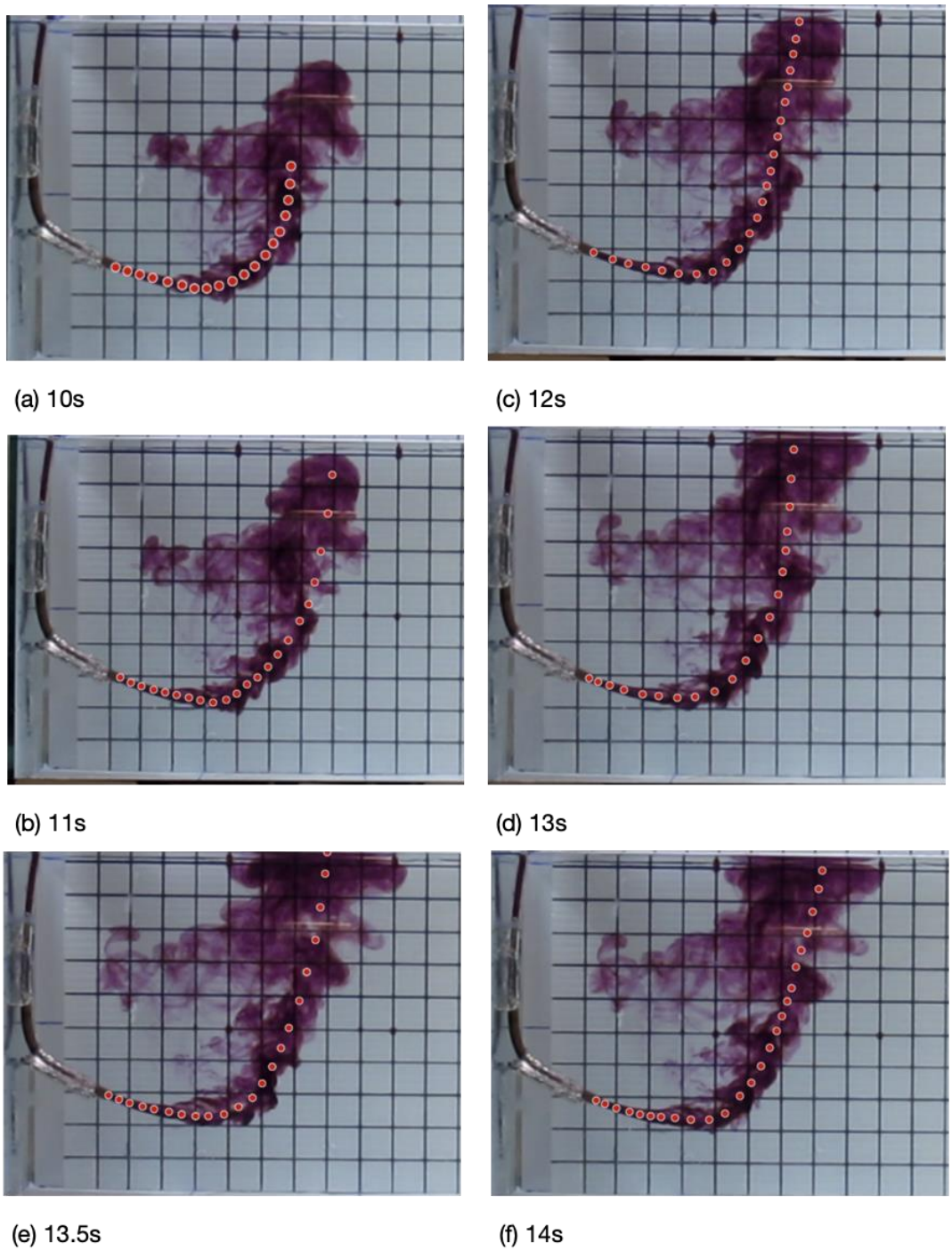

Fig. 3.6.2 Discharge shape and trajectory points selection for jet discharged at(a) 10s, (b)11s, (c)12s, (d)13s, (e)14s in angle -30°, initial velocity 0.2m/s and Froud Number at 10.

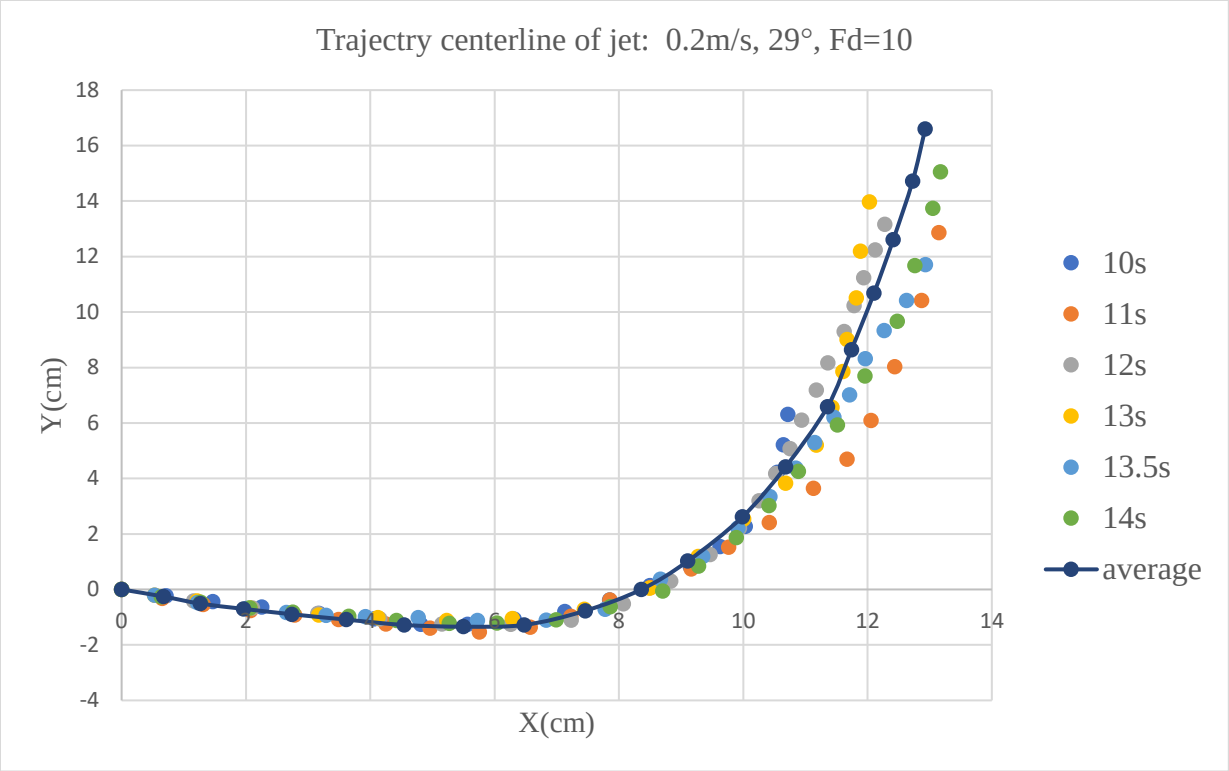

Fig. 3.6.3 Average centerline selection from jet with initial velocity 0.2m/s, Froud Number at 10, discharge angle α = - 29° downwards.

In this project, images of the jet trajectory data were derived from the videos captured by a camera parallel to the front face of tank 2. The camara recorded the whole process since the dyed jet started entering the transparent saline ambient. WebPlotDigitizer was used as a tool to select points from those pictures for trajectory centerline results During data extraction process, in the horizontal and vertical coordinate system, the location of the nozzle where the jet starts was always set as (0, 0), which was same in every single experiment. Four points on horizontal axis and vertical axis were fixed $(x_1,\ 0)$, $(x_2,\ 0)$, $(0,\ y_1)$, $(0,\ y_2)$ to make a Cartesian coordinate system. Then as shown in Fig. 3.6.1, a series of points were manually picked out as the centerline of a jet. In order to eliminate the manual error, an average centerline position was selected for the trajectory shape. For instance, as shown on Fig. 3.6.2, a buoyant jet with an initial velocity of 0.2m/s and Froude number 10 seemed to be almost steady at around 13s. Thus, an average centerline of 10s, 11s, 13s, 13.5s and 14s was selected to record the trajectory position. Fig. 3.6.3 and Table. 3.5 shows how the data of average trajectories came from those points.

Table. 3.5 Centerline points data from jet with initial velocity 0.2m/s, Froud number 10 at 10s, 11s, 13s, 13.5s and 14s.

10s		11s		12s		13s		13.5s		14s		average	
X(cm)	Y(cm)	X(cm)	Y(cm)	X(cm)	Y(cm)	X(cm)	Y(cm)	X(cm)	Y(cm)	X(cm)	Y(cm)	X(cm)	Y(cm)
0	0	0	0	0	0	0	0	0	0	0	0	0	0
0.716	-0.234	0.654	-0.328	1.158	-0.41	0.53	-0.208	0.532	-0.208	0.636	-0.26	0.673	-0.255
1.468	-0.434	1.31	-0.544	2.104	-0.664	1.216	-0.414	1.222	-0.47	1.272	-0.466	1.264	-0.51
2.252	-0.632	2.072	-0.758	3.156	-0.864	2.062	-0.67	2.016	-0.676	2.066	-0.67	1.963	-0.7
3.174	-0.864	2.782	-0.918	4.156	-1.064	3.172	-0.924	2.652	-0.83	2.756	-0.822	2.74	-0.895
4.062	-1.062	3.49	-1.08	5.154	-1.24	4.122	-1.02	3.288	-0.93	3.656	-0.972	3.612	-1.087
4.812	-1.262	4.254	-1.24	6.258	-1.254	5.232	-1.114	3.924	-0.976	4.424	-1.124	4.543	-1.279
5.562	-1.256	4.964	-1.4	7.232	-1.112	6.286	-1.046	4.77	-1.02	5.27	-1.22	5.497	-1.342
6.314	-1.078	5.754	-1.532	8.074	-0.522	7.444	-0.71	5.722	-1.116	6.038	-1.21	6.477	-1.279
7.132	-0.798	6.572	-1.358	8.836	0.304	8.494	0.052	6.832	-1.102	6.99	-1.092	7.457	-0.769
7.85	-0.382	7.228	-0.964	9.468	1.26	9.278	1.186	7.78	-0.716	7.862	-0.626	8.362	0
8.498	0.136	7.854	-0.378	9.94	2.214	10.006	2.534	8.668	0.37	8.706	-0.052	9.109	1.024
9.146	0.826	8.51	0.072	10.256	3.194	10.682	3.828	9.346	1.184	9.284	0.838	9.989	2.62
9.624	1.548	9.164	0.742	10.52	4.172	11.174	5.2	9.916	2.212	9.89	1.864	10.68	4.414
10.034	2.27	9.764	1.524	10.756	5.072	11.426	6.57	10.432	3.348	10.414	3.022	11.357	6.591
10.374	3.264	10.418	2.416	10.94	6.104	11.602	7.856	10.844	4.374	10.886	4.26	11.741	8.64
10.546	4.224	11.128	3.64	11.176	7.188	11.672	9.01	11.15	5.292	11.516	5.928	12.104	10.68
10.648	5.216	11.672	4.698	11.36	8.166	11.82	10.51	11.458	6.208	11.958	7.7	12.414	12.61
10.716	6.312	12.054	6.088	11.624	9.302	11.886	12.198	11.712	7.018	12.48	9.662	12.725	14.717
		12.436	8.03	11.782	10.228	12.032	13.968	11.962	8.312	12.764	11.674	12.928	16.6
		12.872	10.418	11.94	11.232			12.268	9.336	13.048	13.74		
		13.146	12.858	12.124	12.236			12.626	10.416	13.176	15.054		
				12.28	13.162			12.93	11.71				

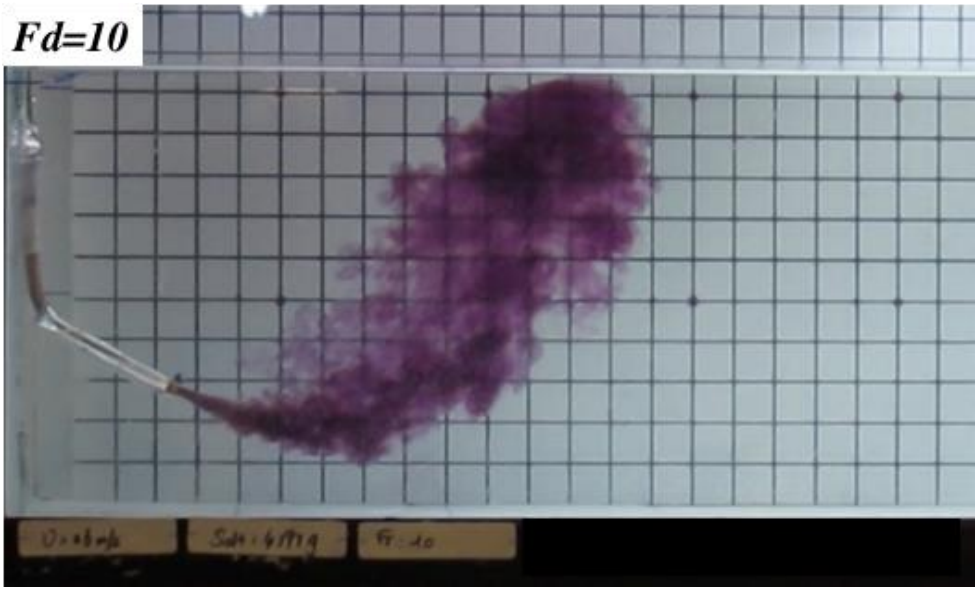

(a)

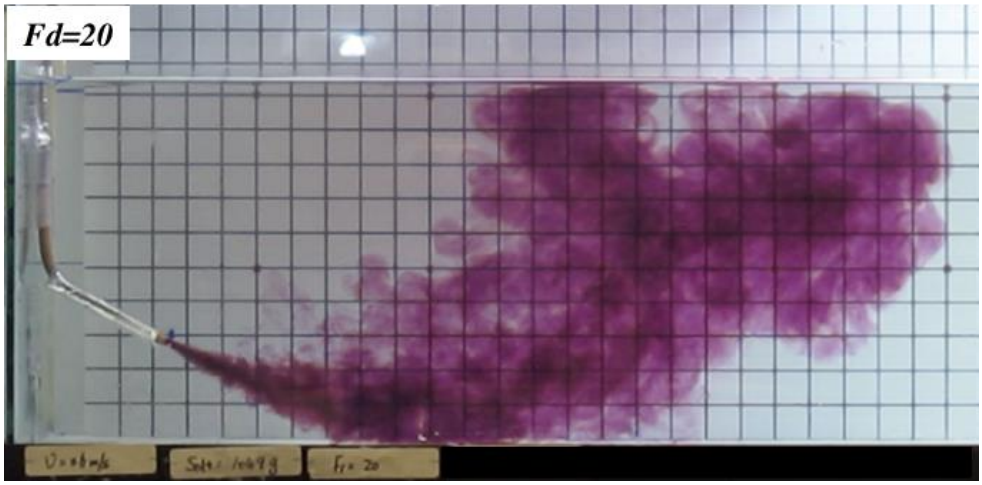

(b)

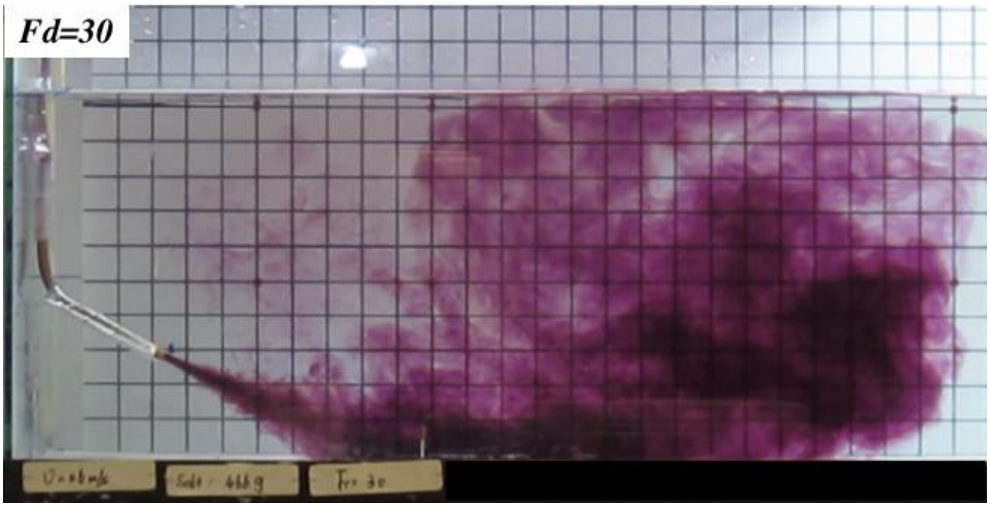

(c)

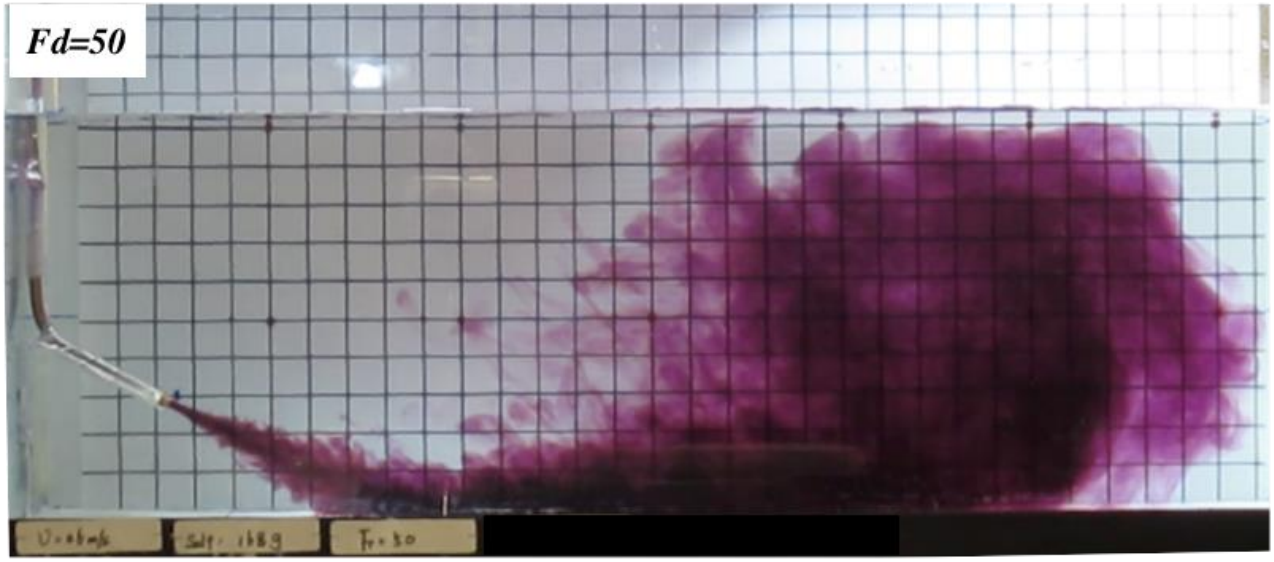

(d)

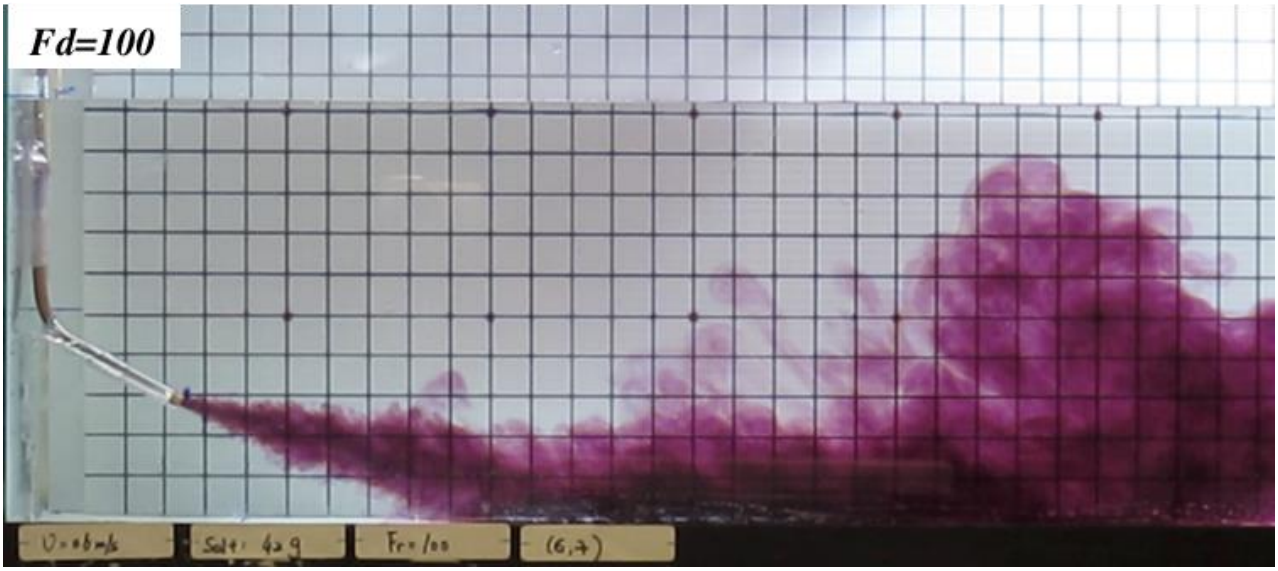

(e)

Fig. 3.7.1 Buoyant jet spread condition changes with the variation of Froude number. All jets had an initial velocity of 0.6 m/s, at -30° downwards jet angle, Froude number: (a) Fd= 10, (b) Fd= 20, (c) Fd= 30, (d) Fd= 50 and (e) Fd= 100.

The group of pictures in Fig. 3.7.1 revealed the effect of Froude number on the jet behavior with initial jet velocity of 0.6 m/s and inclination angle of -30°. Through the comparison in these five experiments, it can be observed that the Froude number acted as an important factor to the jet travel distance. As the Froude number increased from 10 to 100, the jets had a tendency to travel further away from the nozzle. Figures 3.7.1 (a) Fd= 10 and (d) Fd= 50 represent two typical jets. The jet in Figures 3.7.1 (a) was driven by buoyancy and changed the moving direction after it reached the lowest point. The jet with Fd=50 in Figures 3.7.1 (d) touched the bottom and remained attached to it for a long distance before it moved up towards the water surface.

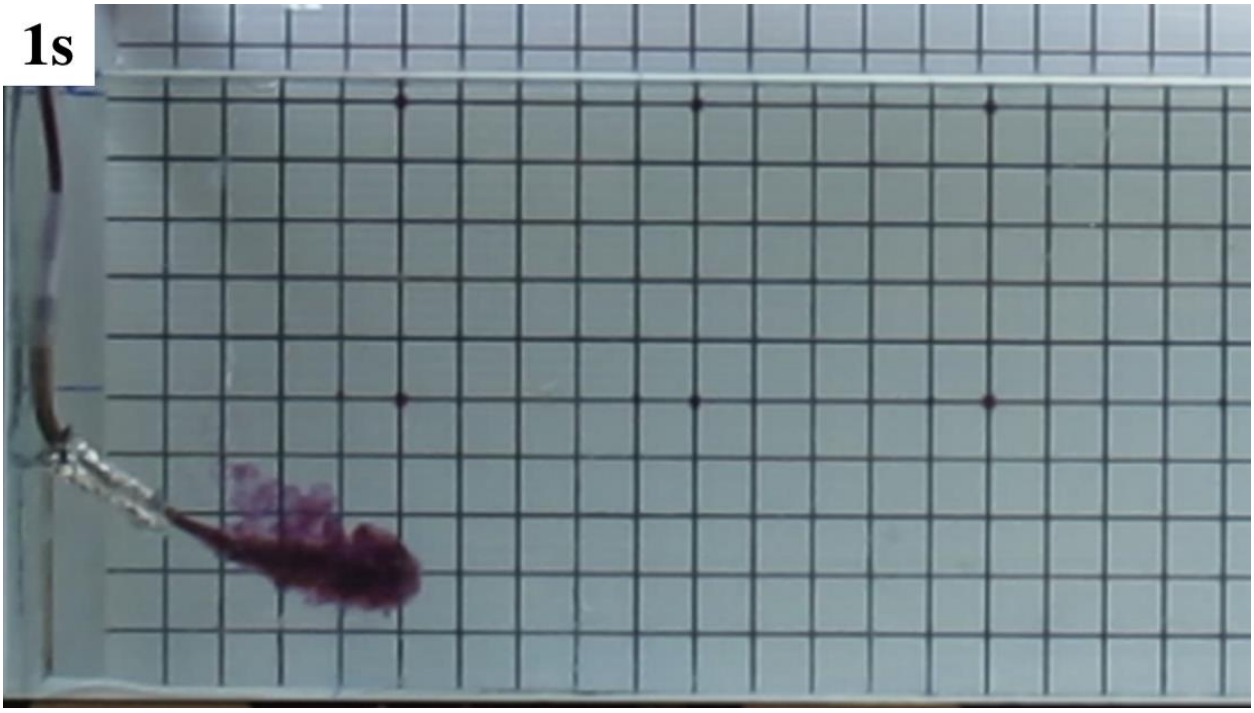

(a)

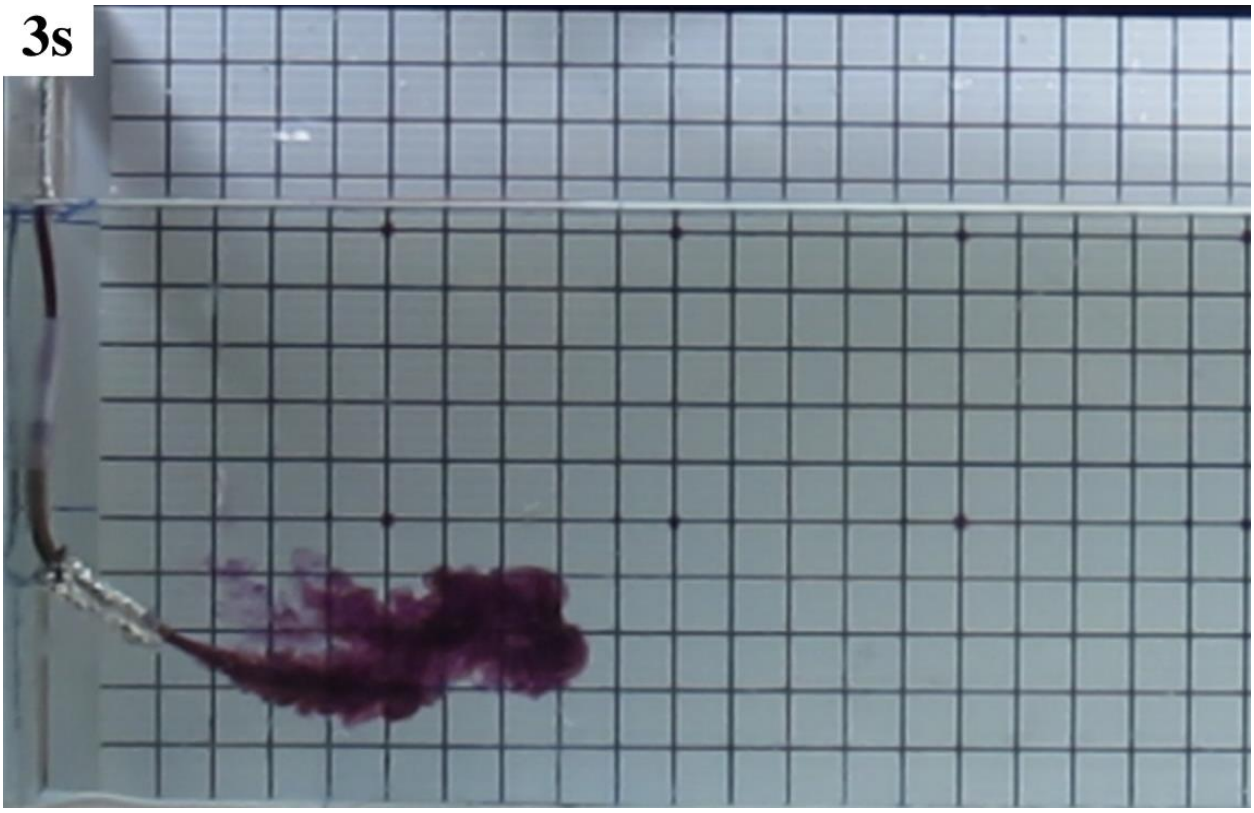

(b)

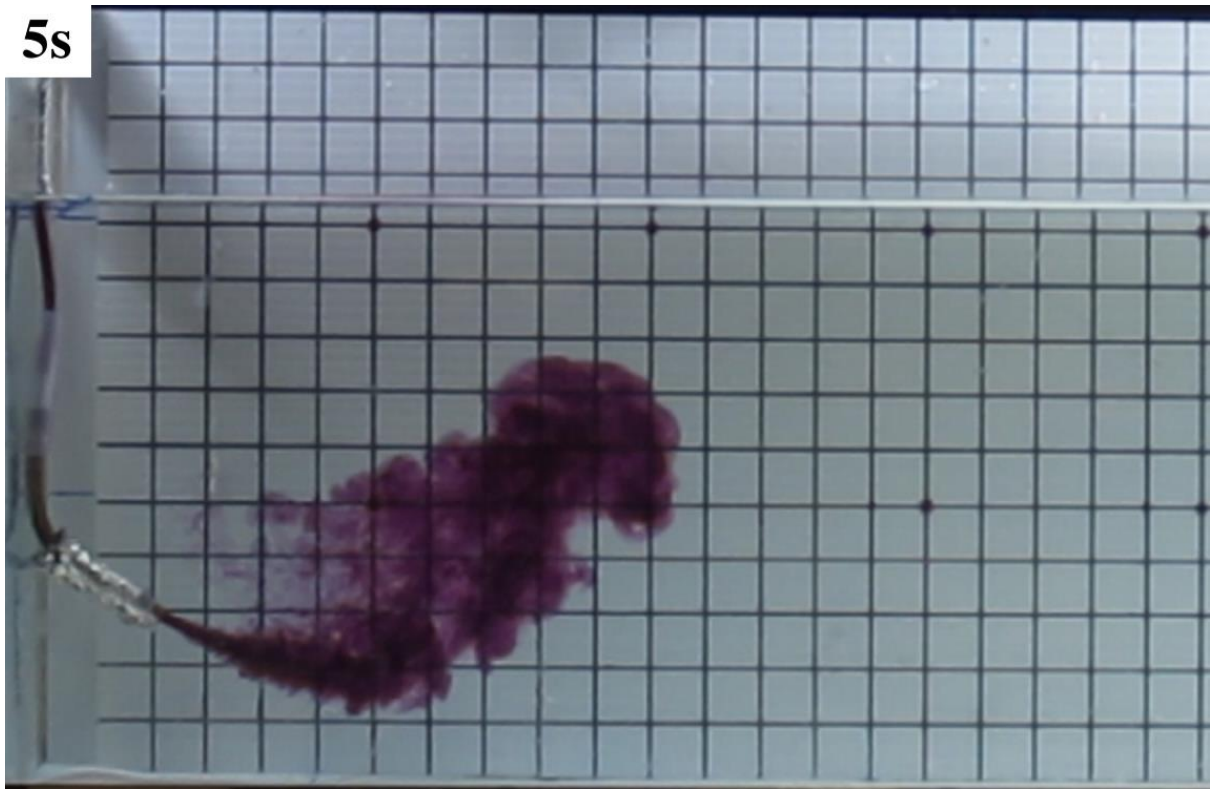

(c)

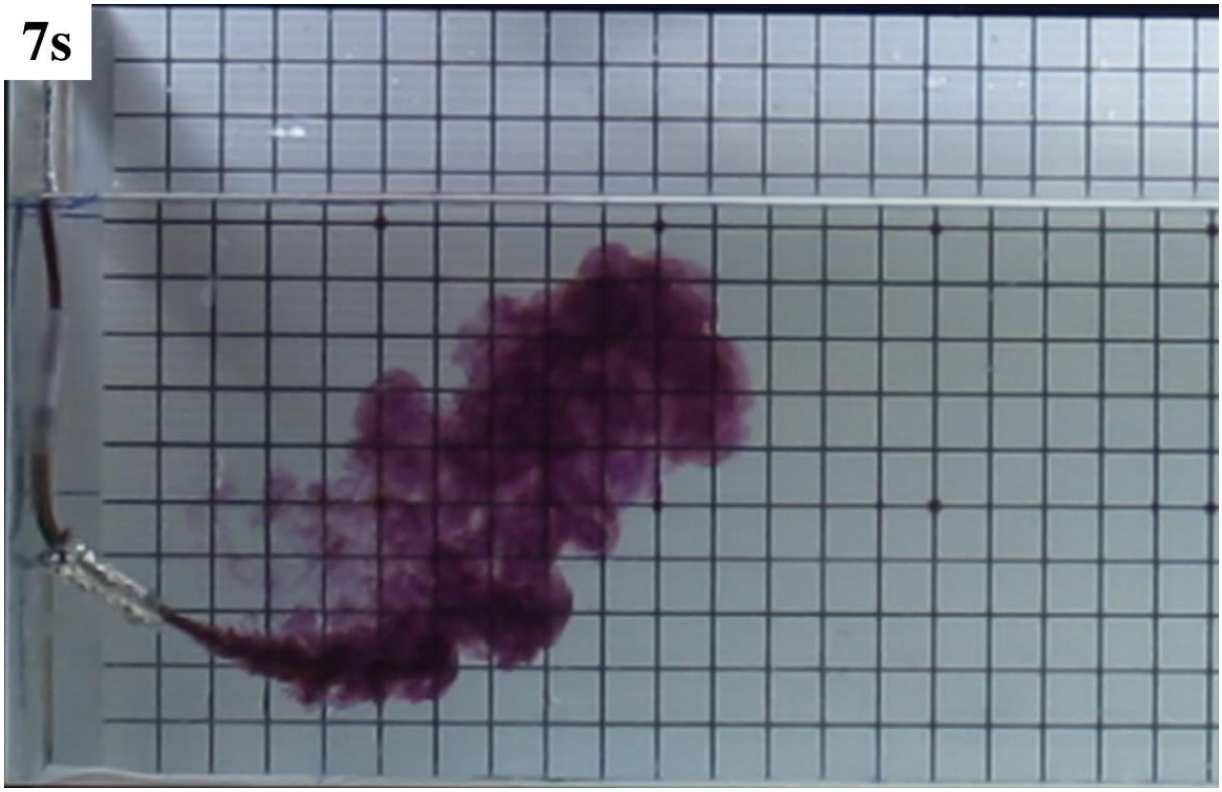

(d)

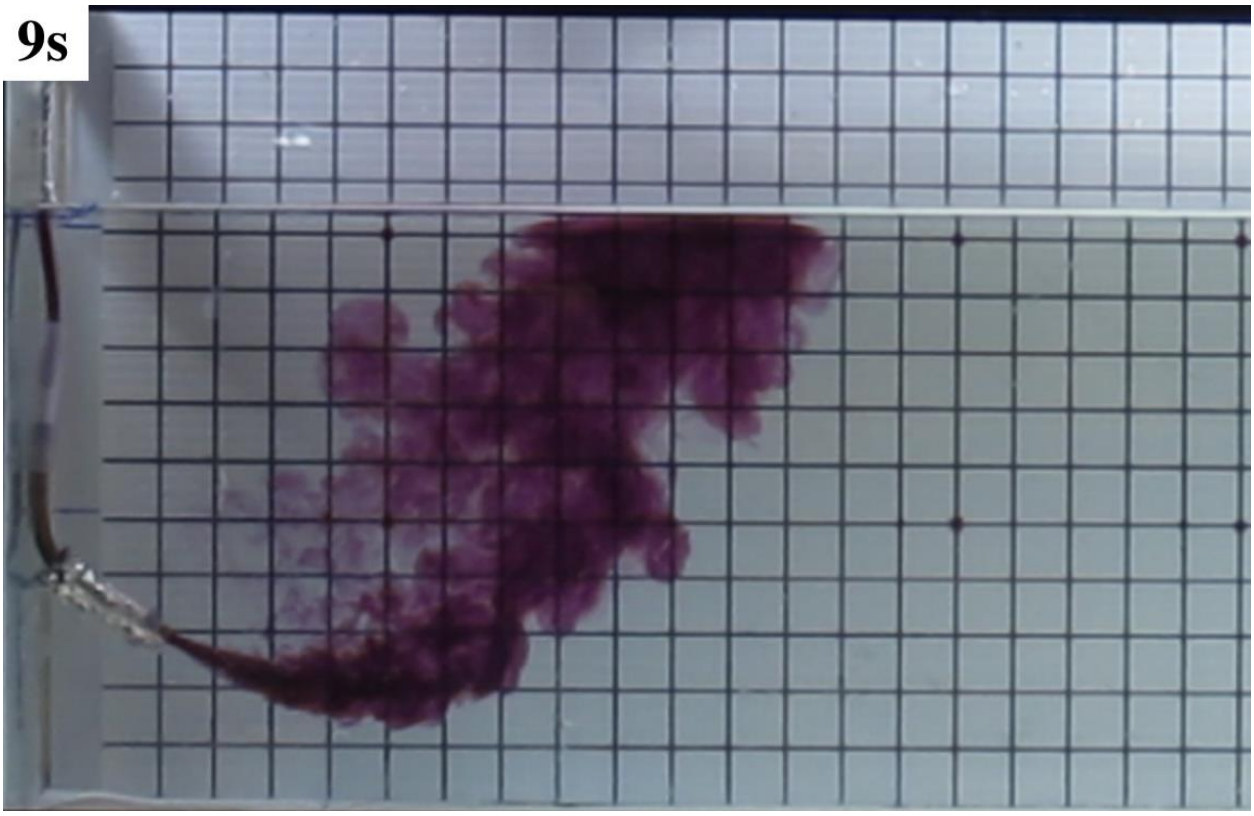

(e)

Fig. 3.7.2 Shapes of jet of velocity 0.41m/s, Fd=10, α=-30° at different times(a) 1s, (b) 3s, (c) 5s, (d) 7s, (e) 9s.

Fig. 3.7.2 offers an example of how a jet developed over time. Comparing the pictures for the jet of 0.41m/s, Fd=10, α=-30° at 1s, 3s, 5s, 7s and 9s, it is clearly known that the jet moved along its original discharge angle for a short distance. However, the centerline bended and became closer to the horizon until it reached to a lowest point. After that, the direction of the jet totally changed from downward to upward. With the jet fully developed, it eventually reached to the water surface.

By using the image analysis and average data extraction method mentions before, a summary of average jet trajectories' data under various Froude numbers of 10, 20, 30,100 were displayed in Table. 3.6.

Table. 3.6 Average centerline data for jets under various Froude numbers of 10, 20, 30,100(a)(b)(c)(d)

Group	1		2		3		4		7	
Initial velocity	0.2m/s		0.41m/s		0.2m/s		0.41m/s		0.41m/s	
Froude Number	10		10		20		20		10	
Discharge angle	-30°		-30°		-30°		-30°		-28°	
Point location	X/cm		Y/cm		X/cm		Y/cm		X/cm	Y/cm
1	0	0	0	0	0	0	0	0	0	0
2	0.673	0.255	0.81	0.359	1.763	0.854	1.789	0.706	1.59	0.654
3	1.264	-0.51	1.719	0.769	3.427	1.386	3.183	1.161	2.884	1.124
4	1.963	0.702	3.131	1.279	5.194	1.708	4.773	1.512	4.477	1.449
5	2.736	0.895	4.344	1.534	6.957	1.652	6.318	1.664	5.919	1.545
6	3.612	1.087	5.556	1.741	8.972	0.747	8.055	1.312	7.608	1.168
7	4.543	1.279	6.617	1.689	10.436	0.425	9.597	0.503	8.954	0.373
8	5.497	1.342	7.479	1.534	12.048	1.919	11.091	0.654	10.296	0.795
9	6.477	1.279	8.388	1.279	13.409	3.412	12.185	1.564	11.338	2.011
10	7.457	0.769	9.298	0.869	14.972	5.867	13.131	2.621	12.532	3.697
11	8.362	0	10.004	0.255	16.333	8.211	14.673	4.185	13.627	5.523
12	9.109	1.024	10.51	0.203	17.394	10.292	16.115	6	14.773	7.394
13	9.989	2.625	11.013	0.614	18.248	12.425	17.157	7.612	15.468	8.61
14	10.684	4.414	11.471	1.128	18.702	14.237	18.203	9.375	16.063	9.874
15	11.357	6.591	11.926	1.741			19.046	11.039	16.861	11.793
16	11.741	8.64	12.429	2.506			19.993	13.006	17.505	13.431
17	12.104	10.684	12.884	3.124			20.492	14.166		
18	12.414	12.606	13.39	3.789						
19	12.725	14.717	13.845	4.503						
20	12.928	16.636	14.399	5.375						
21			15.412	7.116						
22			16.067	8.495						

(a)

Group	8		9		10		16		17	
Initial velocity	0.6 m/s		0.6 m/s		0.6 m/s		0.6m/s		0.41m/s	
Froude Number	10		10		20		100		20	
Discharge angle	-28°		-30°		-29°		-28°		-28°	
Point location	X/cm	Y/cm	X/cm	Y/cm	X/cm	Y/cm	X/cm	Y/cm	X/cm	Y/cm
1	0	0	0	0	0	0	0	0	0	0
2	2.563	1.126	1.59	-0.654	2.563	-1.126	8.071	-2.429	3.533	-1.622
3	4.807	1.919	2.884	-1.124	4.807	-1.919	17.75	-5.179	6.741	-3.022
4	7.133	2.533	4.477	-1.449	7.133	-2.533	29.679	-5.179	10.881	-4.163
5	9.296	2.933	5.919	-1.545	9.296	-2.933	39.571	-3.714	15.237	-4.519
6	11.222	3.044	7.608	-1.168	11.222	-3.044	48.25	-0.393	19.259	-3.815
7	13.867	2.711	8.954	-0.373	13.867	-2.711	52.821	3.071	22.563	-2.148
8	16.356	1.933	10.296	0.795	16.356	-1.933			25.807	-0.089
9	18.681	0.474	11.338	2.011	18.681	-0.474			29.052	2.585
10	20.526	1.089	12.532	3.697	20.526	1.089			31.793	5.259
11	22.526	2.719	13.627	5.523	22.526	2.719			34.156	7.889
12	24.133	4.452	14.773	7.394	24.133	4.452			35.252	9.556
13	25.733	6.193	15.468	8.61	25.733	6.193				
14	26.933	7.763	16.063	9.874	26.933	7.763				
15	28.296	9.444	16.861	11.793	28.296	9.444				
16	29.422	11.126	17.505	13.431	29.422	11.126				
17	30.704	13.311			30.704	13.311				

(b)

Group	18		19		20		22		23		24	
Initial velocity	0.41m/s		0.41m/s		0.41m/s		0.6m/s		0.6m/s		0.41m/s	
Froude Number	30		100		100		30		100		30	
Discharge angle	-27°		-27°		-30°		-29°		-29°		-29°	
Point location	X/cm	Y/cm	X/cm	Y/cm	X/cm	Y/cm	X/cm	Y/cm	X/cm	Y/cm	X/cm	Y/cm
1	0	0	0	0	0	0	0	0	0	0	0	0
2	2.84	-1.425	5.75	-3.036	5.75	-2.821	3.801	-1.624	6.964	-2.714	4.464	-2.177
3	5.514	-2.53	10.821	-5.393	11	-5.393	7.945	-3.215	14.286	-5.607	7.768	-3.569
4	7.878	-3.425	20.571	-5.429	13.571	-5.679	11.89	-4.674	27.643	-5.679	11.691	-4.707
5	11.193	-4.718	30.357	-5.393	21.643	-5.679	15.017	-5.337	37.821	-5.107	16.961	-5.204
6	15.05	-5.381	38.286	-3.536	30.036	-5.679	18.884	-5.624	45.464	-3.857	21.624	-5.315
7	20.077	-5.414	45.607	-0.5	35.607	-4.75	23.304	-5.547	52.393	-1.464	26.685	-4.53
8	24.873	-5.37	50.929	2.893	42.393	-2	27.238	-4.254	57.714	1.036	31.414	-2.928
9	29.812	-4.122	55.893	7.286	47.036	1.429	30.365	-2.796	61.036	2.857	34.387	-1.249
10	34.354	-1.845			50.643	4.75	33.282	-0.961			37.492	0.928
11	38.818	0.873			53.393	7.393	35.801	0.796			39.724	2.707
12	42.884	3.602					38.453	2.63			41.823	4.453
13	46.166	5.878					40.895	4.586			42.972	5.381
14	48.74	8.464										

(c)

Group	30		31		32		33		34	
Initial velocity	0.2m/s		0.2m/s		0.2m/s		0.2m/s		0.2m/s	
Froude Number	10		20		30		50		100	
Discharge angle	-60°		-60°		-60°		-60°		-60°	
Point location	X/cm	Y/cm	X/cm	Y/cm	X/cm	Y/cm	X/cm	Y/cm	X/cm	Y/cm
1	0	0	0	0	0	0	0	0	0	0
2	1.796	-2.692	1.114	-1.81	1.619	-2.605	1.354	-2.278	1.33	-2.333
3	4.075	-5.619	3.417	-5.575	3.532	-5.571	3.345	-5.339	3.032	-5.444
4	7.109	-5.205	7.606	-5.327	8.778	-5.384	9.637	-5.363	10.121	-5.672
5	8.347	-2.019	10.156	-1.526	12.184	-2.229	14.973	-0.342	15.165	-3.573
6	9.569	2.359	12.254	4.162	14.494	1.281	18.159	4.659	20.108	0.159
7	10.557	6.259	13.694	9.118	15.924	5.801	21.027	10.053	25.462	4.958
8	11.381	10.396			16.552	10.388			28.545	8.675

(d)

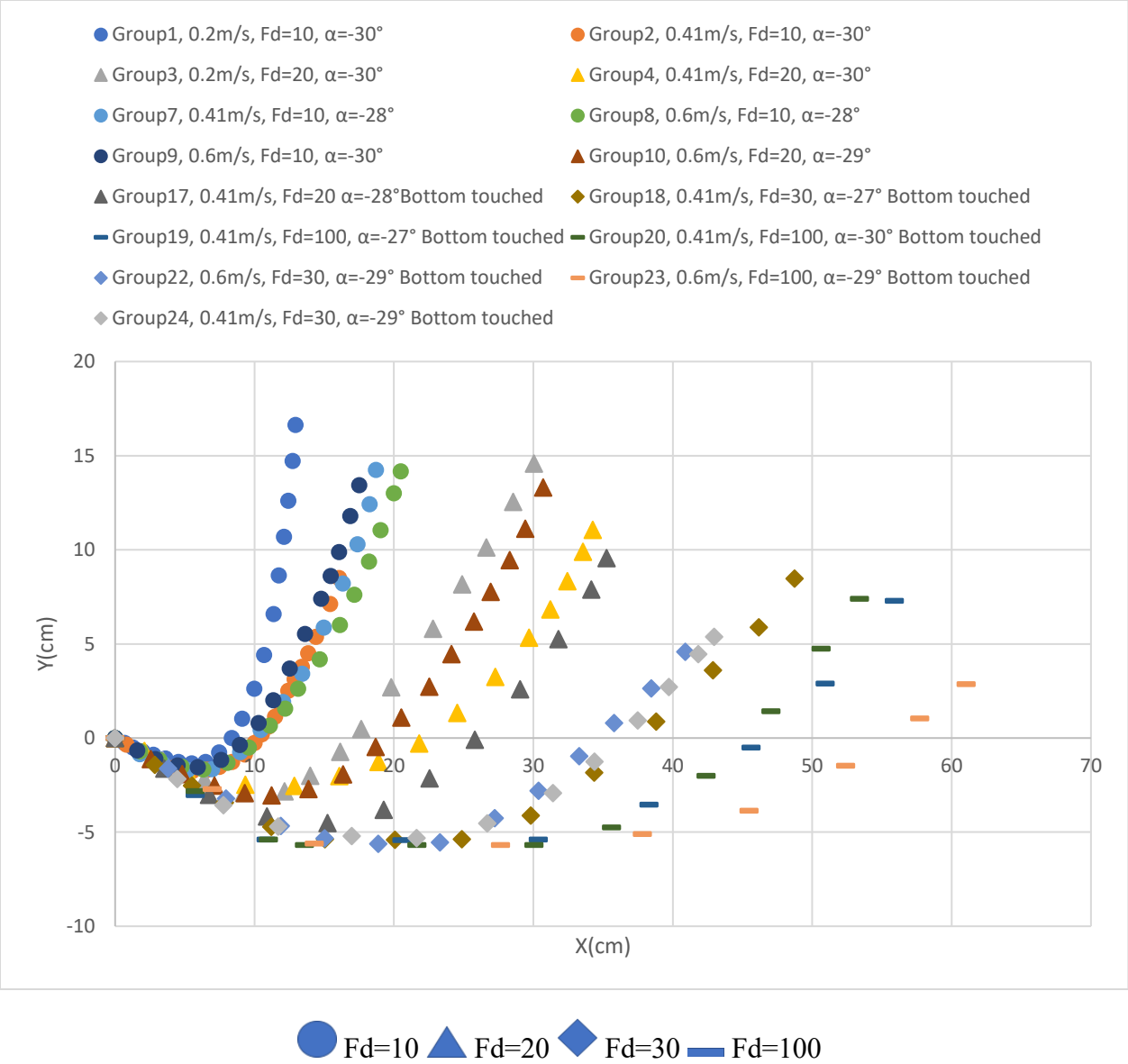

Fig.3.8 Comparison of average centerline trajectory under various Froude number of 10, 20, 30, 100.

Fig.3.8 demonstrates the average trajectories of 15 groups of experiments. All of these jets' discharge angles were about -30° towards the bottom. Their initial velocities were set to 0.2m/s, 0.41m/s and 0.6m/s. Froude number values included Fd=10, Fd=20, Fd=30, Fd=50, Fd=100. During the experimental design stage, Froude number played the role of a comprehensive index that included the impact of velocity and density difference.

The trajectory comparison reflected the relationship between jet behaviour and Froude number. Among all the factors, Froude number represents as the most important parameter. The results

showed that even with the increase of discharge velocity from 0.2m/s to 0.6m/s, jet trajectories could be still grouped based on the Froude number rather than the speed. Jets with highest Froude number in this study always had the longest travel distance.

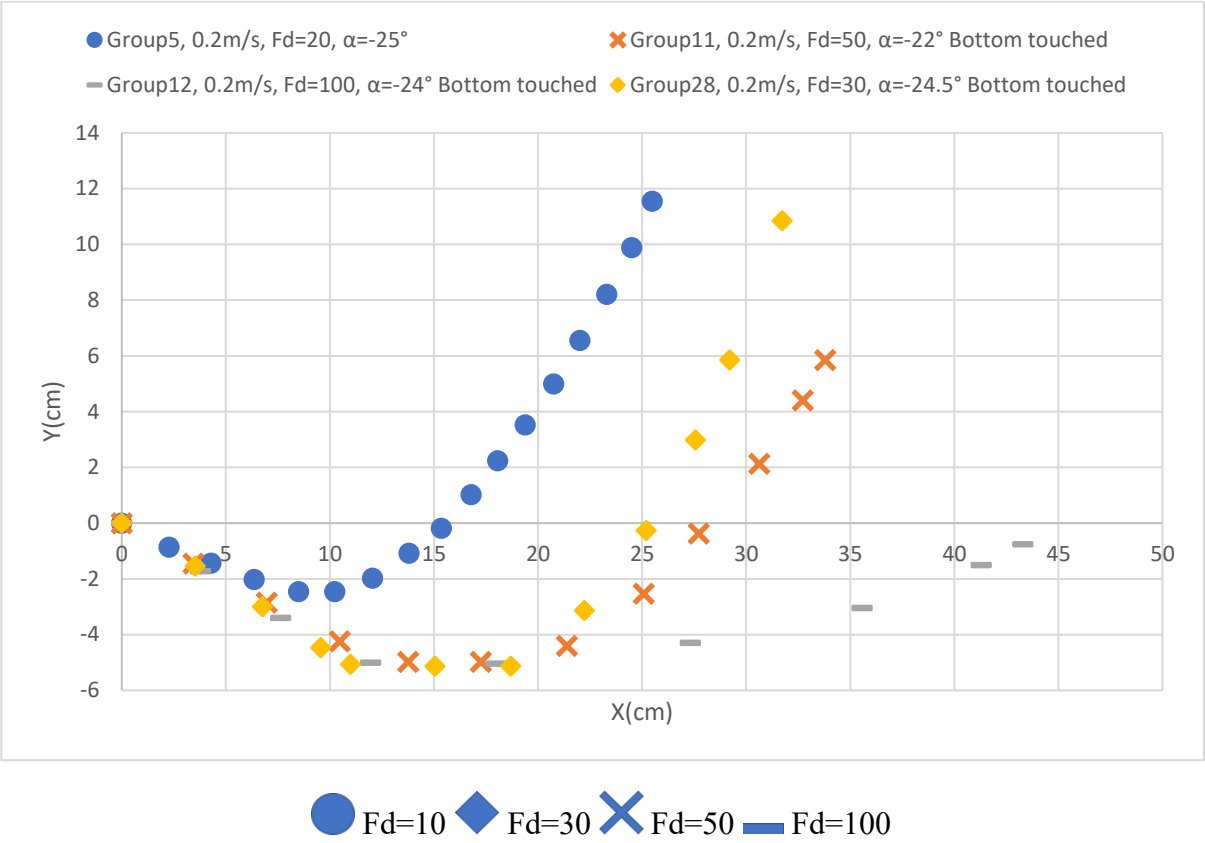

Fig.3.9.1 Trajectory comparison of jets with different Froude numbers of velocity 0.2m/s, around -25° discharge angle.

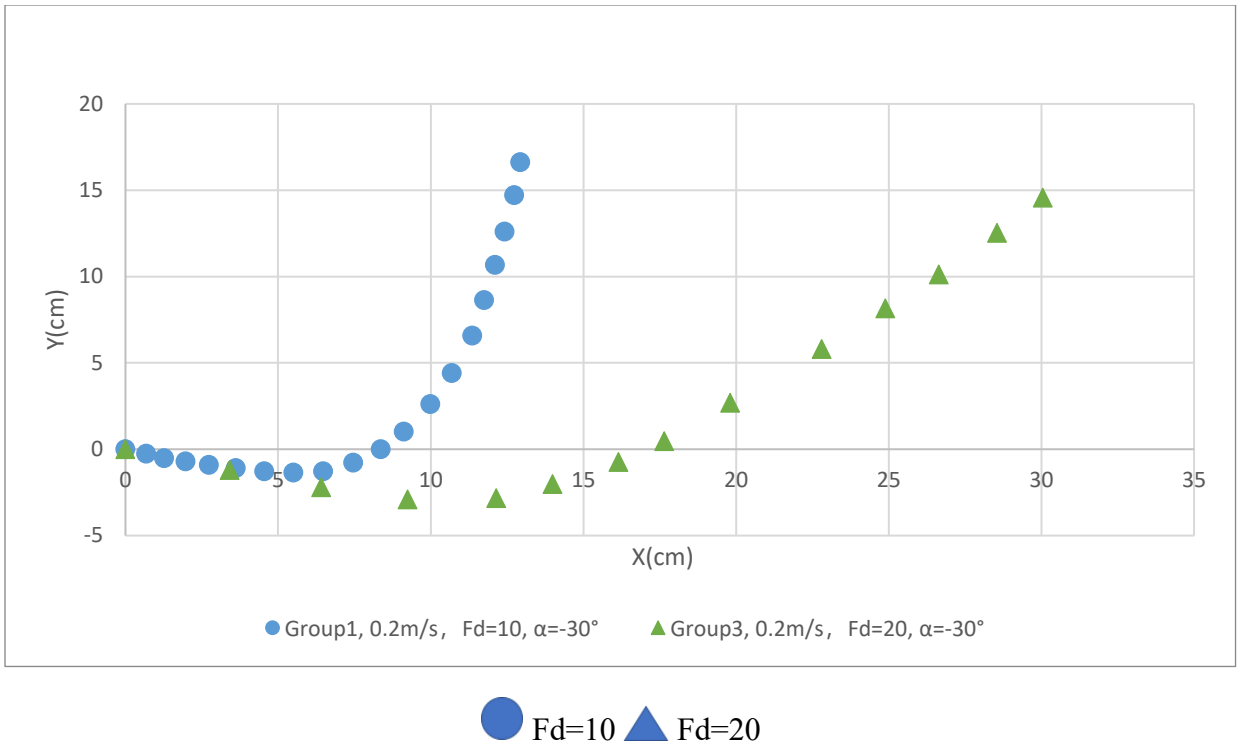

Fig3.9.2 Trajectory comparison of jets with 0.2m/s, discharge angle around -30°

As can be seen in Fig.3.9.1, Group 5 illustrated a typical buoyant jet trajectory that did not touch the bottom of the tank. This group had a higher returning point than the others. Group 11, Group 12 and Group 28 all touched the bottom in laboratory experiments and the trajectories almost overlapped each other in the near nozzle area. For these four jets, a correlation between the Froude number and the jet centerline distance was observed in the graphs. Group 23 with Fd=100 propagated farthest and Group 5 with smallest Fd=10 had the shortest centerline.

The second set of results in Fig.3.9.2, had an angle around -30° from the nozzle towards the bottom. The Froud number was set to 10 and 20 and initial velocity was set to 0.2m/s. A conclusion could be obtained that horizontal distance of a jet is correlated with the Froude number.

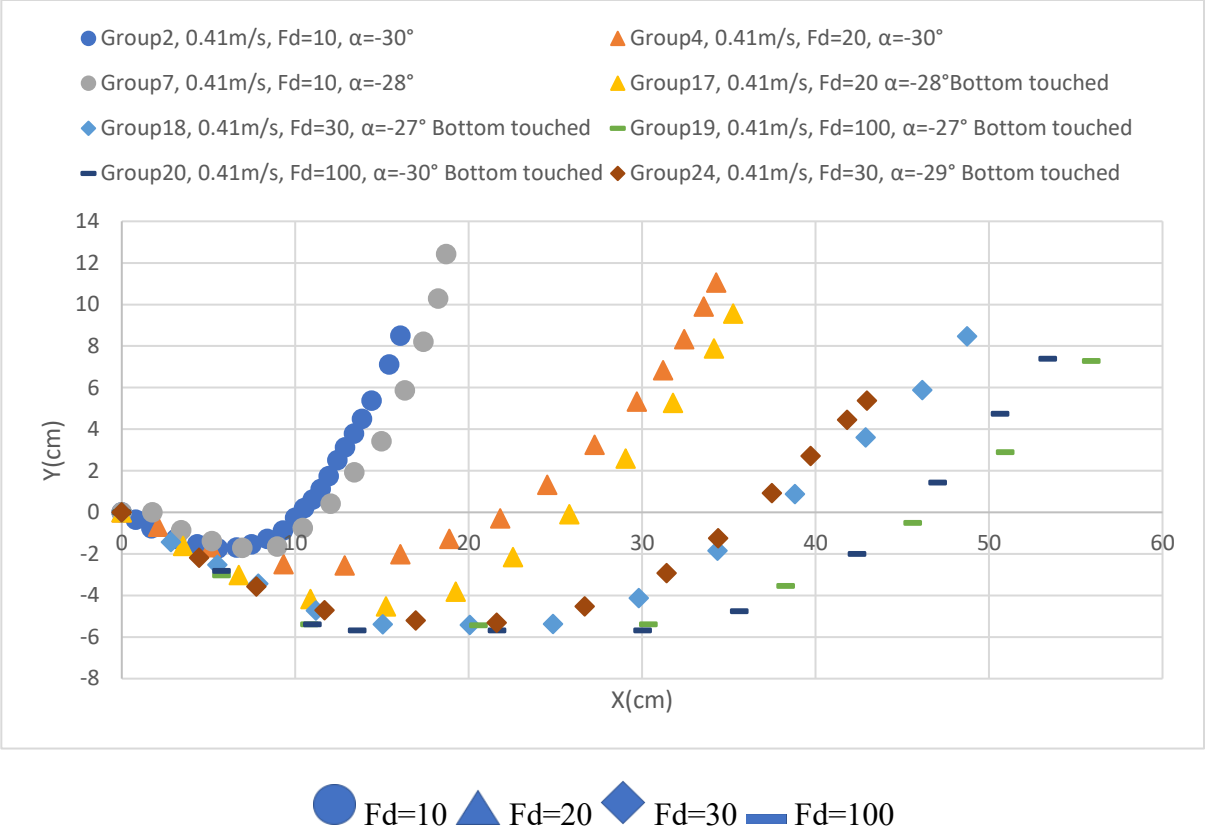

Fig.3.10 Trajectory comparison of jets with 0.41m/s, discharge angle around -30°

Ten groups of buoyant jets were studied in Fig.3.10. They all had a velocity of 0.41m/s and angle of around -30°. Three groups did not touch the bottom of the tank, including group 2, group 4 and group 7. The other groups touched the bottomed (group 7, group 17, group 18, group19, group20, group24). From comparison of the untouched groups, jets with larger Froude number tended to have a lower returning point. Simultaneously, the jet that touched the bottom with higher Froude number had a shorter trajectory before reaching the bottom and longer path after turning upward. In summary, the Froude number has a positive impact on the length of a downward buoyant jet trajectory.

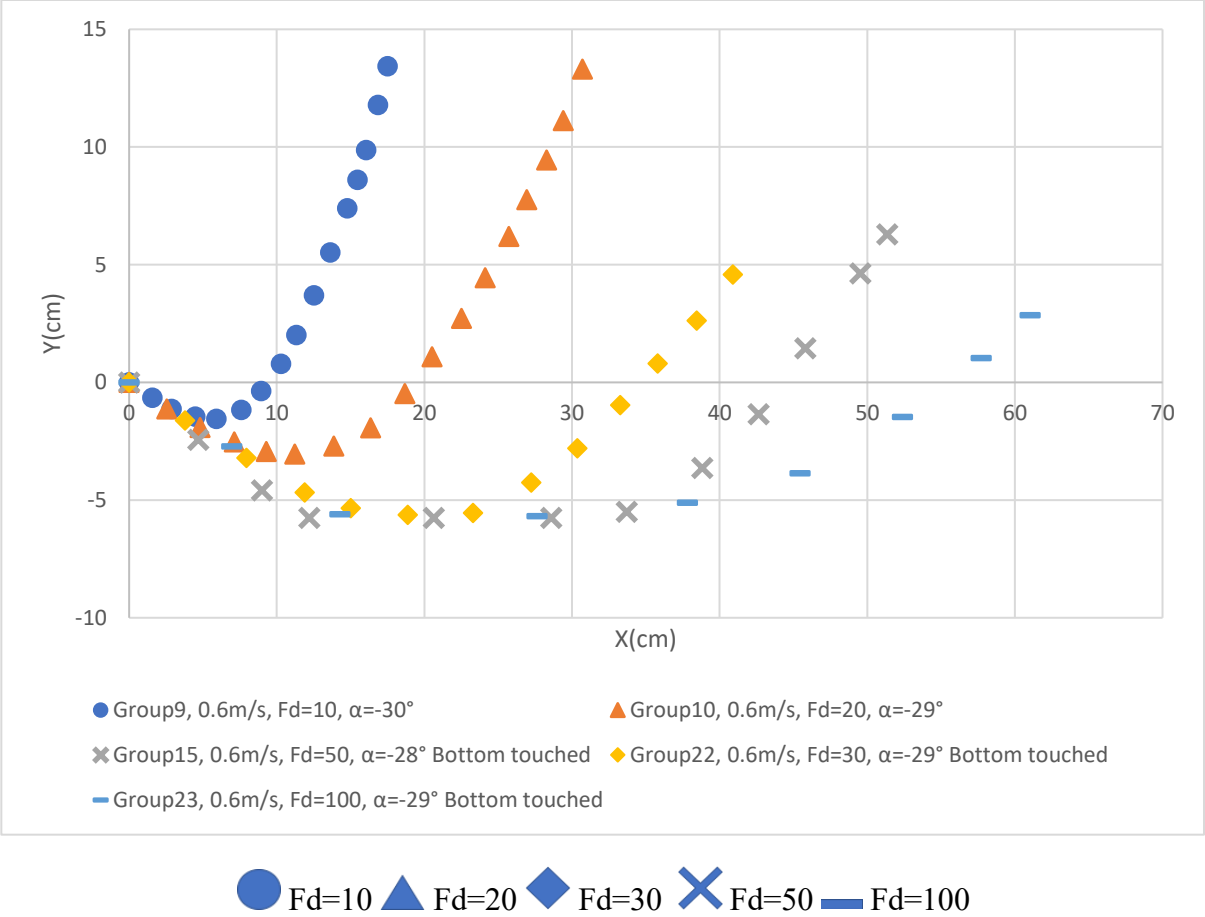

Fig.3.11 Trajectory comparison of jets with 0.6m/s, discharge angle around -30°.

Figure 3.11 presents five jets with initial velocity of 0.6m/s, discharge angle around -30° and Froude number varying from 10 to 100. The results shown in these curves demonstrate that with the increase of the Froude number, the jet moved longer and ended at a farther distance. Among the jets that did not touch the bottom, those with larger Froude number tended to reach a deeper returning point.

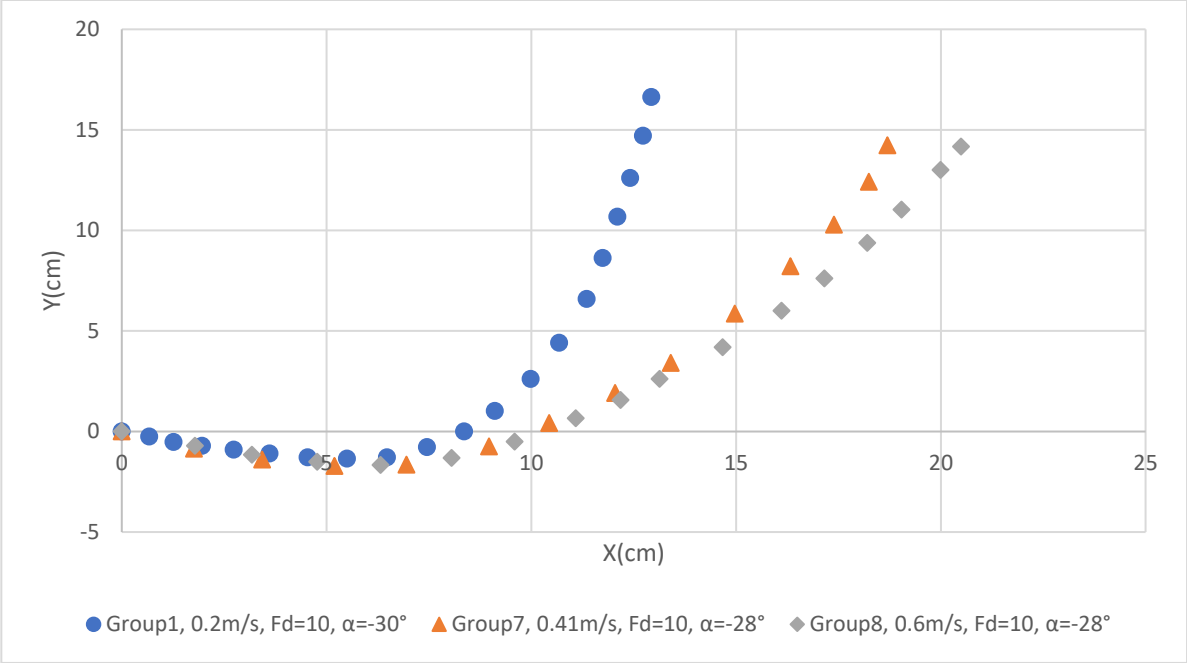

0.2m/s 0.41m/s 0.6m/s

(a)

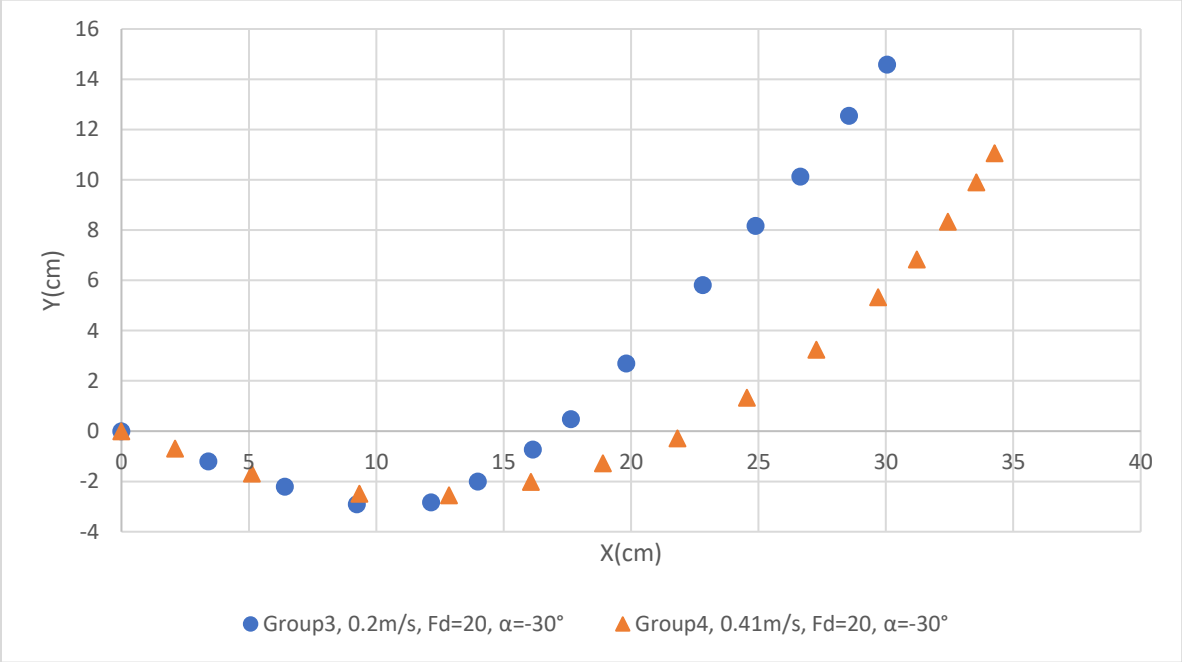

0.2m/s 0.41m/s

(b)

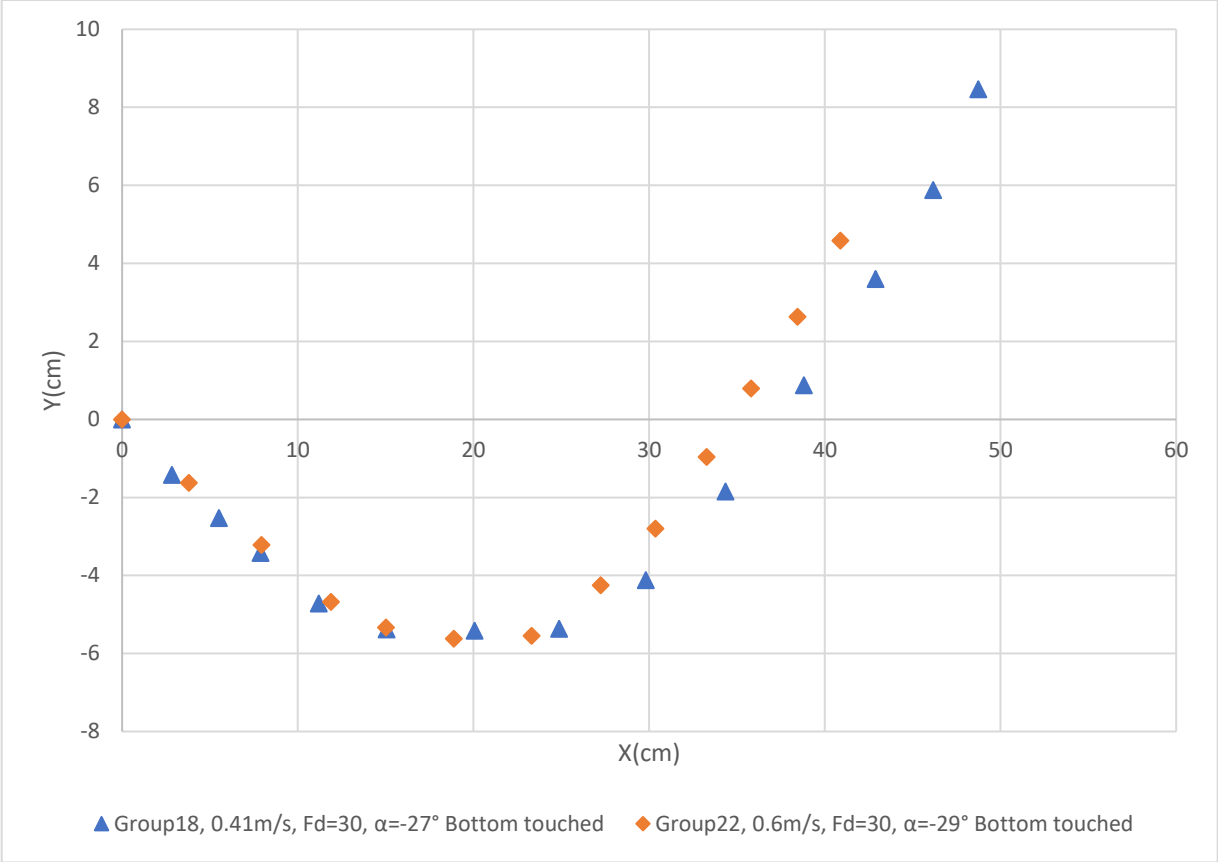
10
8
6
4
2
0
-2
-4
-6
-8
Y(cm)
0
10
20
30
40
50
60
X(cm)
Group18, 0.41m/s, Fd=30, α=-27° Bottom touched
Group22, 0.6m/s, Fd=30, α=-29° Bottom touched

0.41m/s 0.6m/s

(c)

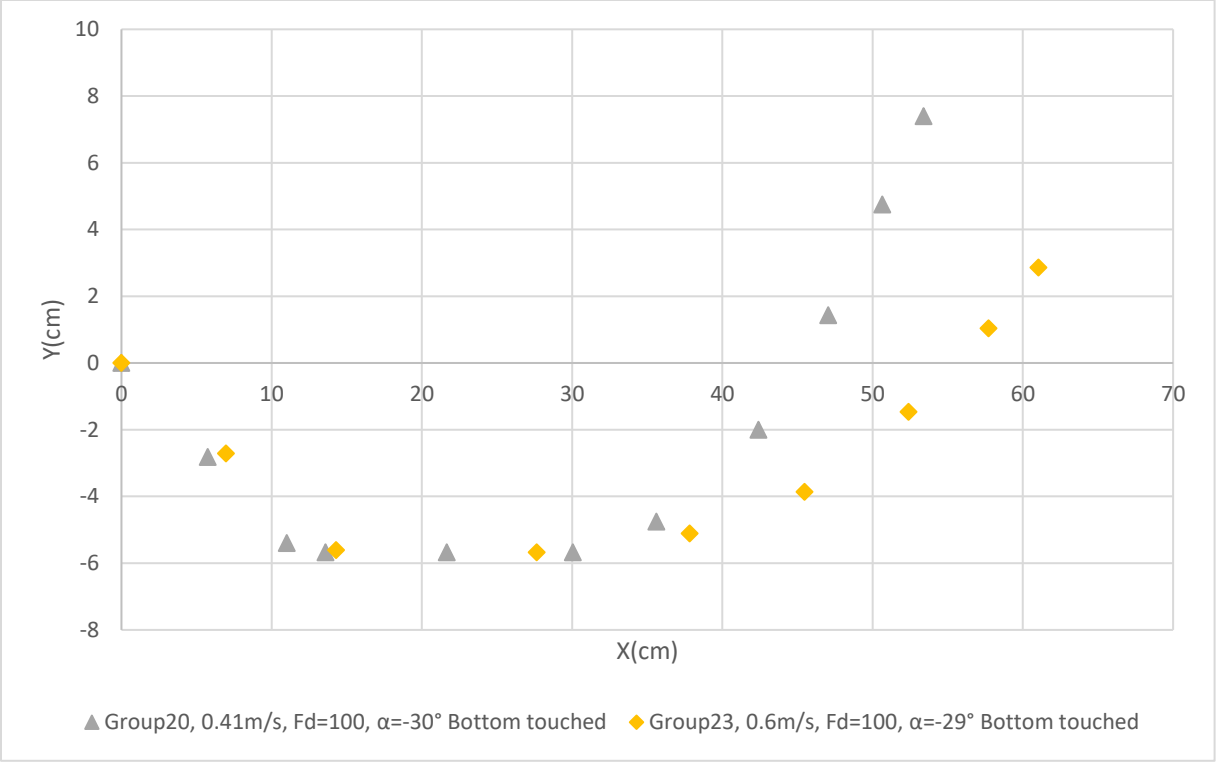

0.41m/s 0.6m/s

(d)

Fig.3.12 Trajectory comparison under different velocities with discharge around -30°(a)Fd=10, (b) Fd=20, (c) Fd=30, (d)Fd=100.

In the laboratory, all the experiments were performed under the same temperature and were carried out in a sequence organized by velocity, angle and Froude number. Reviewing four figures in Fig.3.12, cases with the same Froude number and different velocity were studied. Velocity did make contribution to the jet trajectory length. However, by definition, densimetric Froude number that considered initial velocity, nozzle diameter and density made it more important. As shown in previous figures, even with the change of the velocity, Froude number had a greater impact on the jet trajectory. In summary, Froude number could be used as a more influential parameter to predict the jet behaviour.

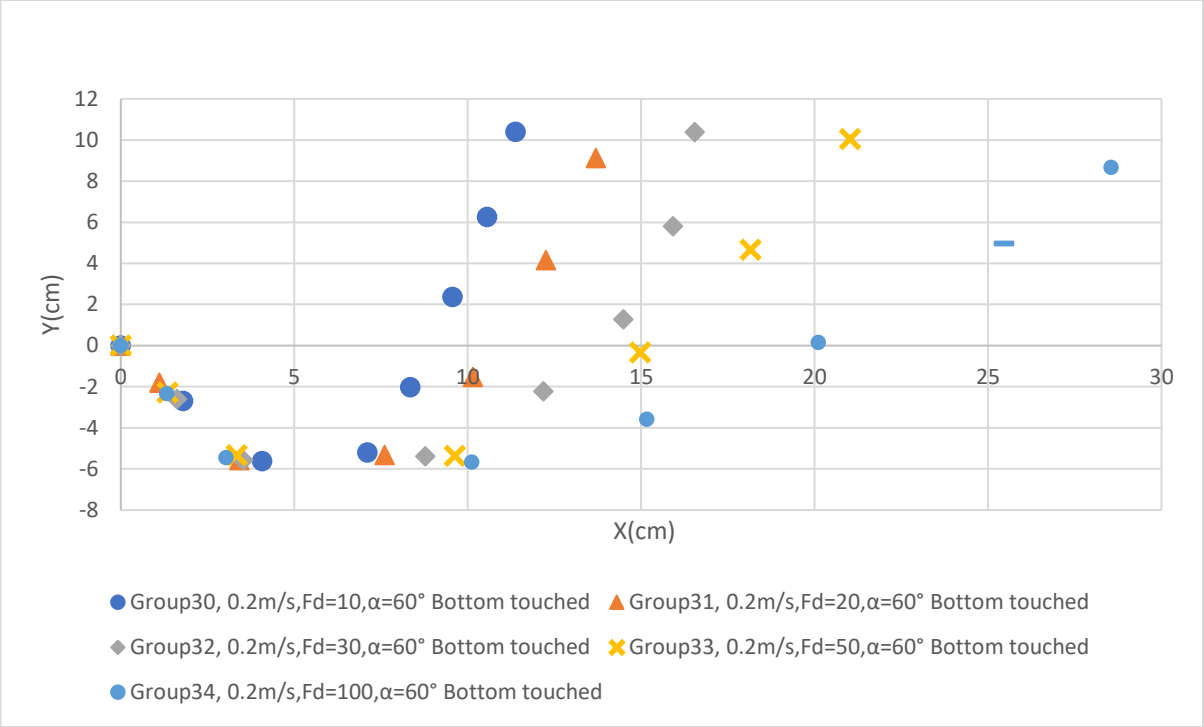

Fig.3.13 Trajectory comparison of jets with 0.2m/s, discharge angle around -60°, Fd=10−100.

Figure 3.13 displays the jet trajectories with downward angle around -60°, velocity of 0.2m/s and Froude number varying from 10 to 100. Even though all five jets touched the tank bottom, the graphs still revealed the significant role of Froude number on jet discharge shape. With the increase of Froude number, jets tend to show a longer and lower centerline, this helps enhance the dilution of the jet.

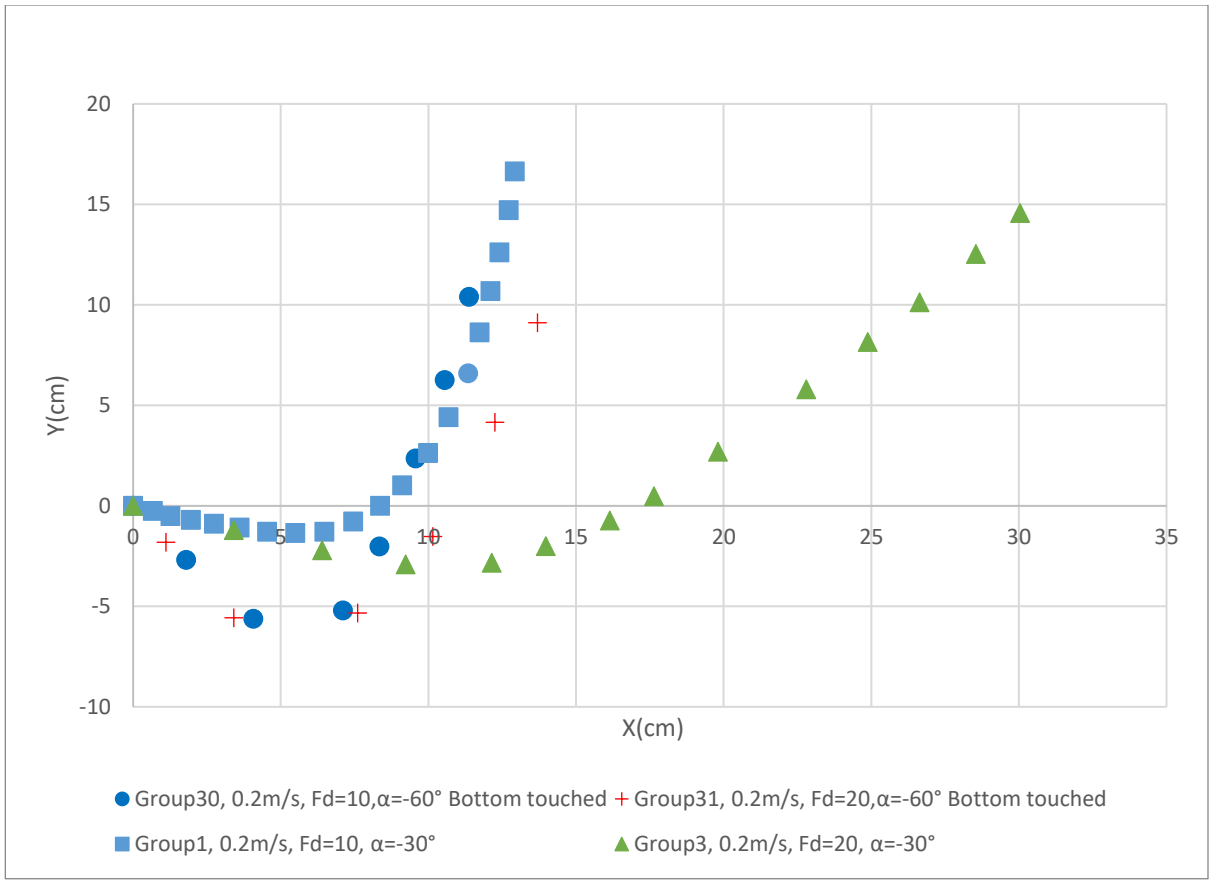

Fig.3.14 Trajectory comparison of jets with different angles

Figure 3.14 shows the centerline comparison of jet at different angle. However, due the confined depth of the tank, jets with 60° reached the bottom too early. But the other two jets with 30° did not touch the bottom. This blurs the effect of angle on buoyant jet behavior and make this comparison less meaningful.

Chapter 4 Numerical study

4.1 Introduction

In fluid dynamics filed, laboratory experiments have been widely applied. However, with the development of computational fluid dynamics, high demand of fluid movement prediction for environmental impact assessment has been observed. OpenFOAM is an open-source tool released in 2004 which is a powerful model that has become widely utilized on numerical simulations of various fluid dynamics problems.

In this chapter, a brief introduction of OpenFOAM will be presented. An optimized Reynolds Averaged Navier Stokes solver called pisoFoamIIII230 was employed for all numerical experiments in this investigation. Comparisons between laboratory experiments and numerical model results will be discussed at the end of this chapter.

4.2 Numerical approach and simulation setup

Governing equations:

The model uses three-dimensional RANS equations as the governing equations for incompressible fluids, as follows:

1. Continuity Equation

$$\frac{\partial u}{\partial x}+\frac{\partial v}{\partial y}+\frac{\partial w}{\partial z}=0 \tag{38}$$

2. Momentum Equations

$$\frac{\partial u}{\partial t} + u\frac{\partial u}{\partial x} + v\frac{\partial u}{\partial y} + w\frac{\partial u}{\partial z}$$
$$= \frac{1}{\rho}\frac{\partial P}{\partial x} + \frac{\partial}{\partial x}\left[\nu_{eff}\left(\frac{\partial}{\partial}\right)\right] + \frac{\partial}{\partial y}\left[\nu_{eff}\left(\frac{\partial}{\partial y}\right)\right] + \frac{\partial}{\partial z}\left[\nu_{eff}\left(\frac{\partial}{\partial z}\right)\right] \quad (39)$$

$$\frac{\partial v}{\partial t} + u\frac{\partial v}{\partial x} + v\frac{\partial v}{\partial y} + w\frac{\partial v}{\partial z} = \frac{1}{\rho}\frac{\partial P}{\partial x} + \frac{\partial}{\partial x}\left[\nu_{eff}\left(\frac{\partial v}{\partial x}\right)\right]$$
$$+ \frac{\partial}{\partial y}\left[\nu_{eff}\left(\frac{\partial v}{\partial y}\right)\right] + \frac{\partial}{\partial z}\left[\nu_{eff}\left(\frac{\partial v}{\partial z}\right)\right] - g\frac{\rho - \rho_0}{\rho} \quad (40)$$

(buoyancy term added to vertical momentum)

$$\frac{\partial w}{\partial t} + u\frac{\partial w}{\partial x} + v\frac{\partial w}{\partial y} + w\frac{\partial w}{\partial z}$$
$$= \frac{1}{\rho}\frac{\partial P}{\partial x} + \frac{\partial}{\partial x}\left[\nu_{eff}\left(\frac{\partial w}{\partial x}\right)\right] + \frac{\partial}{\partial y}\left[\nu_{eff}\left(\frac{\partial w}{\partial y}\right)\right] + \frac{\partial}{\partial z}\left[\nu_{eff}\left(\frac{\partial w}{\partial z}\right)\right] \quad (41)$$

Main parameters:

u, v and w: components of the mean velocity in the x , y and z directions, respectively

P: main fluid pressure

g: gravity acceleration

ρ: fluid density

ν_{eff}: effective kinematic viscosity ($\nu_{\text{eff}} = \nu_t + \upsilon$)

ν_t: turbulent kinematic viscosity

3.The time-history of the concentration and temperature are modelled using the advection-diffusion equation

$$\frac{\partial C}{\partial t} + u\frac{\partial C}{\partial x} + v\frac{\partial C}{\partial y} + w\frac{\partial C}{\partial z} = D\left(\frac{\partial^2 C}{\partial x^2} + \frac{\partial^2 C}{\partial y^2} + \frac{\partial^2 C}{\partial z^2}\right) \quad (42)$$

$$\frac{\partial T}{\partial t} + u\frac{\partial T}{\partial x} + v\frac{\partial T}{\partial y} + w\frac{\partial T}{\partial z} = k_{eff}\left(\frac{\partial^2 T}{\partial x^2} + \frac{\partial^2 T}{\partial y^2} + \frac{\partial^2 T}{\partial z^2}\right) \quad (43)$$

$$k_{eff} = \frac{\upsilon_t}{Pr_t} + \frac{\upsilon}{Pr} \tag{44}$$

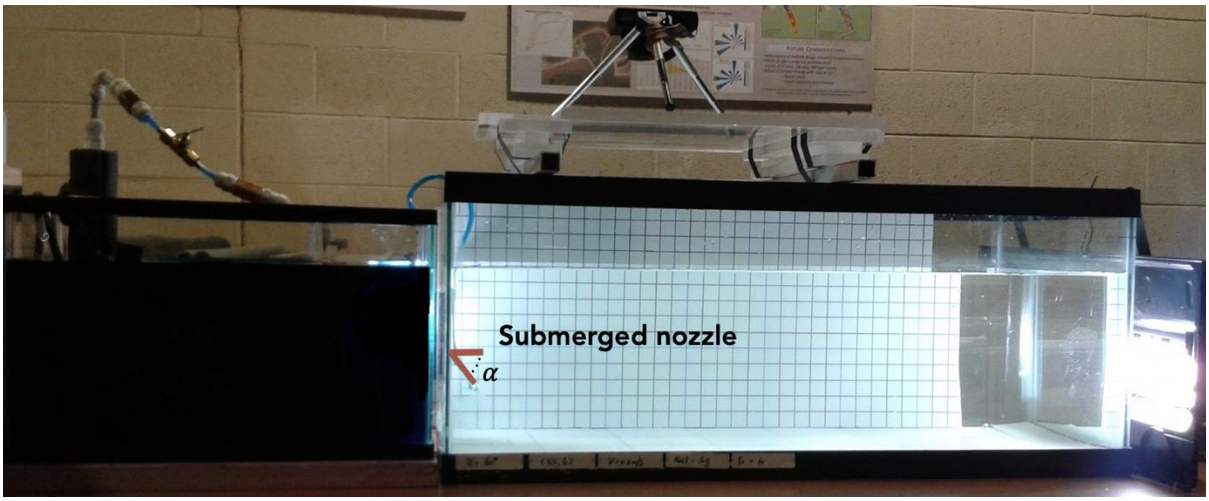

(a)

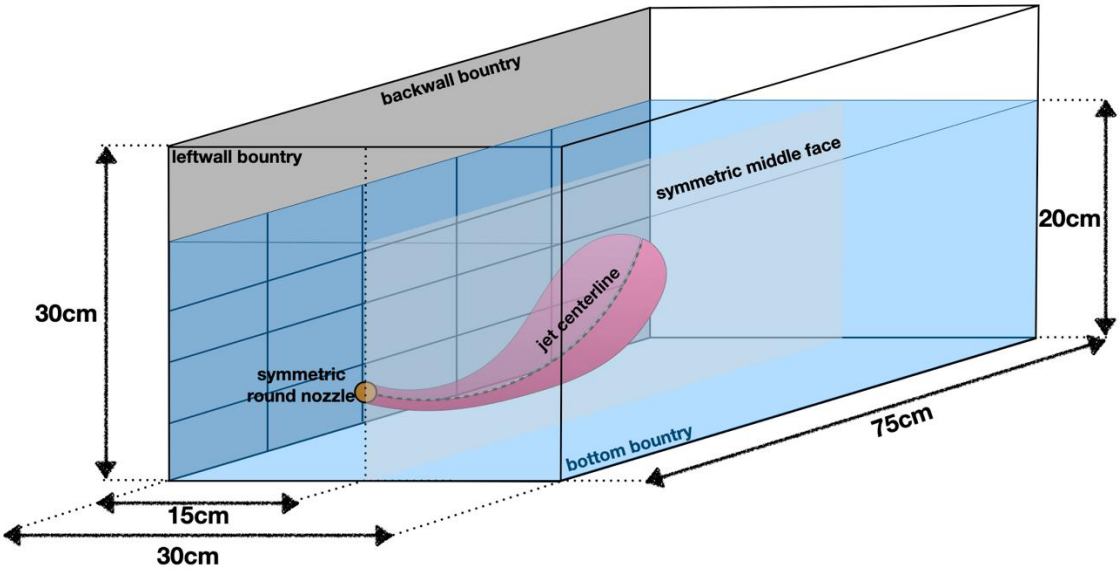

(b)

Fig. 4.1 Scheme of jet and ambient condition in laboratory experiment

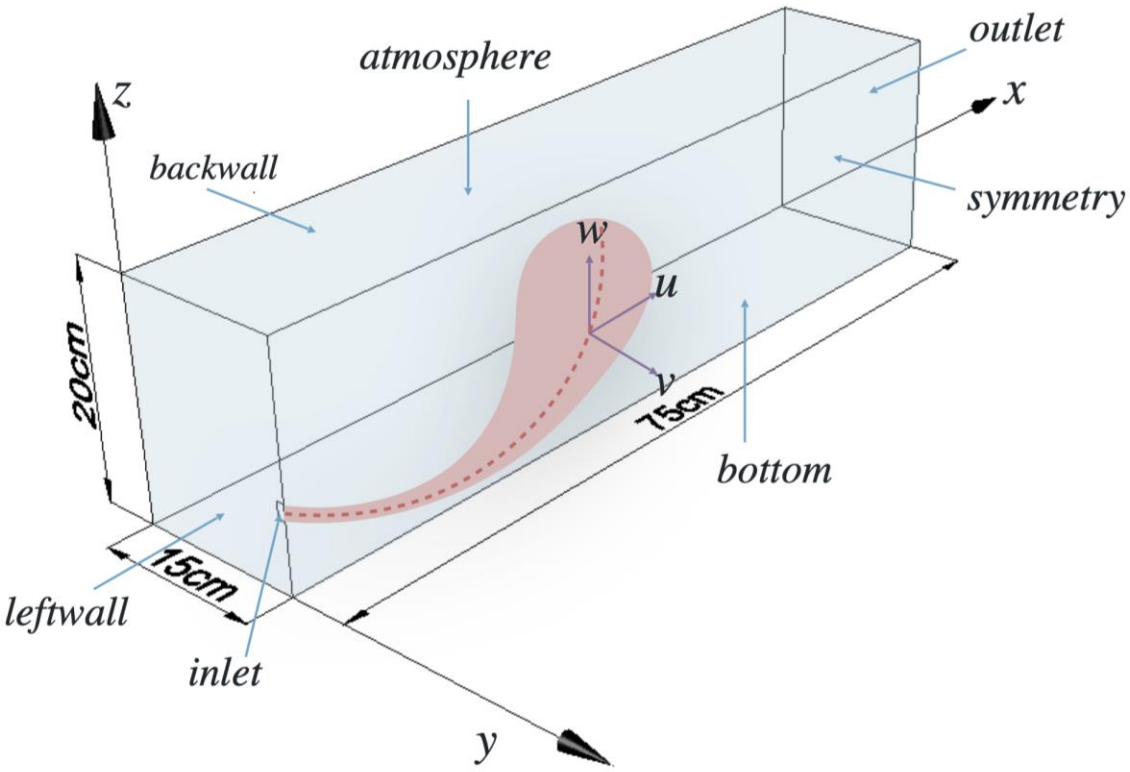

Fig.4.2 Scheme of jet and boundary condition in openFOAM (symmetric half tank)

Figure.4.1 shows a typical experimental setup. A buoyant jet discharged into a stagnant and saline fluid environment with a downward angle. It shows the size of the tank and the boundary conditions. The nozzle in the laboratory was located at the center of the left wall. The jet shape was symmetric by the middle plane between the front wall and the back wall Hence, in the OpenFOAM simulations (Fig.4.2)., only half of the tank was simulated. The simulations focused on the investigation of jet centerline trajectory. The front wall was replaced by a symmetry plane.

The density of the saline water was calculated using

$$\rho = \rho_t + AS + BS^{3/2} + CS \tag{45}$$

where

$$A = 8.24493 \times 10^{-1} - 4.0899 \times 10^{-3}T + 7.6438 \times 10^{-5}T^2 \\ -8.2467 \times 10^{-7}T^3 + 5.3875 \times 10^{-9}T^4 \tag{46}$$

$$B = -5.72466 \times 10^{-3} + 1.0227 \times 10^{-4}T - 1.6546 \times 10^{-6}T^2 \quad (47)$$

$$C = 4.8314 \times 10^{-4} \quad (48)$$

$$\rho_t = 999.842594 + 6.793952 \times 10^{-2}T - 9.095290 \times 10^{-3}T^2 + 1.001685 \times 10^{-4}T^3 - 1.120083 \times 10^{-6}T^4 + 6.536336 \times 10^{-9}T^5 \quad (49)$$

where

S: Salinity

T: jet initial temperature, T=18.8℃

ρ: ambient density, kg/m^3

ρ_t : density of water at temperature T. In this project, ρ_t is jet initial density, kg/m^3

In the present case

T=18.88°C, A=0.7698, B=-0.0044, C=0.0005

Time step size was calculated based on a courant number criterion for stability

$$DeltaT \leq \frac{d}{nU} \quad (50)$$

The boundary conditions were set as following:

$Ux = U\cos\alpha$

$U_y = -U\sin\alpha$

$$\kappa = 0.06U^2,, Huai\ (2010) \quad (51)$$

$$\varepsilon = \frac{0.06U^3}{D}, Huai\ (2010) \quad (52)$$

$$S = \frac{salt\ weight}{Water\ weight} \quad \left(\frac{g}{kg}\right) \quad (53)$$

Table. 4.1 Numerical simulation boundary conditions and parameter settings in the 0 folder

Boundry walls	S	T	U	P	E	K	Rho
internalfield	S_a	$T_0 = 18.8℃$	(1e-10 0 0)	ZeroGradient	$\varepsilon = \frac{0.06U^3}{D}$	$\kappa = 0.06U^2$	ρ_a(ambient)
inlet	$S_0 = 0$	$T_0 = 18.8℃$	(U cos α U sin α 0)	ZeroGradient	$\varepsilon = \frac{0.06U^3}{D}$	$\kappa = 0.06U^2$	ρ_0(jet)
outlet	ZeroGradient	ZeroGradient	ZeroGradient	ZeroGradient	ZeroGradient	ZeroGradient	ZeroGradient
leftwall	ZeroGradient	ZeroGradient	(0 0 0)	ZeroGradient	epsilonwallfunction:0.1	kqRwallfunction:0.1	ZeroGradient
backwall	ZeroGradient	ZeroGradient	(0 0 0)	ZeroGradient	epsilonwallfunction:0.1	kqRwallfunction:0.1	ZeroGradient
bottom	ZeroGradient	ZeroGradient	(0 0 0)	ZeroGradient	epsilonwallfunction:0.1	kqRwallfunction:0.1	ZeroGradient
symmetry	Symmetryplane						
atmosphere	Symmetryplane						

(a)

Group	α	Fd	U(m/s)	Ux(m/s)	Uy(m/s)	κ huai(2010)	ε huai(2010)	ρ_0(jet)	ρ_a(ambient)	S_a	T(°C)
1	-28.89°	10	0.2	0.1751	-0.0966	0.0024	0.012	998.446	1006.1929	10.243	18.8
2	-31.29°	10	0.406	0.3469	-0.2109	0.0096	0.0098	998.446	1028.8634	40.982	18.8
3	-29.03°	20	0.2	0.1749	-0.0971	0.0024	0.012	998.446	1000.4117	2.575	18.8
4	-31.87°	20	0.406	0.3448	-0.2144	0.0096	0.0098	998.446	1006.4378	10.570	18.8
5	-24.41°	20	0.2	0.1821	-0.0827	0.0024	0.012	998.446	1000.4117	2.575	18.8
6	-28.88°	30	0.2	0.1751	-0.0966	0.0024	0.012	998.446	999.3313	1.156	18.8
8	-27.26°	10	0.6	0.5334	-0.2748	0.0216	0.0330	998.446	1060.7898	1.156	18.8
9	-30.69°	10	0.6	0.5160	-0.3062	0.0216	0.0330	998.446	1060.7898	85.431	18.8
10	-29.15°	20	0.6	0.5240	-0.2923	0.0216	0.0330	998.446	1015.5423	22.815	18.8
18	-27.04°	30	0.406	0.3616	-0.1846	0.0096	0.0098	998.446	1002.0358	4.718	18.8
20	-30.12°	100	0.406	0.3512	-0.2037	0.0096	0.0098	998.446	998.7706	0.423	18.8
22	-28.63°	30	0.6	0.5266	-0.2875	0.0216	0.0330	998.446	1006.2092	10.265	18.8
23	-28.98°	100	0.6	0.5249	-0.2907	0.0216	0.0330	998.446	999.1617	0.934	18.8

(b)

d/nU				
U	n=75	n=150	n=300	n=600
0.2	0.0026	0.0013	0.0007	0.0003
0.406	0.0013	0.0007	0.0003	0.0002
0.6	0.0009	0.0004	0.0002	0.0001

(c)

In the preparation stage of numerical studies, the parameters were set with consideration of the laboratory experimental settings. Room temperature in the laboratory was measured at 18.8℃. Salinity of the jet and ambient were calculated after the selection of Froude number, which varied from 10 to 100. Table. 4.1 shows the dominant initial parameters of simulations.

4.3 About CFD and OpenFOAM

In fluid flow research area, computational fluid dynamics (CFD) is a widely used method which takes advantage of numerical solutions and data structures to solve problems. With the rapid progression of computer technology and the increase of computational ability, capacity and efficiency, CFD has become a more economic and accurate choice to investigate flow behaviors by using numerical simulations.

Since 2004, OpenFOAM (Open Field Operation and Manipulation) became one of the most widely used tool to solve computational fluid dynamic problems. It is free, flexible and easily applicable to a wide range of problems. It is widely considered to be the most useful open-source software that is widely used by engineers and researchers in academic applications and engineering problems. OpenFOAM has a wide range of applications to solve complex fluid flow problems, including turbulence, heat transfer, aero hydrodynamics, chemical reactions and even vascular hydrodynamics in medical science.

In this study, OpenFOAM was used to inspect the incompressible buoyant jet via numerical simulations in comparison with experimental results. The objective was to understand the accuracy and applicability of numerical simulations for jet movement prediction in such applications.

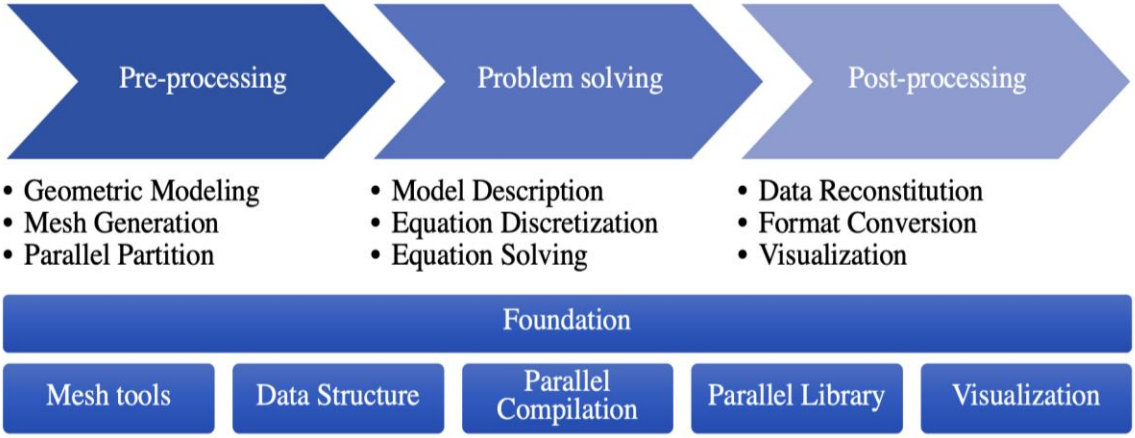

Fig.4.3 Workflow of numerical simulation in openFOAM

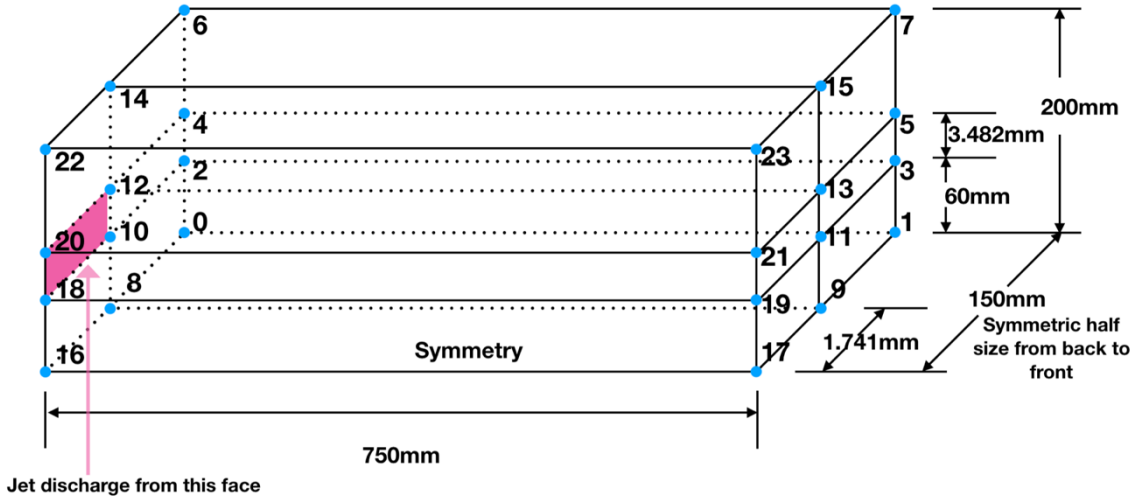

Fig.4.4 BlockMesh definition of half of the tank 2 (from backwall to middle face) and initial jet location.

In a typical openFOAM case, three main steps are considered (Figure. 4.3), including Pre-processing, Problem solving and Post-Processing. Everything starts from a good geometry (Fig.4.4) and mesh generation (Fig.4.5). In this project, mesh size was chosen to be narrow near the nozzle and coarse in locations far from the nozzle. This could increase the accuracy in calculation within jet area, while also save computational time for regions far from the boundary area where jet was not reached. This information was defined in blockMeshDict file in Constant

folder, within which the transport properties and turbulence model were also defined. An LRR turbulence model was chosen, as it is a second order accurate model and is expected to perform accurately. An optimized pisoFoam solver (pisoFoamIIII230) was applied for all simulations (Appendix B). Folder 0 includes the initial parameter values and boundary condition settings for epsilon, k, S, rho, U and P.

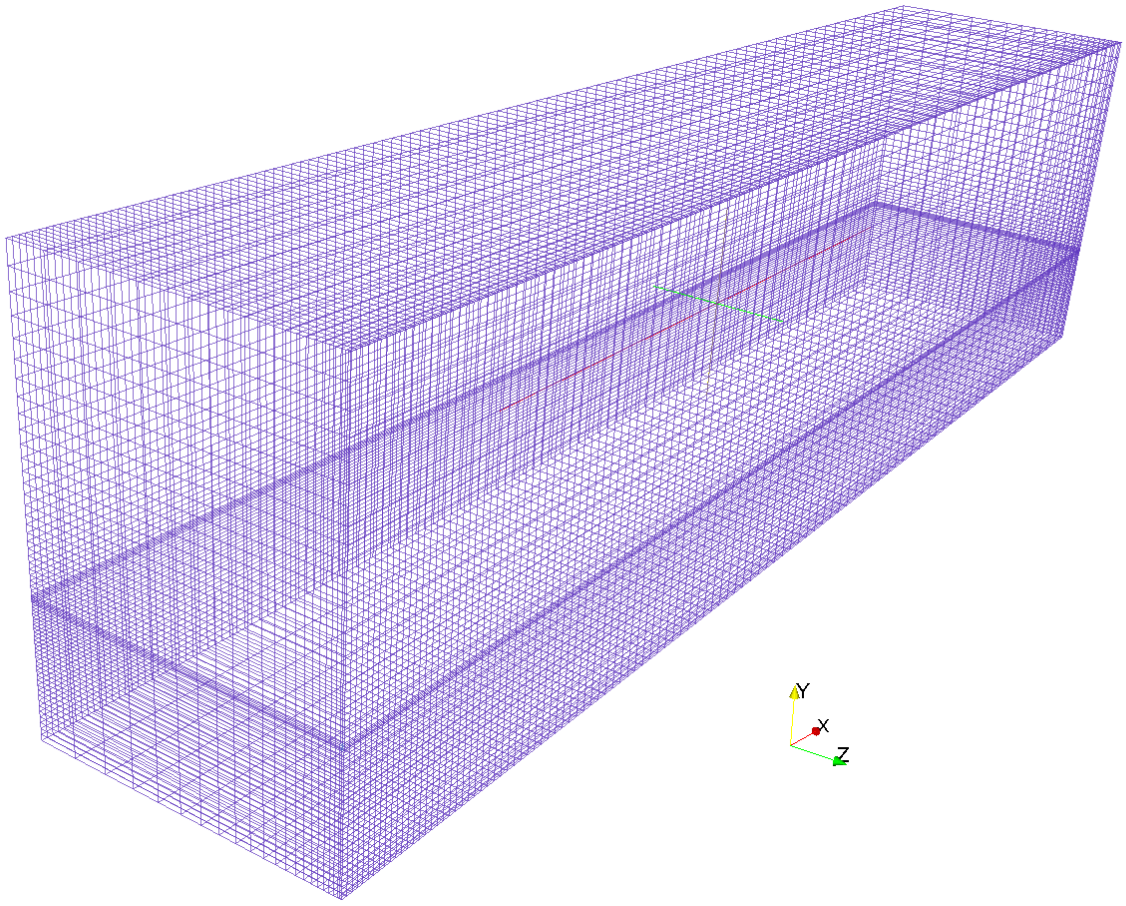

(a)

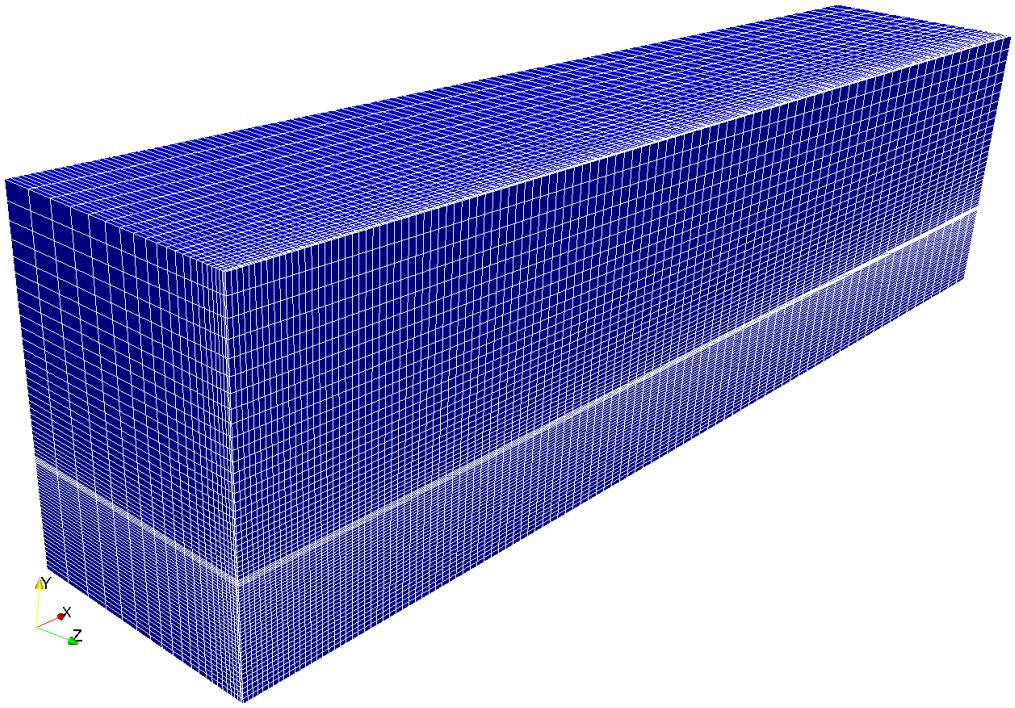

(b)

Fig.4.5 Fine mesh design in this study(a)Wireframe view(b)Surface with wireframe view

4.4 Launder-Reece-Rodi (LRR) Model

Before the computational simulation was introduced as a research method to study fluid discipline and characteristics, field studies and laboratory experiments were the main techniques. In OpenFOAM along with the postprocessing tool ParaView, the simulation results are convenient to view and analyse. The precision of the results relies on the mesh size and chosen turbulence model.

Since the Navier–Stokes system of equations was published in the 19th Century to describe the fluid flow, it enlarged the research possibilities to investigate or predict various flow fields by simulation. However, to get the analytical solution or direct numerical solution of that system is not realistic because it needs a huge amount of time for calculations and requires a lot of

computational resources of computers which is not feasible. Fortunately, a lot of practical engineering flow problems are concerned with macro features of the flow field rather than micro feature. In other words, average flow features are needed. Considering this, Reynolds proposed the concept of averaging treatment on Navier–Stokes equations, that is how Reynolds Average Navier–Stokes (RANS) model was developed.

In RANS, the turbulence effect was presented as "Reynolds stress term $-\rho\overline{u_i{}'u_j{}'}$". The turbulence models are mainly aimed at calculating this Reynolds stress term. However, turbulence models might not always be able to get the exact Reynolds stress value. With the introduction of more differential equations, as long as the number of equations is consistent with the number of unknowns, it is possible to estimate Reynolds stresses. In turbulence models, Reynold stresses are not the only unknowns that are concerned. Other aspects including turbulent energy generation and dissipation, etc., are also sought. Hence, turbulence models play an important role in predicting the flow behavior numerically by calculating the influence of small-scale movements on large-scale turbulence.

Let us rewrite the Navier–Stokes system of equations:

$$\frac{du_i}{dt} = \frac{1}{\rho}\frac{\partial P}{\partial x_i} + \frac{1}{\rho}\frac{\partial}{\partial x_j}\left(\mu\frac{\partial u_i}{\partial x_j}\right) \tag{54}$$

Reynolds-Averaged Navier–Stokes equation are then written are

$$\frac{d\overline{u_i}}{dt} = \frac{1}{\rho}\frac{\partial P}{\partial x_i} + \frac{1}{\rho}\frac{\partial}{\partial x_j}\left[\overline{\tau_{ij}} + \left(-\rho\overline{u_i{}'u_j{}'}\right)\right] \tag{55}$$

Launder-Reece-Rodi (LRR) model, a typical Reynolds Averaged Navier–Stokes model, is a Reynolds stress model that was used in this project. The LRR model was developed by Launder, Reece, and Rodi in 1975. It can be used to calculate Reynolds stresses and is written as

$$\frac{D\overline{u_i}\overline{u_j}}{Dt} = \frac{\partial\overline{u_i{}'u_j{}'}}{\partial t} + \overline{u_k}\frac{\partial\overline{u_i{}'u_j{}'}}{\partial x_k} = D_{ij}{}^{v} + D_{ij}{}^{T} + \emptyset_{ij} + P_{ij} + \varepsilon_{ij} \tag{56}$$

Various terms in this model are provided below:

Viscous diffusion:

$$D_{ij}{}^{v} = v\frac{\partial^2 \overline{u_i{}' u_j{}'}}{\partial x_k x_k} \tag{57}$$

Turbulent diffusion:

$$D_{ij}{}^{T} = \frac{\partial}{\partial x_l}\left(C_s \frac{\varepsilon}{k}\overline{u_i u_k}\frac{\partial \overline{u_i u_j}}{\partial x_k}\right) \tag{58}$$

$C_s = 0.22$

Production:

$$P_{ij} = -\overline{u_i{}' u_k{}'}\frac{\partial \overline{u_j}}{\partial x_k} - \overline{u_j{}' u_k{}'}\frac{\partial \overline{u_i}}{\partial x_k} \tag{59}$$

Dissipation:

$$\varepsilon_{ij} = -2v\overline{\frac{\partial u_i{}'}{\partial x_k}\frac{\partial u_j{}'}{\partial x_k}} \tag{60}$$

$$\frac{\partial}{\partial} + \overline{u_k}\frac{\partial}{\partial x_k} = C_{\varepsilon 1}\frac{P_k \varepsilon}{k} - C_{\varepsilon 2}\frac{\varepsilon^2}{k} + \frac{\partial}{\partial x_j}\left(C_\varepsilon \frac{k}{\varepsilon}\overline{u_i{}' u_j{}'}\frac{\partial \varepsilon}{\partial x_j}\right) \tag{61}$$

$C_{\varepsilon 1} = 1.44, C_{\varepsilon 2} = 1.90$

4.5 Simulation results and comparison with laboratory experiments

The results of for 13 groups of cases of numerical simulations and jet laboratory experiments in this project provided an insight into how jet moved. The discharge angles were precisely set based on the measured values from video records in the actually experimental part of this thesis. As compared results shown from Fig.4.6 to Fig.4.13, all of these jet simulations using the LRR model and pisoFoamIIII230 solver illustrated a reasonable agreement with laboratory experimental results. Summary speaking, LRR model and pisoFoamIIII230 solver were proved to work well on simulating and predicting the submerged inclined positively buoyant jets' behavior.

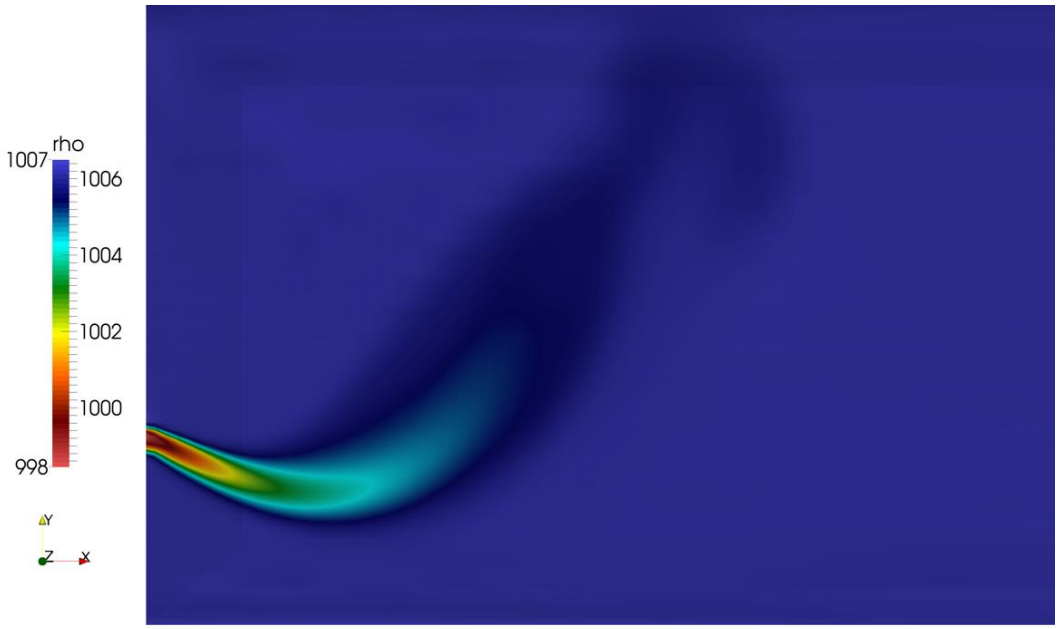

(a) LRR Simulation

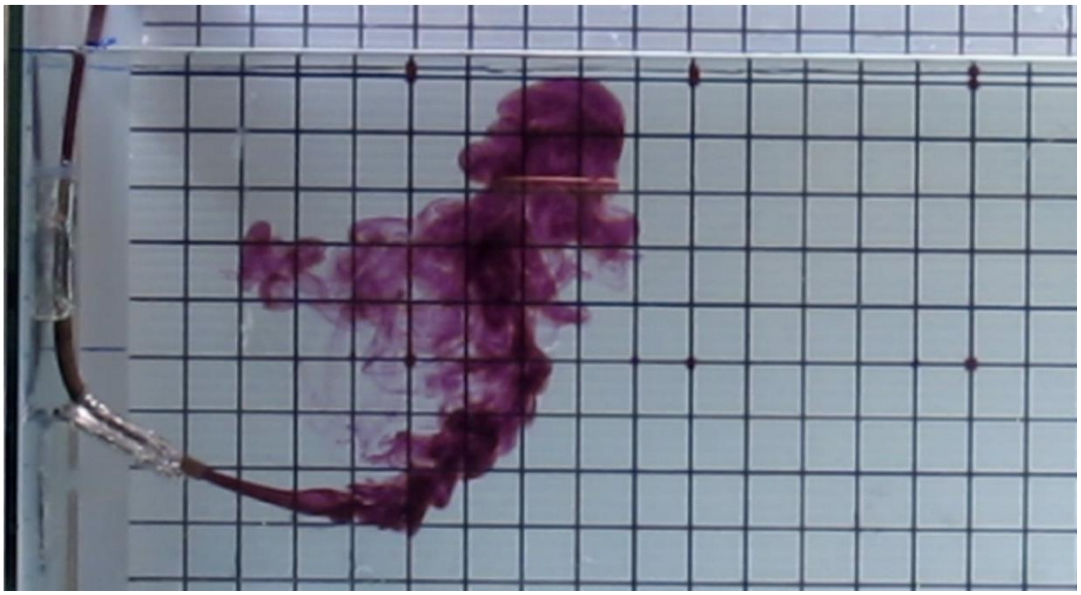

(b) Laboratory Experiment

Fig.4.6 Comparison between numerical simulation and laboratory experiment for Group1 (0.2 m/s, Fd=10, α =-28.89°)

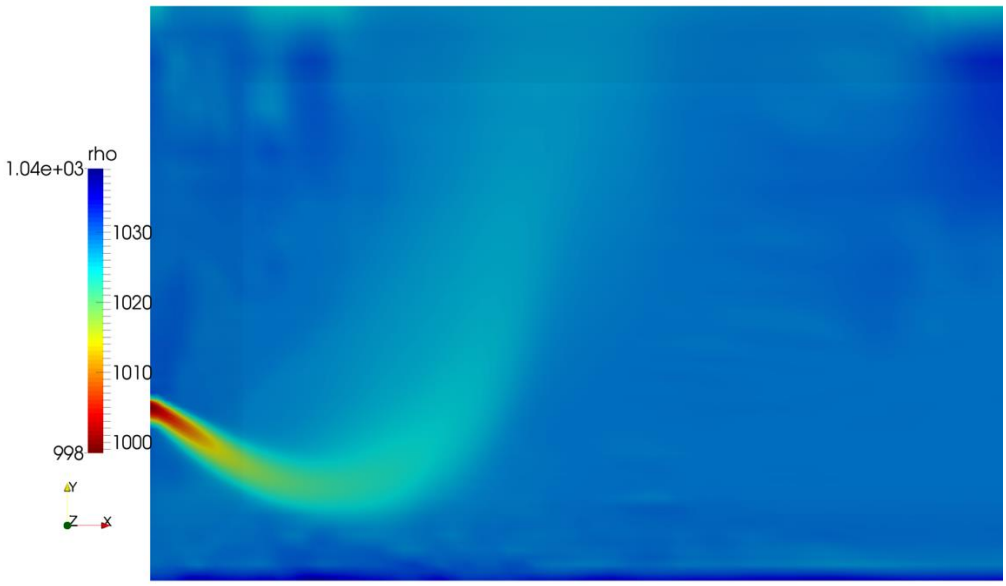

(a) LRR Simulation

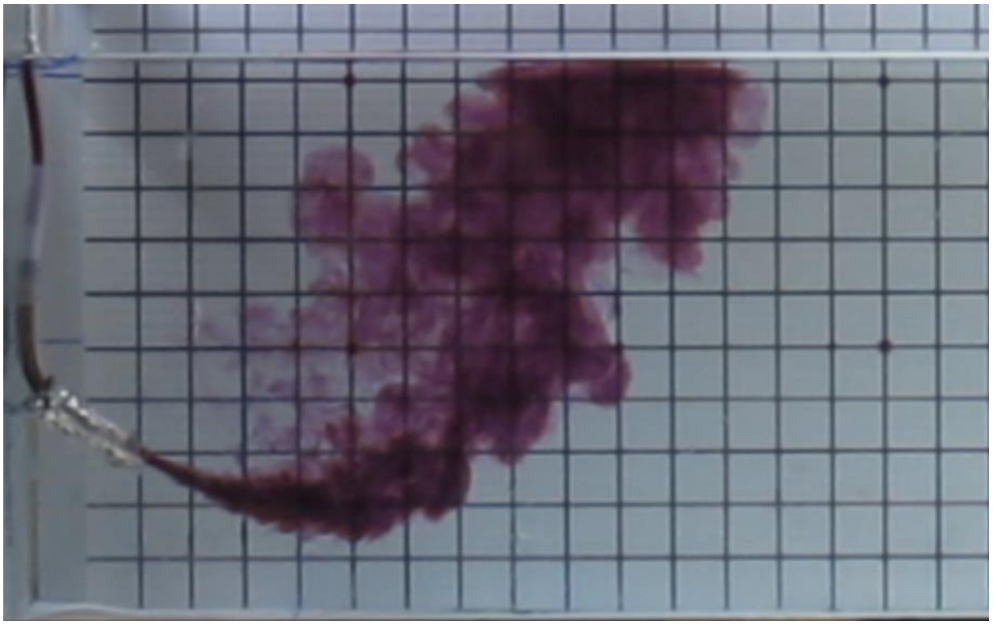

(b) Laboratory Experiment

Fig.4.7 Comparison between numerical simulation and laboratory experiment for Group2 (0.4 m/s, Fd=20, α =-31.29°)

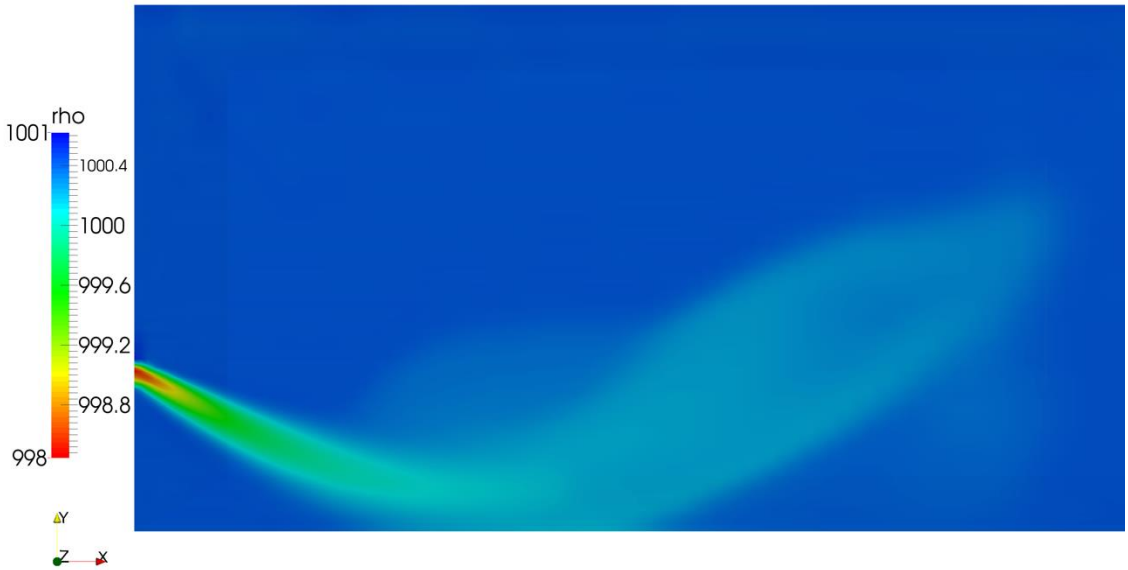

(a) LRR Simulation

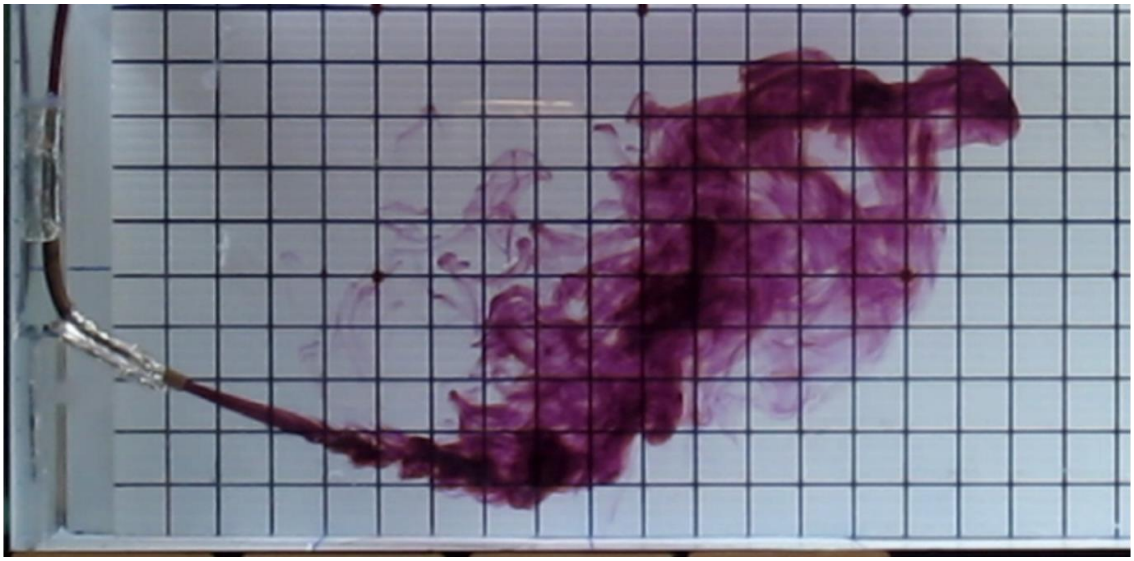

(b) Laboratory Experiment

Fig.4.8 Comparison between numerical simulation and laboratory experiment for Group 3 (0.2 m/s, Fd=20, α =-29.03°)

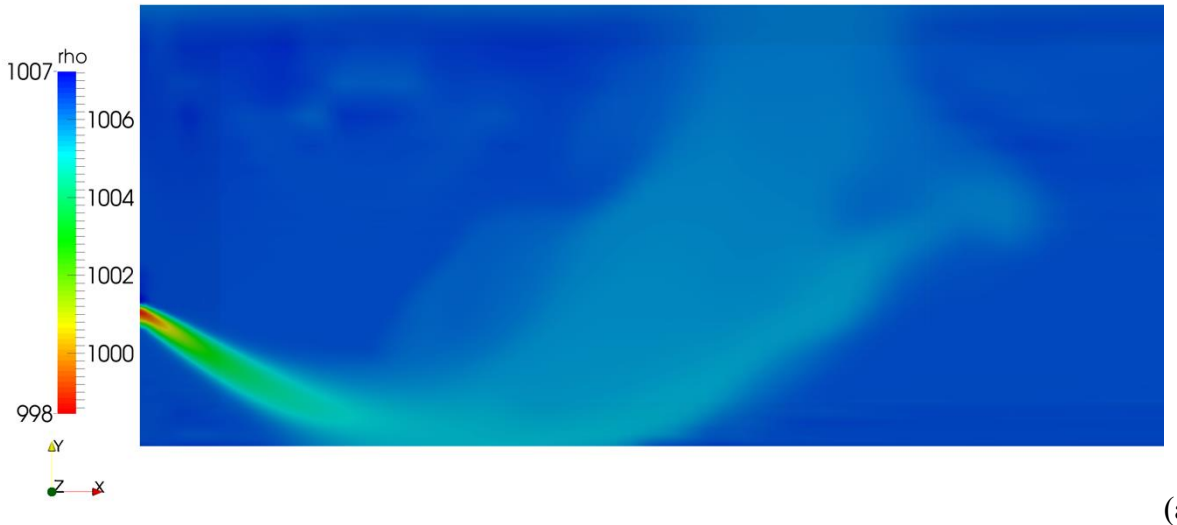

(a)

(a) LRR Simulation

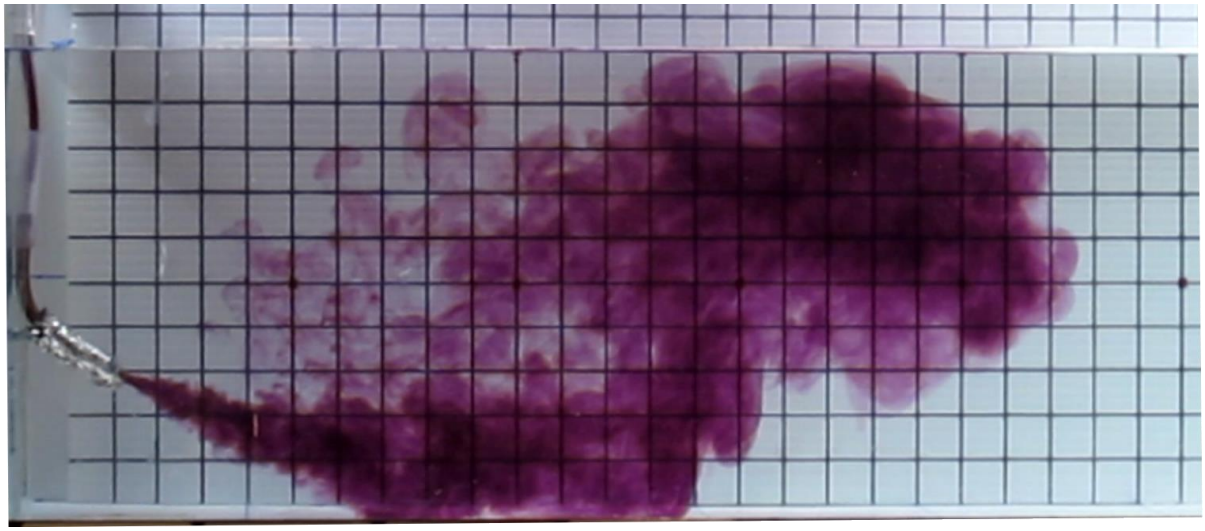

(b) Laboratory Experiment

Fig.4.9 Comparison between numerical simulation and laboratory experiment for Group 4 (0.4 m/s, Fd=20, α =-31.87°)

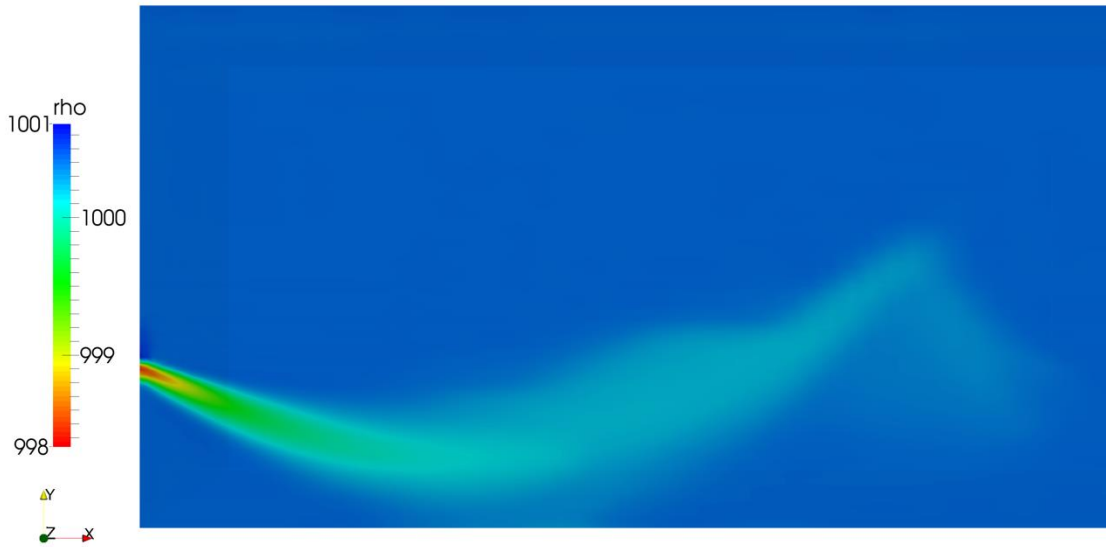

(a) LRR Simulation

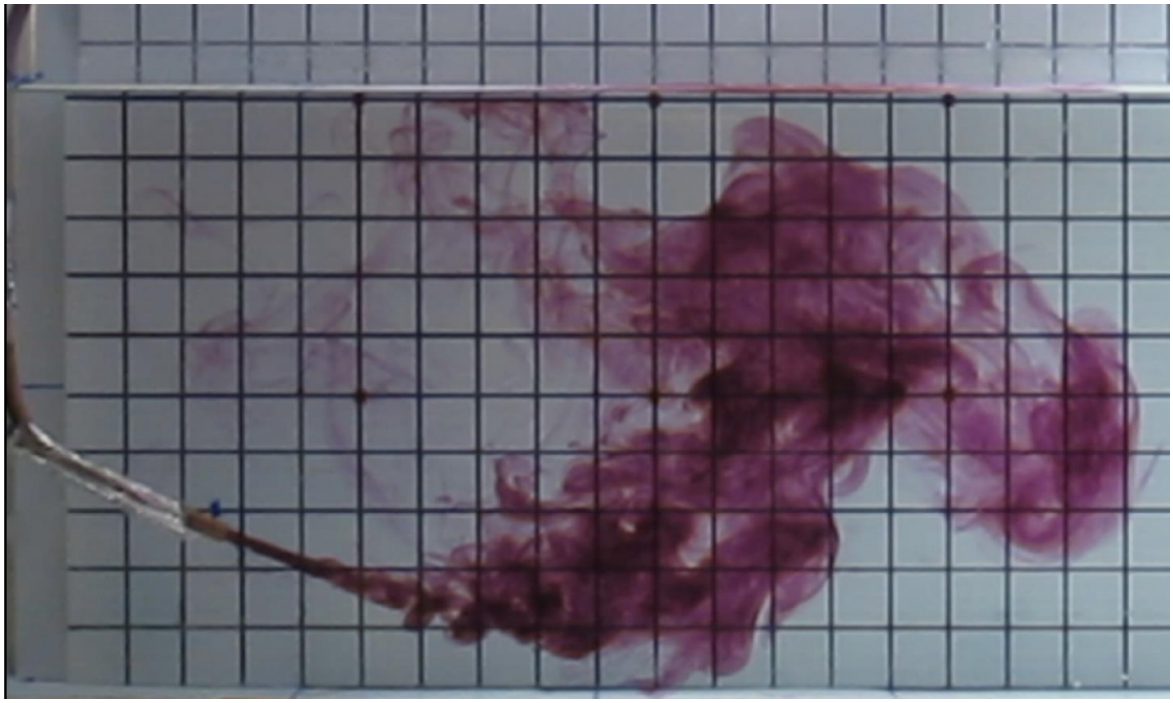

(b) Laboratory Experiment

Fig.4.10 Comparison between numerical simulation and laboratory experiment for Group 5 (0.2m/s, Fr=20, α =-24.41°)

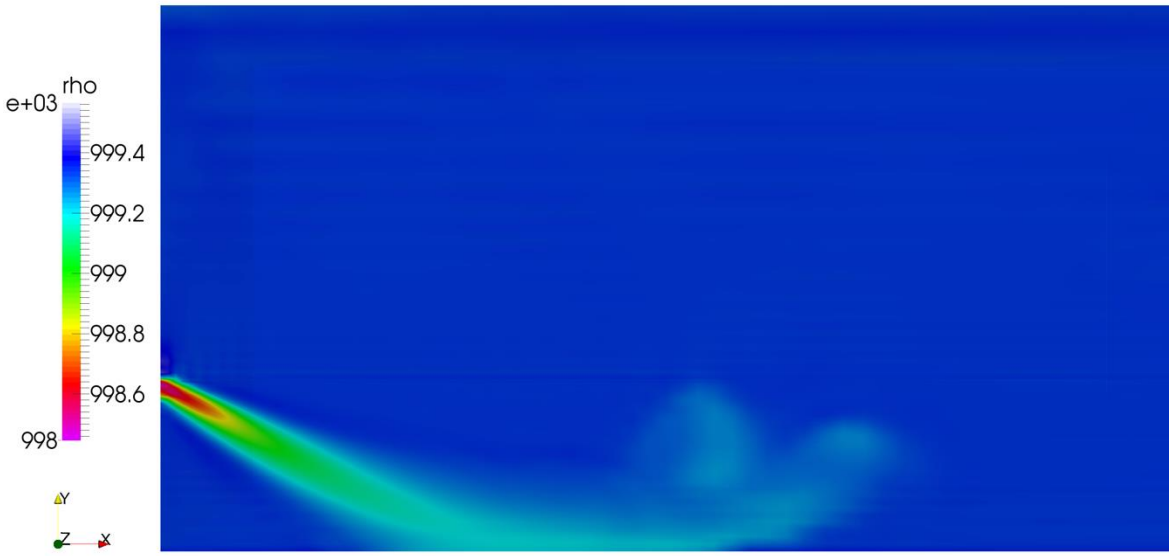

(a) LRR Simulation, 29s

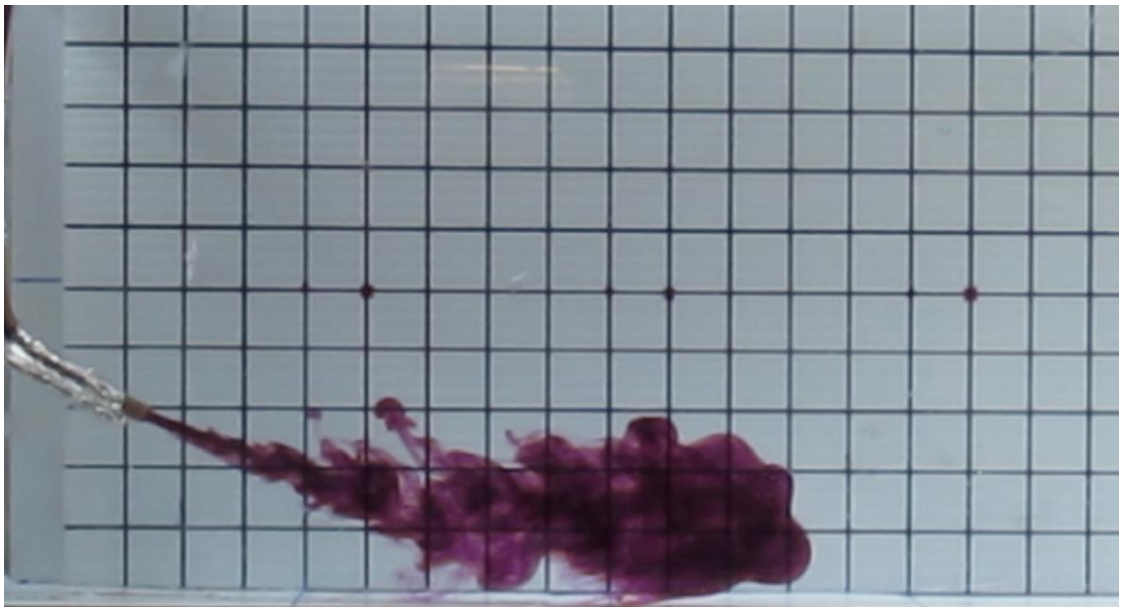

(b) Laboratory Experiment, 29s

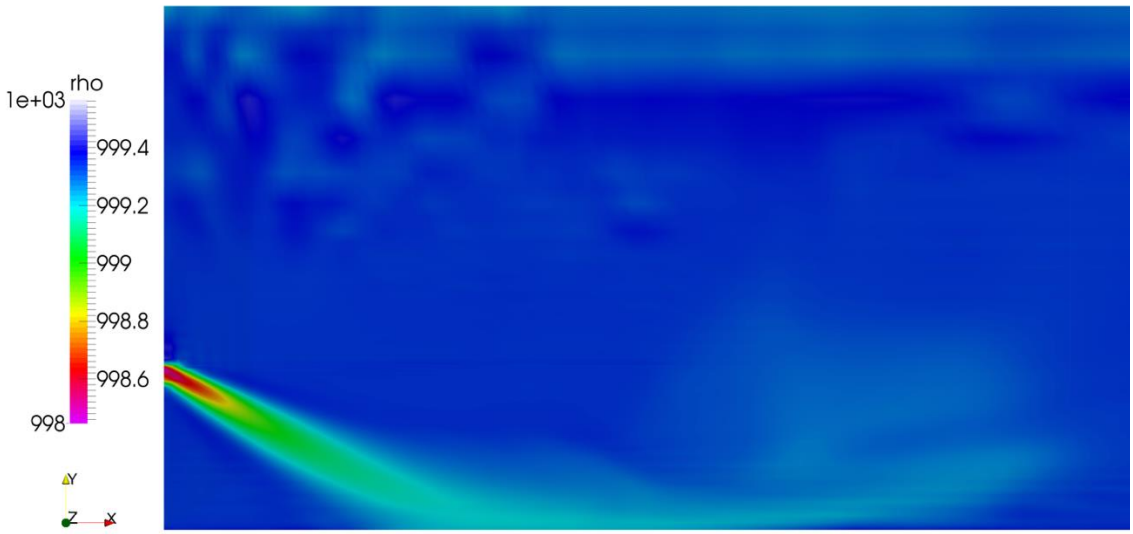

(c) LRR Simulation, 65s

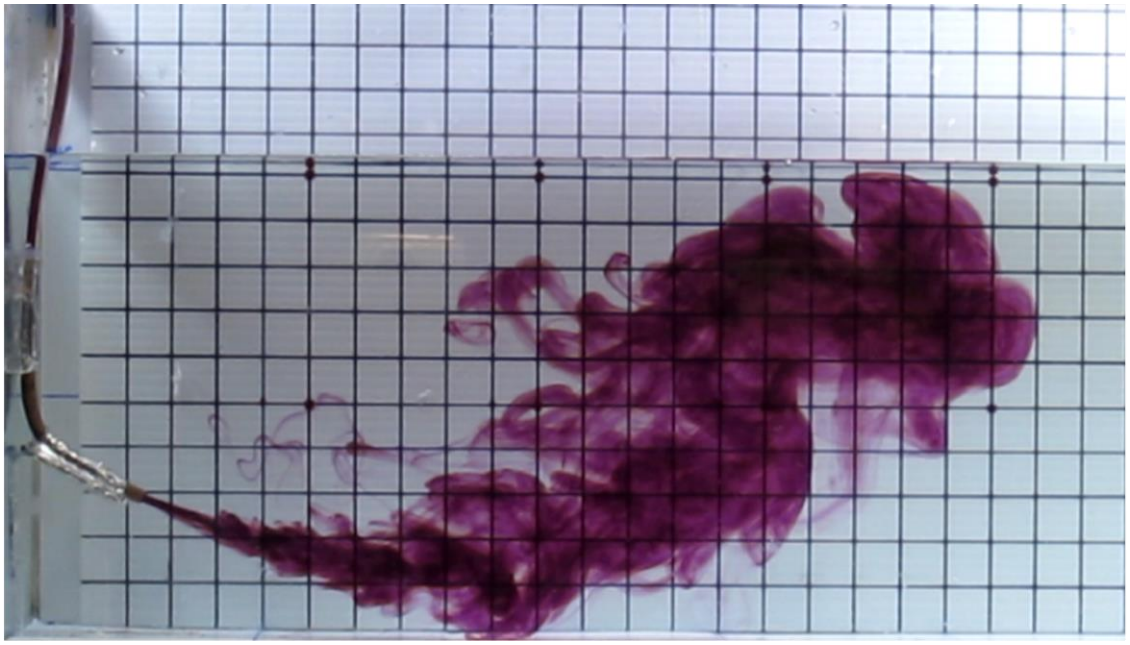

(d) Laboratory Experiment, 65s

Fig.4.11 Comparison between numerical simulation and laboratory experiment for Group 6 (0.2 m/s, Fd=30, α =-28.88°)

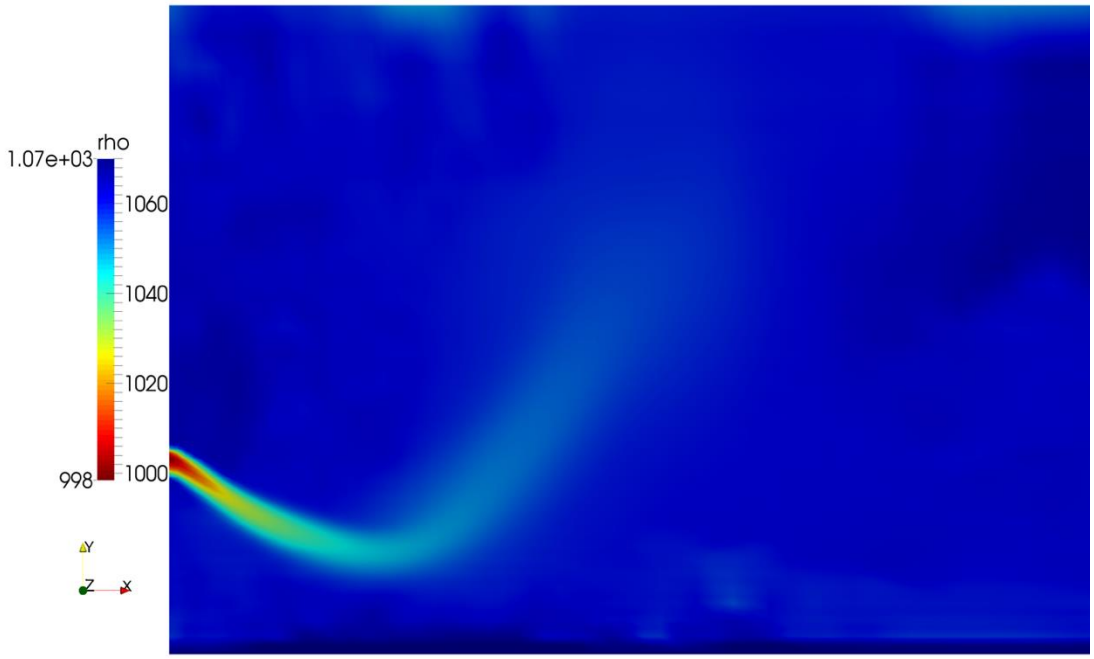

(a) LRR Simulation

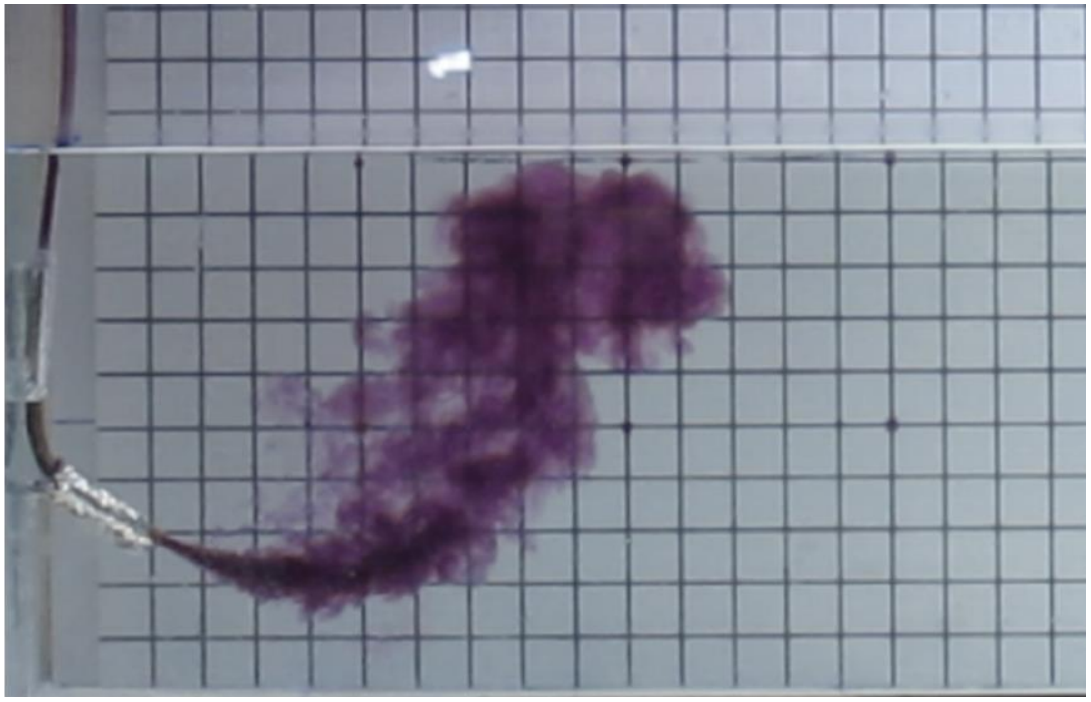

(b) Laboratory Experiment

Fig.4.12 Comparison between numerical simulation and laboratory experiment for Group 9 (0.6 m/s, Fd=10, α=-30.69°)

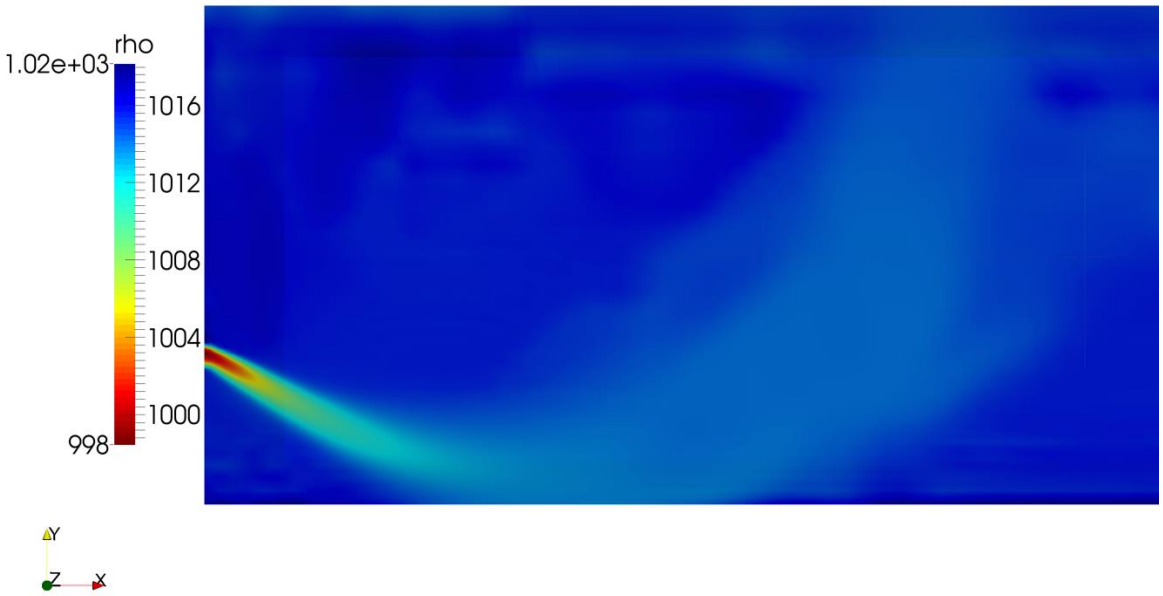

(a) LRR Simulation

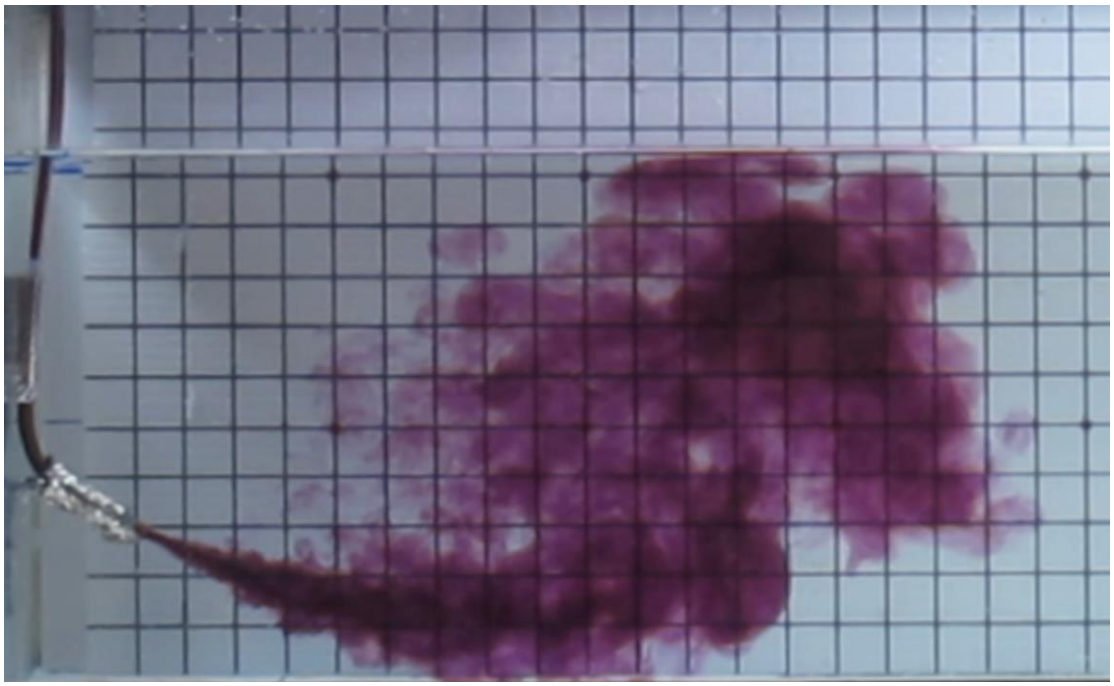

(b) Laboratory Experiment

Fig.4.13 Comparison between numerical simulation and laboratory experiment for Group 10 (0.6 m/s, Fd=20, α=-29.15°)

(a) LRR Simulation, 6.5s

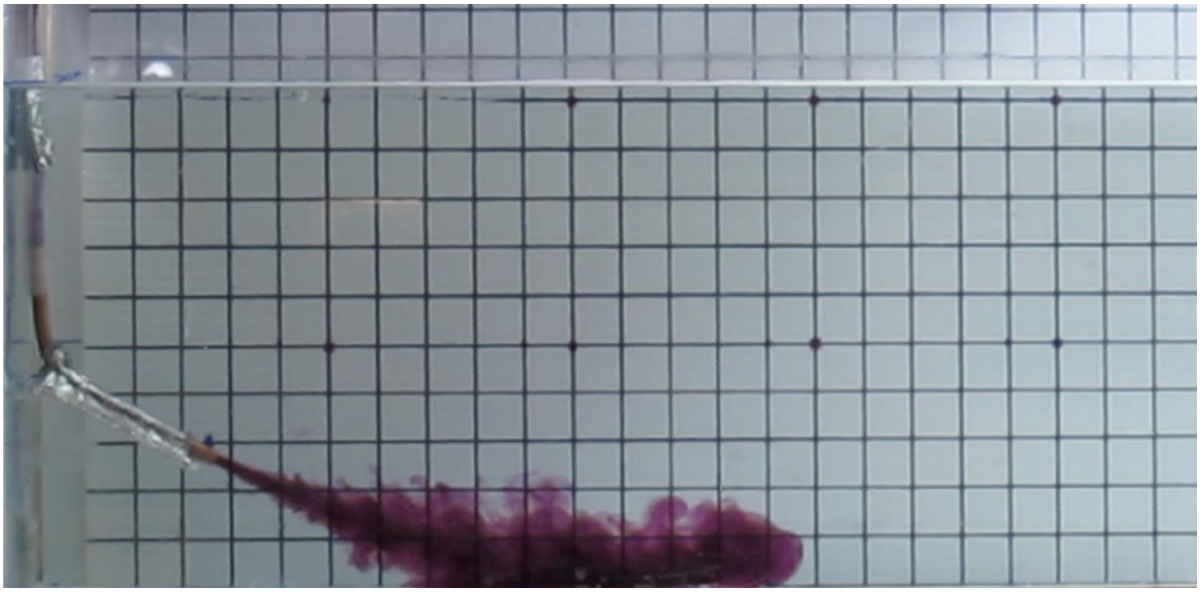

(b) Laboratory Experiment, 6.5s

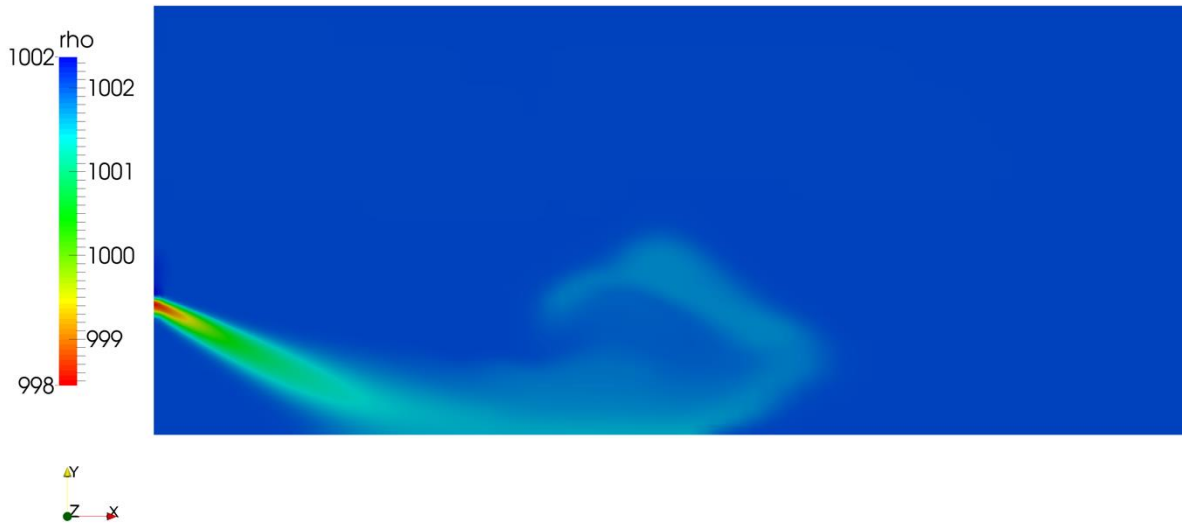

(c) LRR Simulation, 13s

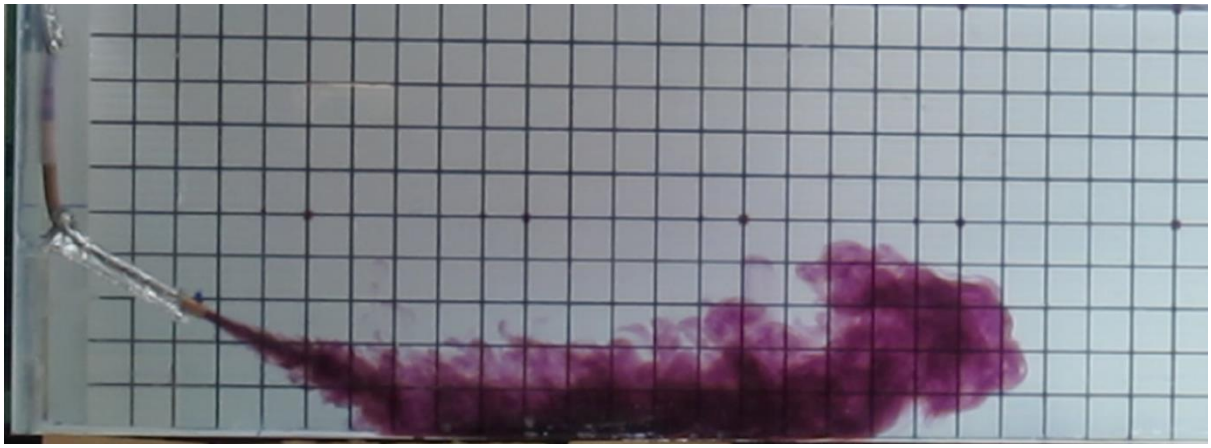

(d) Laboratory Experiment, 13s

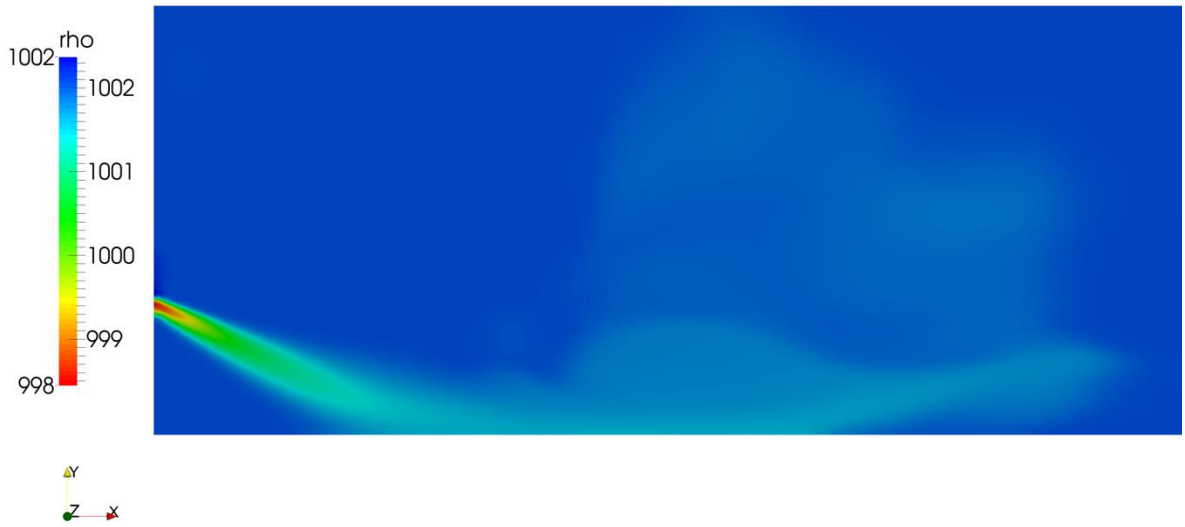

(e) LRR Simulation, 29s

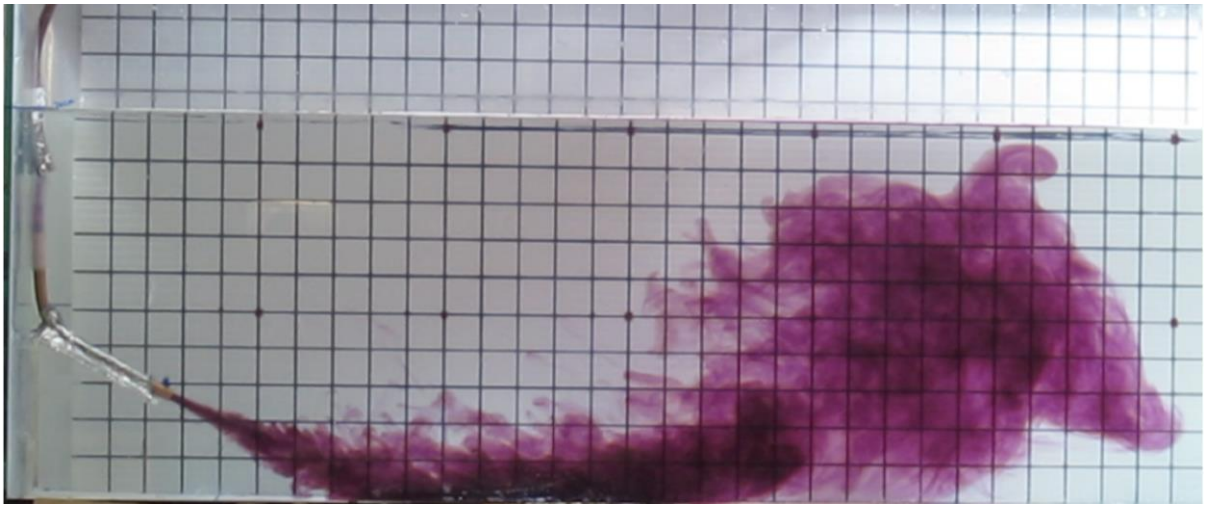

(f) Laboratory Experiment, 29s

Fig.4.14 Comparison between numerical simulation and laboratory experiment for Group 18 (0.41m/s, Fd=30, α=-27.04°)

Chapter 5 Conclusions and Suggestions for future work

5.1 Conclusions

Effluent pollution problems are not only a fluid dynamic issue, but also significant environmental and ecological concern to where the effluent is discharged. A number of studies about brine and thermal outfalls have been conducted in the past few years. Most of them focused on analyzing the jets' geometric characteristics while it is getting mixed. They aimed at finding out the optimal ways that help minimizing the environmental impact of the outfall system within the discharge area at the least economic cost. However, positively buoyant jets have not been thoroughly studied unlike negatively buoyant ones. This thesis is focused on both experimental and numerical study of the trajectory of positively buoyant jets.

The jets in this study were discharged from an inclined nozzle submerged below the receiving liquid water surface. In the experiments, the dyed tap water was discharged from the nozzle at velocities of 0.2m/s, 0.41m/w and 0.6m/s with discharge angles around 30° and 60° towards the bottom. The salinities of the still and homogenous ambient saline water were set based on the jets' initial velocity. Values of the Froude number were set at 10, 20, 30, 50 and 100. Videos of the experiments were recorded; image analysis was employed to extract the trajectories of the jets in various conditions.

From this study, in line with previous research, the Froude number (a dimensionless parameter that considers flow inertial and density difference) was found to be closely related to the jet trajectory in the case of a positively buoyant jet with an inclination of the jet nozzle. Compared to the impact of the velocity, the Froude number played a more significant role in the process of mixing. High velocities also made contributions to the dilution. However, jets with the same Froude number had closer trajectories, even when the velocity values were not very close to each other. The larger the Froude number was, the longer the jet trajectory formed. Two angles of the jet discharge were considered in the experiments (30° and 60°). Due to the confined depth of the tank, the jets with 60° inclined angle of the nozzle, reached the bottom and were blocked by

the bed which affected the centerline trajectory development of the jet.

Numerical simulations were conducted using OpenFOAM based on related laboratory experiments setting for comparison purposes. The Launder-Reece-Rody (LRR) model was used for turbulence modeling which is a second order turbulence model and calculates the Reynolds stresses directly without the Boussinesq approximation. A modified pisoFOAM solver (pisoFoamIIII230) was utilized for solving incompressible Navier-Stokes equations in all simulations in which the density effects and buoyancy terms are incorporated in the model. A structured grid using cubic control volumes was generated using the BLOCKMESH software (which is part of the OpenFOAM software) in order to enhance the efficiency of the model. Only half of the domain was simulated noting the symmetry of the problem to further expedite the simulations. The finite volume method was used in the simulations which ensures conservation of mass and is highly stable and accurate. Second order discretization methods where used in the simulations to enhance the accuracy of the system. Mesh independency was ensured by try different grid sizes and selecting the grid size that leads to mesh-independent results. Comparing the jet behavior in experimental and numerical results on several cases, a reasonable agreement was observed between experimental and numerical results. In other words, the LRR model and pisoFoamIIII230 solver in the OpenFOAM framework were found to be good options for numerical prediction of submerged inclined positively buoyant jets.

5.2 Suggestions for future works

The dynamic fluid principles of positively buoyant jets are not thoroughly understood yet. Further studies on related problems can lead to deeper understanding in the problems. The following suggestions may be considered for future research.

- Researchers can carry out experiments that focus on the discharge angles over a wider range between 0° to 90°.
- The impact of moving ambient condition could be considered.
- Similar experiments on thermal jets but with a wider range of Froude numbers can be

conducted.

- More turbulence models and solvers could be employed on the numerical investigation of positively buoyant jets.
- Large eddy simulation (LES), Detached eddy simulation (DES) and Delayed detached eddy simulations (DDES) can be performed.
- SnappyHexMesh could be used to get higher quality mesh.
- Laser Induced Fluorescence (LIF), Particle Image Velocimetry (PIV) and their combination can be used to develop further insight into flow and mixing features and details of positively buoyant jets.

Reference

Abessi, O., & Roberts, P. J. (2015). Effect of nozzle orientation on dense jets in stagnant environments. Journal of Hydraulic Engineering, 141(8), 06015009.

Abessi, O., Saeedi, M., Davidson, M., & Zaker, N. H. (2012). Flow classification of negatively buoyant surface discharge in an ambient current. Journal of Coastal Research, 28(1A), 148-155.

Alfaifi, H., Mohammadian, A., & Gildeh, H. K. (2015). Experimental and numerical study of thermal buoyant wall jet in calm ambient water.

Argyropoulos, C. D., & Markatos, N. C. (2015). Recent advances on the numerical modelling of turbulent flows. Applied Mathematical Modelling, 39(2), 693-732.

Bashitialshaaer, R., Larson, M., & Persson, K. M. (2012). An experimental investigation on inclined negatively buoyant jets. Water, 4(3), 720-738.

Bashitialshaaer, R., Larson, M., & Persson, K. M. (2013). An experimental study to improve the design of brine discharge from desalination plants. American Journal of Environmental Protection, 2(6), 176-182.

Belcaid, A., Le Palec, G., & Draoui, A. (2015). Numerical and experimental study of Boussinesq wall horizontal turbulent jet of fresh water in a static homogeneous environment of salt water. Journal of Hydrodynamics, 27(4), 604-615.

Bemporad, G. A. (1994). Simulation of round buoyant jet in stratified flowing environment. Journal of hydraulic Engineering, 120(5), 529-543.

Bigg, P. H. (1967). Density of water in SI units over the range 0-40 C. British Journal of Applied Physics, 18(4), 521.

Bleninger, T., & Jirka, G. H. (2008). Modelling and environmentally sound management of brine discharges from desalination plants. Desalination, 221(1-3), 585-597.

Bleninger, T., Niepelt, A., & Jirka, G. (2010). Desalination plant discharge

calculator. Desalination and Water Treatment, 13(1-3), 156-173.

Bloomfield, L. J., & Kerr, R. C. (2002). Inclined turbulent fountains. Journal of Fluid Mechanics, 451, 283.

Christodoulou, G. C., Papakonstantis, I. G., & Nikiforakis, I. K. (2015). Desalination brine disposal by means of negatively buoyant jets. Desalination and Water Treatment, 53(12), 3208-3213.

Crowe, A. (2013). Inclined negatively buoyant jets and boundary interaction.

Devenish, B. J., Rooney, G. G., Webster, H. N., & Thomson, D. J. (2010). The entrainment rate for buoyant plumes in a crossflow. Boundary-layer meteorology, 134(3), 411-439.

Gildeh, H. K., Mohammadian, A., Nistor, I., & Qiblawey, H. (2014, May). Numerical modelling of brine discharges using OpenFOAM. In Proc. Int. Conf. New Trends Transp. Phenom., Ottawa, Ontario, Canada.

Hargreaves, D. M., Scase, M. M., & Evans, I. (2012). A simplified computational analysis of turbulent plumes and jets. Environmental fluid mechanics, 12(6), 555-578.

Holford, j. M., & linden, p. F. (1999). The development of layers in a stratified fluid. In institute of mathematics and its applications conference series (vol. 68, pp. 165-180). Oxford university press.

Huai, W. X., Li, Z. W., Qian, Z. D., Zeng, Y. H., Han, J., & Peng, W. Q. (2010). Numerical simulation of horizontal buoyant wall jet. Journal of Hydrodynamics, 22(1), 58-65.

Ivey, G. N., Imberger, J., & Koseff, J. R. (1998). Buoyancy fluxes in a stratified fluid. Coastal and Estuarine Studies, 377-388.

Jiang, M., Law, A. W. K., & Zhang, S. (2018). Mixing behavior of 45 inclined dense jets in currents. Journal of hydro-environment research, 18, 37-48.

Jirka, G. H., & Harleman, D. R. (1973). The mechanics of submerged multiport diffusers for bouyant discharges in shallow water. MIT Energy Lab.

Jirka, G. H. (2004). Integral model for turbulent buoyant jets in unbounded stratified flows. Part I: Single round jet. Environmental Fluid Mechanics, 4(1), 1-56.

Kheirkhah Gildeh, H., Mohammadian, A., Nistor, I., & Qiblawey, H. (2014). Numerical modeling of turbulent buoyant wall jets in stationary ambient water. Journal of Hydraulic Engineering, 140(6), 04014012.

Kheirkhah Gildeh, H., Mohammadian, A., Nistor, I., & Qiblawey, H. (2015). Numerical modeling of 30◦ and 45◦ inclined dense turbulent jets in stationary ambient. Environmental Fluid Mechanics (Dordrecht, Netherlands : 2001), 15(3), 537–562.

Kheirkhah Gildeh, H., Mohammadian, A., Nistor, I., Qiblawey, H., & Yan, X. (2016). CFD modeling and analysis of the behavior of 30 and 45 inclined dense jets–new numerical insights. Journal of Applied Water Engineering and Research, 4(2), 112-127.

Kheradmand, S., Mohammadian, A., Seidou, O., & Gildeh, H. K. (2015). Numerical and experimental investigation of saline discharges in stationary ambient.

Kim, Y. D., Seo, I. W., Kang, S. W., & Oh, B. C. (2002). Jet integral–particle tracking hybrid model for single buoyant jets. Journal of Hydraulic Engineering, 128(8), 753-760.

Kikkert, G. A., Davidson, M. J., & Nokes, R. I. (2007). Inclined negatively buoyant discharges. Journal of Hydraulic Engineering, 133(5), 545-554.

Lai, C. C., & Lee, J. H. (2012). Mixing of inclined dense jets in stationary ambient. Journal of hydro-environment research, 6(1), 9-28.

Lai, C. K. (2009). Mixing of inclined dense jets. University of Hong Kong, 1-0.

Lattemann, S., & Höpner, T. (2008). Environmental impact and impact assessment of seawater desalination. Desalination, 220(1-3), 1-15.

Millero, F. J., & Poisson, A. (1981). International one-atmosphere equation of state of seawater. Deep Sea Research Part A. Oceanographic Research Papers, 28(6), 625-629.

Millero, F. J., & Huang, F. J. O. S. (2009). The density of seawater as a function of salinity (5 to

70 g kg-1) and temperature (273.15 to 363.15 K). Ocean Science, 5(2).

Michas, S. N., & Papanicolaou, P. N. (2009). Horizontal round heated jets into calm uniform ambient. Desalination, 248(1-3), 803-815.

Nikiforakis, I. K., Stamou, A. I., & Christodoulou, G. C. (2015). A modified integral model for negatively buoyant jets in a stationary ambient. Environmental Fluid Mechanics, 15(5), 939-957.

Oliver, C. (2012). Near field mixing of negatively buoyant jets.

Oliver, C. J., Davidson, M. J., & Nokes, R. I. (2013). Behavior of dense discharges beyond the return point. Journal of hydraulic engineering, 139(12), 1304-1308.

Palomar, P., & Losada, I. J. (2011). Impacts of brine discharge on the marine environment. Modelling as a Predictive Tool.

Palomar, P., Lara, J. L., Losada, I. J., & Tarrade, L. (2013). Numerical modeling of brine discharge: commercial models, MEDVSA online simulation tools and advanced computational fluid dynamics. Desalination and Water Treatment, 51(1-3), 543-559.

Pantzlaff, L., & Lueptow, R. M. (1999). Transient positively and negatively buoyant turbulent round jets. Experiments in fluids, 27(2), 117-125.

Papakonstantis, I. G., & Christodoulou, G. C. (2010). Spreading of round dense jets impinging on a horizontal bottom. Journal of Hydro-environment Research, 4(4), 289-300.

Papakonstantis, I. G., Christodoulou, G. C., & Papanicolaou, P. N. (2011). Inclined negatively buoyant jets 1: geometrical characteristics. Journal of Hydraulic Research, 49(1), 3-12.

Papanicolaou, P. N., Papakonstantis, I. G., & Christodoulou, G. C. (2008). On the entrainment coefficient in negatively buoyant jets. Journal of Fluid Mechanics, 614, 447-470.

Pincince, A. B., & List, E. J. (1973). Disposal of brine into an estuary. Journal (Water Pollution Control Federation), 2335-2344.

Roberts, D. A., Johnston, E. L., & Knott, N. A. (2010). Impacts of desalination plant discharges

on the marine environment: A critical review of published studies. Water research, 44(18), 5117-5128.

Roberts, P. J., & Toms, G. (1987). Inclined dense jets in flowing current. Journal of Hydraulic Engineering, 113(3), 323-340.

Roberts, P. J., Ferrier, A., & Daviero, G. (1997). Mixing in inclined dense jets. Journal of Hydraulic Engineering, 123(8), 693-699.

Saeedi, M., Farahani, A. A., Abessi, O., & Bleninger, T. (2012). Laboratory studies defining flow regimes for negatively buoyant surface discharges into crossflow. Environmental fluid mechanics, 12(5), 439-449.

Scheepbouwer, E. (2013). The evolution of discharges with two and three dimensional trajectories.

Shao, D., & Law, A. W. K. (2010). Mixing and boundary interactions of 30 and 45 inclined dense jets. Environmental fluid mechanics, 10(5), 521-553.

Sharp JJ (1975) The use of a buoyant wall jet to improve the dilution of a submerged outfall. Proc. Instn. Civ. Eng. (London) Part 2, 59(2): 527-534

Sharp, J. J., Vyas, B. D., & FROUDE. (1977). The buoyant wall jet. Proceedings of the Institution of Civil Engineers, 63(3), 593-611.

Ungate, C. D., Harleman, D. R., & Jirka, G. H. (1975). Stability and mixing of submerged turbulent jets at low Reynolds numbers. MIT Energy Lab.

Vafeiadou, P., Papakonstantis, I., & Christodoulou, G. (2005, September). Numerical simulation of inclined negatively buoyant jets. In The 9th international conference on environmental science and technology, September (pp. 1-3).

Van Maele, K., & Merci, B. (2006). Application of two buoyancy-modified k–ε turbulence models to different types of buoyant plumes. Fire Safety Journal, 41(2), 122-138.

Wright, S. J. (1984). Buoyant jets in density-stratified crossflow. Journal of Hydraulic

Engineering, 110(5), 643-656.

Xiao, J., Travis, J. R., & Breitung, W. (2009). Non-Boussinesq integral model for horizontal turbulent buoyant round jets. Science and Technology of Nuclear Installations, 2009.

Yannopoulos, P. C. (2010). Advanced integral model for groups of interacting round turbulent buoyant jets. Environmental fluid mechanics, 10(4), 415-450.

Zhang, H., & Baddour, R. E. (1998). Maximum penetration of vertical round dense jets at small and large Froude numbers. Journal of Hydraulic Engineering, 124(5), 550-553.

Zhang, S., Jiang, B., Law, A. W. K., & Zhao, B. (2016). Large eddy simulations of 45 inclined dense jets. Environmental Fluid Mechanics, 16(1), 101-121.

Appendix A: Numerical preparation in openFOAM in Case: Group 4, 0.4 m/s, F_d =20, α =-31.87°.

Constant dictionary

blockMeshDict file

```
FoamFile
{
   version     2.0;
   format      ascii;
   class       dictionary;
   object      blockMeshDict;
}

convertToMeters 0.001;

vertices
(
        (0 0 0)//0
        (750 0 0)//1
        (0 60 0)//2
        (750 60 0)//3
        (0 63.482 0)//4
        (750 63.482 0)//5
        (0 200 0)//6
        (750 200 0)//7

        (0 0 148.259)//8
        (750 0 148.259)//9
        (0 60 148.259)//10
        (750 60 148.259)//11
        (0 63.482 148.259)//12
        (750 63.482 148.259)//13
        (0 200 148.259)//14
        (750 200 148.259)//15

        (0 0 150)//16
        (750 0 150)//17
```

```
    (0 60 150)//18
    (750 60 150)//19
    (0 63.482 150)//20
    (750 63.482 150)//21
    (0 200 150)//22
    (750 200 150)//23
);

blocks
(
   hex (0 1 3 2 8 9 11 10) (100 30 20) simpleGrading (6 .5 .1)//0
   hex (8 9 11 10 16 17 19 18) (100 30 2) simpleGrading (6 .5 1)//1
   hex (2 3 5 4 10 11 13 12) (100 5 20) simpleGrading (6 1 .1)//2
   hex (10 11 13 12 18 19 21 20) (100 5 2) simpleGrading (6 1 1)//3
   hex (4 5 7 6 12 13 15 14) (100 28 20) simpleGrading (6 5 .1)//4
   hex (12 13 15 14 20 21 23 22) (100 28 2) simpleGrading (6 5 1)//5
);

edges
(
);

boundary
(
   inlet
   {
        type patch;
        faces
        (
           (10 18 20 12)
        );
   }
   leftWall
   {
      type wall;
      faces
      (
         (0 8 10 2)
            (8 16 18 10)
            (2 10 12 4)
         (4 12 14 6)
         (12 20 22 14)
      );
   }
   outlet
   {
```

```
    type patch;
    faces
    (
        (1 3 11 9)
        (9 11 19 17)
        (3 5 13 11)
            (11 13 21 19)
        (5 7 15 13)
        (13 15 23 21)
    );
}
lowerWall
{
    type wall;
    faces
    (
        (8 0 1 9)
        (16 8 9 17)
    );
}
atmosphere
{
    type symmetryPlane;
    faces
    (
        (22 23 15 14)
        (14 15 7 6)
        );
}
backWall
{
    type wall;
    faces
    (
        (0 1 3 2)
        (2 3 5 4)
        (4 5 7 6)
    );
}
symmetry
{
        type symmetryPlane;
        faces
        (
            (16 17 19 18)
            (18 19 21 20)
```

```
        (20 21 23 22)
        );
    }
);

mergePatchPairs
(
);
```

turbulenceProperties file

```
FoamFile
{
    version     2.0;
    format      ascii;
    class       dictionary;
    location    "constant";
    object      turbulenceProperties;
}

simulationType  RASModel;
```

RASProperties file

```
FoamFile
{
    version     2.0;
    format      ascii;
    class       dictionary;
    location    "constant";
    object      RASProperties;
}

RASModel        LRR;

turbulence      on;

printCoeffs     on;


transportProperties:
FoamFile
```

```
{
    version     2.0;
    format      ascii;
    class       dictionary;
    location    "constant";
    object      transportProperties;
}
// * * * * * * * * * * * * * * * * * * * * * * * * * * * * * * * * * * * * * * * * * * * * //

transportModel  Newtonian;

nu              nu [ 0 2 -1 0 0 0 0 ] 1e-06;
mykappaEff      mykappaEff [ 1 -1 -1 0 0 0 0 ] 1e-03;

CrossPowerLawCoeffs
{
    nu0             nu0 [ 0 2 -1 0 0 0 0 ] 1e-06;
    nuInf           nuInf [ 0 2 -1 0 0 0 0 ] 1e-06;
    m               m [ 0 0 1 0 0 0 0 ] 1;
    n               n [ 0 0 0 0 0 0 0 ] 1;
}

BirdCarreauCoeffs
{
    nu0             nu0 [ 0 2 -1 0 0 0 0 ] 1e-06;
    nuInf           nuInf [ 0 2 -1 0 0 0 0 ] 1e-06;
    k               k [ 0 0 1 0 0 0 0 ] 0;
    n               n [ 0 0 0 0 0 0 0 ] 1;
}

 g :
FoamFile
{
    version     2.0;
    format      ascii;
    class       uniformDimensionedVectorField;
    location    "constant";
    object      g;
}

dimensions      [0 1 -2 0 0 0 0];
value           ( 0 -9.81 0 );
```

0 dictionary

epsilon file

```
FoamFile
{
   version     2.0;
   format      ascii;
   class       volScalarField;
   location    "0";
   object      epsilon;
}

dimensions      [0 2 -3 0 0 0 0];

internalField   uniform 0.1;

boundaryField
{
   inlet
   {
      type            fixedValue;
      value           uniform 0.977348;
   }
   leftWall
   {
      type            epsilonWallFunction;
      value           uniform 0.1;
   }
   outlet
   {
      type            zeroGradient;
   }
   lowerWall
   {
      type            epsilonWallFunction;
      value           uniform 0.1;
   }
   atmosphere
   {
      type            symmetryPlane;
   }
   backWall
```

```
    {
        type            epsilonWallFunction;
        value           uniform 0.1;
    }
    symmetry
    {
        type            symmetryPlane;
    }
}
```

k file

```
FoamFile
{
    version     2.0;
    format      ascii;
    class       volScalarField;
    location    "0";
    object      k;
}

dimensions      [0 2 -2 0 0 0 0];

internalField   uniform 0.1;

boundaryField
{
    inlet
    {
        type            fixedValue;
        value           uniform 0.0096;
    }
    leftWall
    {
        type            kqRWallFunction;
        value           uniform 0.1;
    }
    outlet
    {
        type            zeroGradient;
    }
    lowerWall
    {
        type            kqRWallFunction;
        value           uniform 0.1;
```

```
    }
    atmosphere
    {
        type            symmetryPlane;
    }
    backWall
    {
        type            kqRWallFunction;
        value           uniform 0.1;
    }
    symmetry
    {
        type            symmetryPlane;
    }
}
```

Rho file

```
FoamFile
{
    version     2.0;
    format      ascii;
    class       volScalarField;
    object      rho;
}
// * * * * * * * * * * * * * * * * * * * * * * * * * * * * * * * * * * * * * * * * * * * * //

dimensions      [0 0 0 0 0 0 0];

internalField   uniform 1006.4378;
boundaryField
{
    inlet
    {
        type            fixedValue;
        value           uniform 998.4462;
    }
    leftWall
    {
        type            zeroGradient;
    }

    outlet
```

```
    {
        type            zeroGradient;
    }

    lowerWall
    {
        type            zeroGradient;
    }

    atmosphere
    {
        type            symmetryPlane;
    }

    backWall
    {
        type            zeroGradient;
    }
    symmetry
    {
        type            symmetryPlane;
    }

}
```

S file

```
FoamFile
{
    version     2.0;
    format      ascii;
    class       volScalarField;
    object      S;
}
// * * * * * * * * * * * * * * * * * * * * * * * * * * * * * * * * * * * * * * * * * * * * //

dimensions      [0 0 0 0 0 0 0];

internalField   uniform 10.5703;

boundaryField
{
    inlet
    {
```

```
    type            fixedValue;
    value           uniform 0;
  }
  leftWall
  {
    type            zeroGradient;
  }

  outlet
  {
    type            zeroGradient;
  }

  lowerWall
  {
    type            zeroGradient;
  }

  atmosphere
  {
    type            symmetryPlane;
  }

  backWall
  {
    type            zeroGradient;
  }
  symmetry
  {
    type            symmetryPlane;
  }

}
```

T file

```
FoamFile
{
  version     2.0;
  format      ascii;
  class       volScalarField;
  object      T;
}
```

```
dimensions      [0 0 0 0 0 0 0];

internalField   uniform 18.8;

boundaryField
{
   inlet
   {
      type           fixedValue;
      value          uniform 18.8;
   }
   leftWall
   {
      type           zeroGradient;
   }

   outlet
   {
      type           zeroGradient;
   }

   lowerWall
   {
      type           zeroGradient;
   }

   atmosphere
   {
      type           symmetryPlane;
   }

   backWall
   {
      type           zeroGradient;
   }
   symmetry
   {
      type           symmetryPlane;
   }

}
```

U file

```
FoamFile
```

```
{
    version     2.0;
    format      ascii;
    class       volVectorField;
    location    "0";
    object      U;
}

dimensions      [0 1 -1 0 0 0 0];

internalField   uniform (1e-10 0 0);

boundaryField
{
    inlet
    {
        type            fixedValue;
        value           uniform (0.3448 -0.2144 0);
    }
    leftWall
    {
        type            fixedValue;
        value           uniform (0 0 0);
    }
    outlet
    {
        type            zeroGradient;
    }
    lowerWall
    {
        type            fixedValue;
        value           uniform (0 0 0);
    }
    atmosphere
    {
        type            symmetryPlane;
    }
    backWall
    {
        type            fixedValue;
        value           uniform (0 0 0);
    }
    symmetry
    {
        type            symmetryPlane;
    }
```

}

System dictionary

controlDict file

```
FoamFile
{
   version     2.0;
   format      ascii;
   class       dictionary;
   location    "system";
   object      controlDict;
}
// * * * * * * * * * * * * * * * * * * * * * * * * * * * * * * * * * * * * * * * * * * * * //

application     pisoFoamIIII230;

startFrom       startTime;

startTime       10;

stopAt          endTime;

endTime         20;

deltaT          0.0002;

writeControl    adjustableRunTime;

writeInterval   0.25;

purgeWrite      0;

writeFormat     ascii;

writePrecision  6;

writeCompression off;
```

```
timeFormat      general;

timePrecision   6;

runTimeModifiable true;

maxCo     0.5;
```

fvSchemes file

```
FoamFile
{
   version     2.0;
   format      ascii;
   class       dictionary;
   location    "system";
   object      fvSchemes;
}
// * * * * * * * * * * * * * * * * * * * * * * * * * * * * * * * * * * * * * * * * //

ddtSchemes
{
   default         Euler;
//    default         CrankNicholson 0.5;
}

gradSchemes
{

   default         Gauss linear;
   grad(p)         Gauss linear;
   grad(U)         Gauss linear;
/*
   default         fourth;
   grad(p)         fourth;
   grad(U)         fourth;
*/
}

divSchemes
{
   default         none;
/*
```

```
    div(phi,U)      Gauss limitedLinearV 1;
    div(phi,S)      Gauss limitedLinear 1;
    div(phi,T)      Gauss limitedLinear 1;
    div(rhophi,S)       Gauss limitedLinear 1;
    div(rhophi,T)       Gauss limitedLinear 1;
    div(phi,k)      Gauss limitedLinear 1;
    div(phi,epsilon) Gauss limitedLinear 1;
    div(phi,R)      Gauss limitedLinear 1;
    div(R)          Gauss linear;
    div(phi,nuTilda) Gauss limitedLinear 1;
    div((nuEff*dev(T(grad(U))))) Gauss linear;
///
    div(nonlinearStress) Gauss linear;
///
*/

    div(phi,U)      Gauss linearUpwindV Gauss linear;
    div(phi,S)      Gauss upwind;
    div(phi,T)      Gauss upwind;
    div(rhophi,S)       Gauss limitedLinear 1;
    div(rhophi,T)       Gauss limitedLinear 1;
    div(phi,k)      Gauss limitedLinear 1;
    div(phi,epsilon) Gauss limitedLinear 1;
    div(phi,R)      Gauss limitedLinear 1;
    div(R)          Gauss linear;
    div(phi,nuTilda) Gauss limitedLinear 1;
    div((nuEff*dev(T(grad(U))))) Gauss linear;
    div(nonlinearStress) Gauss linear;

}

laplacianSchemes
{
    default         none;

    laplacian(nuEff,U) Gauss linear corrected;
    laplacian(kappaEff,S) Gauss linear corrected;
    laplacian(kappaEff,T) Gauss linear corrected;
    laplacian(kappaEff,rhoT) Gauss linear corrected;
    laplacian(kappaEff,rhoS) Gauss linear corrected;
    laplacian((1|A(U)),p) Gauss linear corrected;
    laplacian(DkEff,k) Gauss linear corrected;
    laplacian(DepsilonEff,epsilon) Gauss linear corrected;
    laplacian(DREff,R) Gauss linear corrected;
    laplacian(DnuTildaEff,nuTilda) Gauss linear corrected;
```

```
/*
    laplacian(nuEff,U) Gauss cubic corrected;
    laplacian(kappaEff,S) Gauss cubic corrected;
    laplacian(kappaEff,T) Gauss cubic corrected;
    laplacian(kappaEff,rhoT) Gauss cubic corrected;
    laplacian(kappaEff,rhoS) Gauss cubic corrected;
    laplacian((1|A(U)),p) Gauss linear corrected;
    laplacian(DkEff,k) Gauss linear corrected;
    laplacian(DepsilonEff,epsilon) Gauss linear corrected;
    laplacian(DREff,R) Gauss linear corrected;
    laplacian(DnuTildaEff,nuTilda) Gauss linear corrected;
*/
}

interpolationSchemes
{
    default         linear;
    interpolate(U)  linear;
}

snGradSchemes
{
    default         corrected;
}

fluxRequired
{
    default         no;
    p               ;
}
```

fvSolution file

```
FoamFile
{
    version     2.0;
    format      ascii;
    class       dictionary;
    location    "system";
    object      fvSolution;
}

solvers
{
```

```
    p
    {
        solver          PCG;
        preconditioner  DIC;
        tolerance       1e-06;
        relTol          0.1;
    }

    pFinal
    {
        solver          PCG;
        preconditioner  DIC;
        tolerance       1e-06;
        relTol          0;
    }

    U
    {
        solver          PBiCG;
        preconditioner  DILU;
        tolerance       1e-05;
        relTol          0;
    }
//
    S
    {
        solver          PBiCG;
        preconditioner  DILU;
        tolerance       1e-05;
        relTol          0;
    }
    T
    {
        solver          PBiCG;
        preconditioner  DILU;
        tolerance       1e-05;
        relTol          0;
    }

    rhoS
    {
        solver          PBiCG;
        preconditioner  DILU;
        tolerance       1e-05;
        relTol          0;
    }
```

```
    rhoT
    {
        solver          PBiCG;
        preconditioner  DILU;
        tolerance       1e-05;
        relTol          0;
    }
//

    k
    {
        solver          PBiCG;
        preconditioner  DILU;
        tolerance       1e-05;
        relTol          0;
    }

    epsilon
    {
        solver          PBiCG;
        preconditioner  DILU;
        tolerance       1e-05;
        relTol          0;
    }

    R
    {
        solver          PBiCG;
        preconditioner  DILU;
        tolerance       1e-05;
        relTol          0;
    }

    nuTilda
    {
        solver          PBiCG;
        preconditioner  DILU;
        tolerance       1e-05;
        relTol          0;
    }
}

PISO
{
    nCorrectors     2;
    nNonOrthogonalCorrectors 0;
```

```
    pRefCell        0;
    pRefValue       0;
}
```

Appendix B: pisoFoamIIII230

pisoFoamIIII230.C

```
#include "fvCFD.H"
#include "singlePhaseTransportModel.H"
#include "turbulenceModel.H"

// * * * * * * * * * * * * * * * * * * * * * * * * * * * * * * * * * * * * * //

int main(int argc, char *argv[])
{
  #include "setRootCase.H"

  #include "createTime.H"
  #include "createMesh.H"
  #include "createFields.H"
  #include "initContinuityErrs.H"

  // * * * * * * * * * * * * * * * * * * * * * * * * * * * * * * * * * * * //

  Info<< "\nStarting time loop\n" << endl;

  while (runTime.loop())
  {
    Info<< "Time = " << runTime.timeName() << nl << endl;

    #include "readPISOControls.H"
    #include "CourantNo.H"
/// Modification Start
// 01. Add equation of state start
rho==1000;
rho==(rho/1000*(999.842594+6.793952e-2*T-(9.095290e-3*pow(T,2))+(1.001685e-
4*pow(T,3))-(1.120083e-6*pow(T,4))+(6.536336e-9*pow(T,5))+S*(8.24493e-1-4.0899e-
3*T+(7.6438e-5*pow(T,2))-(8.2467e-7*pow(T,3))+(5.3875e-
9*pow(T,4)))+(pow(S,1.5))*(-5.72466e-3+1.0227e-4*T-1.6546e-
6*pow(T,2))+S*(4.8314e-4)));
```

```
// 01. Add equation of state end

// 02. Add Variables and A-D Equations start
{

// 02-01. Add heat transfer coefficient start

kappaEff=rho*(turbulence->nu()+turbulence->nut());
// 02-01. Add heat transfer coefficient end
// 02-02. Add rhoU start

   volVectorField rhoU
    (
        IOobject
        (
            "rhoU",
            runTime.timeName(),
            mesh,
            IOobject::MUST_READ,
            IOobject::AUTO_WRITE
        ),
        rho*U
    );
// 02-02. Add rhoU end
// 02-03. Add rhophi start
surfaceScalarField rhophi
(
    IOobject
    (
        "rhophi",
        runTime.timeName(),
        mesh,
        IOobject::READ_IF_PRESENT,
        IOobject::AUTO_WRITE
    )
,
    linearInterpolate(rhoU) & mesh.Sf()
);
// 02-03. Add rhophi end
// 02-04. Add temperature AD equation start
```

```
    fvScalarMatrix TEqn
    (
        fvm::ddt(rho,T)
      + fvm::div(rhophi, T)
      - fvm::laplacian(kappaEff, T)
    );

    TEqn.relax();
    TEqn.solve();
// 02-04. Add temperature AD equation end
// 02-05. Add salinity AD equation start
    fvScalarMatrix SEqn
    (
        fvm::ddt(rho,S)
      + fvm::div(rhophi, S)
      - fvm::laplacian(kappaEff, S)
    );

    SEqn.relax();
    SEqn.solve();
// 02-05. Add salinity AD equation end

}

        // Pressure-velocity PISO corrector
        {
            // Momentum predictor
// 02-06. Modify the gravatational start
            fvVectorMatrix UEqn
            (
                fvm::ddt(U)
              + fvm::div(phi, U)
              + turbulence->divDevReff(U)
              - g*(rho-1000)/1000
            );
// 02-06. Modify the gravatational end
            UEqn.relax();

            if (momentumPredictor)
            {
```

```
    solve(UEqn == -fvc::grad(p));
}

// --- PISO loop

for (int corr=0; corr<nCorr; corr++)
{
    volScalarField rAU(1.0/UEqn.A());

    volVectorField HbyA("HbyA", U);
    HbyA = rAU*UEqn.H();
    surfaceScalarField phiHbyA
    (
        "phiHbyA",
        (fvc::interpolate(HbyA) & mesh.Sf())
      + fvc::interpolate(rAU)*fvc::ddtCorr(U, phi)
    );

    adjustPhi(phiHbyA, U, p);

    // Non-orthogonal pressure corrector loop
    for (int nonOrth=0; nonOrth<=nNonOrthCorr; nonOrth++)
    {
        // Pressure corrector

        fvScalarMatrix pEqn
        (
            fvm::laplacian(rAU, p) == fvc::div(phiHbyA)
        );

        pEqn.setReference(pRefCell, pRefValue);

        if
        (
            corr == nCorr-1
         && nonOrth == nNonOrthCorr
        )
        {
            pEqn.solve(mesh.solver("pFinal"));
        }
```

```
            else
            {
                pEqn.solve();
            }

            if (nonOrth == nNonOrthCorr)
            {
                phi = phiHbyA - pEqn.flux();
            }
        }

        #include "continuityErrs.H"

        U = HbyA - rAU*fvc::grad(p);
        U.correctBoundaryConditions();
    }
}

turbulence->correct();

runTime.write();

Info<< "ExecutionTime = " << runTime.elapsedCpuTime() << " s"
    << "  ClockTime = " << runTime.elapsedClockTime() << " s"
    << nl << endl;
}

Info<< "End\n" << endl;

return 0;
}


// ************************************************************************* //
```

createFields.H

```
Info<< "Reading field p\n" << endl;
```

```
    volScalarField p
    (
        IOobject
        (
            "p",
            runTime.timeName(),
            mesh,
            IOobject::MUST_READ,
            IOobject::AUTO_WRITE
        ),
        mesh
    );

    Info<< "Reading field U\n" << endl;
    volVectorField U
    (
        IOobject
        (
            "U",
            runTime.timeName(),
            mesh,
            IOobject::MUST_READ,
            IOobject::AUTO_WRITE
        ),
        mesh
    );
// 01. Add salinity start
    Info<< "Reading field S\n" << endl;
    volScalarField S
    (
        IOobject
        (
            "S",
            runTime.timeName(),
            mesh,
            IOobject::MUST_READ,
            IOobject::AUTO_WRITE
        ),
        mesh
    );
```

```
// 01. Add salinity end
// 02. Add temperature start

Info<< "Reading field T\n" << endl;
    volScalarField T
    (
        IOobject
        (
            "T",
            runTime.timeName(),
            mesh,
            IOobject::MUST_READ,
            IOobject::AUTO_WRITE
        ),
        mesh
    );
// 02. Add temperature end
// 03. Add rho start
    Info<< "Reading field rho\n" << endl;
    volScalarField rho
    (
        IOobject
        (
            "rho",
            runTime.timeName(),
            mesh,
            IOobject::READ_IF_PRESENT,
            IOobject::AUTO_WRITE
        ),
        mesh
    );
// 03. Add rho end
// 04. Add rhoS start
    Info<< "Reading field S\n" << endl;
    volScalarField rhoS
    (
        IOobject
        (
            "rhoS",
            runTime.timeName(),
```

```
            mesh,
            IOobject::MUST_READ,
            IOobject::AUTO_WRITE
        ),
        rho*S
    );
// 04. Add rhoS end
// 05. Add rhoT start
  Info<< "Reading field T\n" << endl;
    volScalarField rhoT
    (
        IOobject
        (
            "rhoT",
            runTime.timeName(),
            mesh,
            IOobject::MUST_READ,
            IOobject::AUTO_WRITE
        ),
        rho*T
    );
// 05. Add rhoT end
// 06. Add temperature transfer coeff start
volScalarField kappaEff
(
IOobject
        (
            "kappaEff",
            runTime.timeName(),
            mesh,
            IOobject::READ_IF_PRESENT,
            IOobject::AUTO_WRITE
        ),
        mesh
          );
// 06. Add temperature transfer coeff end
// 07. Include gravitational acceleration start
    #include "readGravitationalAcceleration.H"
// 07. Include gravitational acceleration end
#   include "createPhi.H"
```

```
// 08. Calcuate rhoU start
Info<< "Reading/calculating face flux field phi\n" << endl;

   volVectorField rhoU
    (
        IOobject
        (
            "rhoU",
            runTime.timeName(),
            mesh,
            IOobject::MUST_READ,
            IOobject::AUTO_WRITE
        ),
        rho*U
    );
// 08. Calculate rhoU end
// 09. Calculate rhophi start
surfaceScalarField rhophi
(
    IOobject
    (
        "rhophi",
        runTime.timeName(),
        mesh,
        IOobject::READ_IF_PRESENT,
        IOobject::AUTO_WRITE
    )
,
    linearInterpolate(rhoU) & mesh.Sf()
);
// 09. Calculate rhophi end


    label pRefCell = 0;
    scalar pRefValue = 0.0;
    setRefCell(p, mesh.solutionDict().subDict("PISO"), pRefCell, pRefValue);


    singlePhaseTransportModel laminarTransport(U, phi);
```

```
autoPtr<incompressible::turbulenceModel> turbulence
(
    incompressible::turbulenceModel::New(U, phi, laminarTransport)
);
```